



12-2015

Wide-Area Synchrophasor Measurement Applications and Power System Dynamic Modeling

Yin Lei

University of Tennessee - Knoxville, ylei6@vols.utk.edu

Recommended Citation

Lei, Yin, "Wide-Area Synchrophasor Measurement Applications and Power System Dynamic Modeling." PhD diss., University of Tennessee, 2015.

https://trace.tennessee.edu/utk_graddiss/3549

This Dissertation is brought to you for free and open access by the Graduate School at Trace: Tennessee Research and Creative Exchange. It has been accepted for inclusion in Doctoral Dissertations by an authorized administrator of Trace: Tennessee Research and Creative Exchange. For more information, please contact trace@utk.edu.

To the Graduate Council:

I am submitting herewith a dissertation written by Yin Lei entitled "Wide-Area Synchrophasor Measurement Applications and Power System Dynamic Modeling." I have examined the final electronic copy of this dissertation for form and content and recommend that it be accepted in partial fulfillment of the requirements for the degree of Doctor of Philosophy, with a major in Electrical Engineering.

Yilu Liu, Major Professor

We have read this dissertation and recommend its acceptance:

Kevin Tomsovic, Fangxing Li, Chen Chien-fei

Accepted for the Council:

Carolyn R. Hodges

Vice Provost and Dean of the Graduate School

(Original signatures are on file with official student records.)

Wide-Area Synchrophasor Measurement Applications and Power System Dynamic Modeling

A Dissertation Presented for the
Doctor of Philosophy
Degree
The University of Tennessee, Knoxville

Yin Lei
December 2015

Copyright © 2015 by Yin Lei
All rights reserved.

ACKNOWLEDGEMENTS

First, I would like to express my deepest gratitude and appreciation to my advisor, Dr. Yilu Liu, for her patient guidance and consistent encouragement in both academic area and personal life throughout the past four years. I will always remember the inspiration and wisdom she has passed on. I could not be any luckier to have an advisor like Dr. Liu. In addition, I would also like to thank Dr. Kevin Tomsovic, Dr. Fangxing Li, and Dr. Chien-fei Chen for serving in my dissertation committee. I appreciate their precious time and valuable advice and comments. Besides, I would like to thank my supervisor Dr. Reynaldo Nuqui from ABB, for his kind guidance during my internship.

Then, special thanks go to those graduated Power IT Lab colleagues for the foundation work and contribution for my work, especially from Dr. Lang Chen, Dr. Yong Liu and Dr. Changgang Li. Also, I would like to thank Yalong Li and Siqi Wang for the collaboration and great teamwork. My special thanks are extended to all of my wonderful colleagues in FNET group: I am greatly appreciated the support and consistent friendship from Dr. Ye Zhang, Dr. Lingwei Zhan, Gefei Kou, Jiahui Guo, Jidong Chai, Dao Zhou and many other wonderful friends. I also like to thank all my friends outside my academic life for the remarkable kindness and help. I particularly want to thank Dr. Xiaojing Xu, Dr. Zhi Li, Meng Li, Xuan Liu, Haoyu Yuan and Yiwei Ma for all the happiness we have shared. I will never forget the memorable time during the past four years in Knoxville with all your friendship.

Last but not least I would like to express my deepest love and gratitude to my family: my father Xiaoming Lei, my mother Li Luo, and my boyfriend Shun Wan for their unconditional love and support.

ABSTRACT

The use of synchrophasor measurements system-wide has been providing significant assistance for grid dynamic monitoring, situation awareness and reliability improvement. Frequency Monitoring Network (FNET), as an academia-run synchrophasor measurement system, utilizes a large number of Internet-connected low-cost Frequency Disturbance Recorders (FDRs) installed at the distribution level to measure power system dynamics and provide both online and off-line applications, such as event detection, oscillation modes estimation, event replay, etc. This work aims to further explore applications of the FNET measurements and utilize measurement-based method in dynamic modeling.

Measurement-based dynamic reduction is an important application of synchrophasor measurement, especially considering the fact that when the system model is large, measurements provide a precise insight of system dynamics in order to determine equivalent regions. Another important application is to investigate Super Bowl games as an example to evaluate the influence of synchronized human activities on the power system. Featured characteristics drawn from the frequency data detected during the Super Bowl games are discussed.

Increased penetration levels of wind generation and retirements of conventional plants have caused concerns about a decline of system inertia and primary frequency response. This work evaluates the impact of wind power on the system inertial response, simulation scenarios with different wind penetration levels are developed based on the U.S. Northeast Power Coordinating Council (NPCC) system. A user-defined electrical control model is also introduced to provide inertia and governor control to wind generations.

Except for wind generation, frequency regulation can also be achieved by supplementary control of High Voltage Direct Current (HVDC) transmission line. A multi-terminal Voltage Source Converter (VSC) HVDC model is constructed to prove the effective control. In order to transmit large amount of intermittent and remote renewable energy over long distance to load centers, a potential solution is to upgrade the transmission system at a higher voltage by constructing an overlay HVDC grid on top of the original transmission

system. The VSC HVDC model is utilized to build the HVDC overlay grid, and the overlay grid is tested with interconnection models.

Conclusions and possible future research topics are given in the end.

TABLE OF CONTENTS

Chapter 1	Introduction to Frequency Monitoring Network.....	1
1.1	Frequency Monitoring Network (FNET).....	1
1.2	Frequency Disturbance Recorder (FDR)	2
Chapter 2	Eastern Interconnection Model Reduction Based on Phasor Measurements..	4
2.1	Power System Dynamic Model Reduction	4
2.2	Dynamic Equivalence of EI System	4
2.2.1	Coherency Determination	5
2.2.1	Generation and Load Aggregation.....	9
2.2.2	Network Reduction	13
2.3	PSS/E Model and Simulation Results.....	13
2.3.1	Load Flow Model.....	14
2.3.2	Dynamic Model	14
2.3.3	Preliminary Simulation Results	15
2.4	Conclusion	17
Chapter 3	Impact of Synchronized Human Activities on Power System Frequency....	18
3.1	Background	18
3.2	Super Bowl Information	18
3.3	FNET Observations and Analysis of Power System Frequency	19
3.3.1	Observation 1: high density of frequency events during broadcasting period	19
3.3.2	Observation 2: Frequency events tend to happen during commercial breaks	21
3.3.3	Observation 3: large frequency fluctuation during halftime show	21
3.3.4	Observation 4: Sharp drop of frequency at the beginning of halftime show	23
3.3.5	Observation 5: All US interconnections tend to oscillate together during large frequency disturbances.....	25
3.4	Conclusions.....	28
Chapter 4	Wind Frequency Control under High Wind Penetration on an NPCC System Model	29
4.1	Background	29
4.2	Model Development.....	30
4.2.1	Base Case without Wind	30
4.2.2	Wind Case without Control	34
4.2.3	Wind Case with Control.....	38
4.3	Simulation Results Comparison.....	39
4.3.1	Wind Impact of System Inertial Responses	39
4.3.1	Wind Frequency Control.....	39
4.4	Conclusion	44
Chapter 5	VSC-HVDC Model Development	46
5.1	Background	46
5.2	Multi-terminal VSC HVDC Model Development.....	47
5.2.1	Static Model.....	48

5.2.2	Dynamic Model	49
5.2.1	Simulation Results	51
5.3	VSC HVDC Supplementary Control	51
5.3.1	Frequency Droop Control	52
5.3.2	Inertia Control	52
5.3.3	Oscillation Damping Control	53
5.3.4	Test system and results	54
5.4	Conclusion	57
Chapter 6	Building an HVDC Overlay for US Power Grid Using Multi-terminal VSC-HVDC Technology	58
6.1	Background	58
6.2	Required Characteristics of the Overlay Grid	60
6.3	Transmission Technology	61
6.3.1	HVAC Technology	61
6.3.2	HVDC Technology	61
6.4	Regional HVDC Overlay Planning	62
6.4.1	Overlay HVDC grid for NPCC system	62
6.4.2	Overlay HVDC grid for WECC and EI system	63
6.4.3	Simulation results with overlay grid	64
6.5	Conclusion	67
Chapter 7	Virtual Grid Simulator	68
7.1	Background	68
7.2	Different Toolboxes for Comparison	69
7.2.1	Power System Analysis Toolbox (PSAT)	69
7.2.2	ePMU	70
7.2.3	PowerWorld Dynamic Simulator	72
7.2.4	ePHASORsim	72
7.3	Conclusion	75
Chapter 8	Conclusions and Future Work	76
8.1	Conclusions	76
8.2	Possible Future Work	78
	LIST OF REFERENCES	80
	VITA	85

LIST OF TABLES

Table 2-1 Clustering results of selected cases	10
Table 2-2 FDR clustering results	11
Table 2-3 Generator and load capacities for each cluster	12
Table 3-1 Super Bowl Audience Rating	19
Table 5-1 PSS/E convertor models	47
Table 5-2 Power flow results comparison in TSAT and Matlab	49
Table 6-1 Five-terminal VSC HVDC system operating mode	63

LIST OF FIGURES

Figure 1-1 FNET Architecture.....	1
Figure 1-2 Second Generation FDR	2
Figure 1-3 FDR Location Map (As of October 2014)	3
Figure 1-4 FNET World-wide Deployment Map	3
Figure 2-1 Voltage angle response from FNET.....	5
Figure 2-2 Voltage angle response from FNET.....	6
Figure 2-3 The flowchart for the clustering algorithm	7
Figure 2-4 Distribution of selected cases.....	8
Figure 2-5 Coherent Regions Map.....	11
Figure 2-6 Reduced EI system Structure	13
Figure 2-7 PSS/E load flow model	14
Figure 2-8 Simulation results of frequency deviations during a 1100 MW generation trip case.....	15
Figure 2-9 Frequency measurements of a 1100MW generation trip case	16
Figure 2-10 Simulated frequency deviations caused by a line fault	16
Figure 3-1 EI daily events histogram.....	20
Figure 3-2 Super Bowl events histogram.....	20
Figure 3-3 Frequency events occurrence distribution for Super Bowl XLVI, 2012 and XLVII, 2013.....	21
Figure 3-4 30 minutes frequency plot during halftime show on Super Bowl XLVII.....	22
Figure 3-5 30 minutes frequency plot on an ordinary Sunday Evening	22
Figure 3-6 Halftime 30 minutes plot for Super Bowl XLVII, 2013	23
Figure 3-7 Halftime 30 minutes plot for Super Bowl XLVI, 2012	24
Figure 3-8 Halftime 30 minutes plot for Super Bowl XLV, 2011	24
Figure 3-9 Halftime 30 minutes plot for Super Bowl XLV, 2011	25
Figure 3-10 Different interconnections frequency swings during halftime 2013.....	26
Figure 3-11 Different interconnections frequency swings on an ordinary Sunday evening	26
Figure 3-12 NERC interconnections frequency swings during Super Bowl XLVII	27
Figure 3-13 NERC interconnections frequency swings during random event	27
Figure 4-1 NPCC one-line diagram	31
Figure 4-2 NPCC system topology	31
Figure 4-3 Base case tuning steps comparison	32
Figure 4-4 Machine speed deviation after a generation trip for base case.....	33
Figure 4-5 Machine terminal voltage after a generation trip for base case	33
Figure 4-6 Structure of WT3 Wind Turbine Stability Model in PSS/E [25].....	34
Figure 4-7 Wind farm locations for 20% wind case	35
Figure 4-8 Machine speed deviation after a generation trip for 20% wind case without control	36
Figure 4-9 Machine terminal voltage after a generation trip for 20% wind case without control	36

Figure 4-10 Frequency deviation after a generation trip for 90% wind case without control	37
Figure 4-11 Machine terminal voltage after a generation trip for 90% wind case without control	37
Figure 4-12 Wind Inertia Control Structure.....	38
Figure 4-13 Wind Governor Control Structure.....	39
Figure 4-14 Machine speed deviation after a generation trip for 20% wind case with control	40
Figure 4-15 Machine terminal voltage after a generation trip for 20% wind case with control	40
Figure 4-16 Machine speed deviation after a generation trip for 90% wind case with control	41
Figure 4-17 Machine terminal voltage after a generation trip for 90% wind case with control	41
Figure 4-18 Frequency deviation after a generation trip under different wind penetration levels	42
Figure 4-19 Frequency deviation after a generation trip for 20% wind case with different controls.....	42
Figure 4-20 Active power output after a generation trip for 20% wind case with different controls.....	43
Figure 4-21 Frequency deviation after a generation trip for 90% wind case with different controls.....	43
Figure 4-22 Active power output after a generation trip for 90% wind case with different controls.....	44
Figure 5-1 Voltage-Sourced Converter Model in TSAT[29]	47
Figure 5-2 Four terminal VSC HVDC in NPCC system	48
Figure 5-3 Static MTDC model in PSAT	48
Figure 5-4 Control diagrams of MTDC converters	50
Figure 5-5 System response for a 350MW generation trip.....	51
Figure 5-6 Control diagram for frequency droop control	52
Figure 5-7 Control diagram for inertia control	53
Figure 5-8 Control diagram for oscillation damping control.....	53
Figure 5-9 Test system topology for HVDC controls.....	54
Figure 5-10 System response with or without frequency droop control.....	55
Figure 5-11 System response with or without inertia control.....	56
Figure 5-12 System response comparison	57
Figure 6-1 AEP conceptual 765kV backbone system.....	59
Figure 6-2 Renewable energy map, United States (Image courtesy of NREL).....	60
Figure 6-3 Five-terminal HVDC overlay of NPCC system.....	63
Figure 6-4 MISO proposed HVDC overlay topology.....	64
Figure 6-5 WECC system with HVDC overlay.....	65
Figure 6-6 EI system with HVDC overlay	65
Figure 7-1 Data structure	68
Figure 7-2 PSAT Results of adding load profile	69

Figure 7-3 ePMU structure 71

Figure 7-4 example of ePMU streaming data 71

Figure 7-5 ePMU control command 71

Figure 7-6 PWDS user interface 72

Figure 7-7 ePHASORsim HIL demo 74

Figure 7-8 Simulation results validation with PSS/E 74

Chapter 1 INTRODUCTION TO FREQUENCY MONITORING NETWORK

1.1 Frequency Monitoring Network (FNET)

The evolving technology of wide-area measurement system (WAMS) and the use of synchronized phasor measurement units (PMUs) have made monitoring the power system dynamics in real-time a promising aspect to enhance and maintain power system stability [1]. As an alternative to WAMS, frequency monitoring network (FNET) at the University of Tennessee, Knoxville (UTK) has been continuously providing high accuracy, GPS synchronized measurements on distribution level since 2003[2][3].

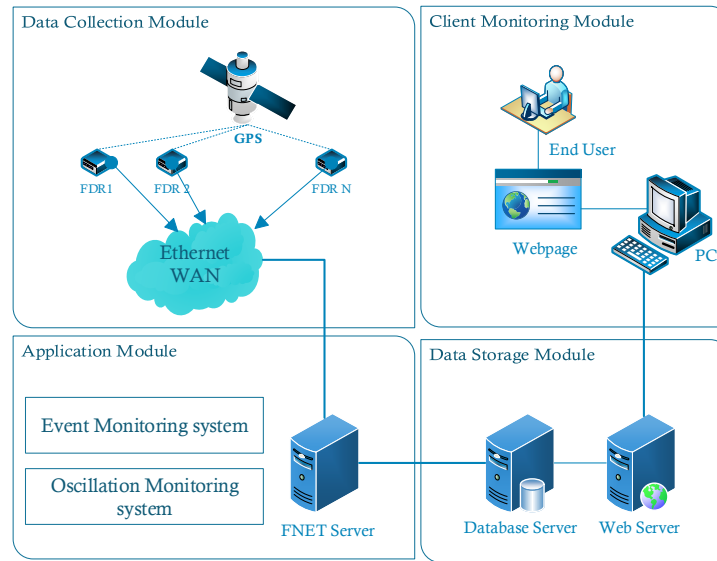


Figure 1-1 FNET Architecture

As shown in Figure 1-1, FNET system consists of four major modules: a) Data collection module includes hundreds of frequency disturbance recorders (FDRs), the ground-level sensor which perform local GPS-synchronized frequency measurements and send data to a server through the Internet at 100ms intervals, and b) Application module, which has event detection, oscillation detection, event location estimation and various applications installed on FNET application server located at UTK. c) Data storage module, which

archives and store different types of FNET data and d) Client monitoring module, which provides end users with real-time event alert emails and web-based visualization services.

1.2 Frequency Disturbance Recorder (FDR)

The measuring device used in FNET is called Frequency Disturbance Recorder (FDR, Figure 1-2) that is an essentially GPS time-synchronized single-phase phasor measurement units (PMU) to capture the distribution level dynamic responses like frequency, voltage magnitude and phase angle [4].



Figure 1-2 Second Generation FDR

And the installation of FDR is simple and low cost comparing with PMUs which are normally installed at high voltage substations. FDRs are currently installed in offices, residential households and renewable generation sites all over the world. Figure 1-3 **Error! Reference source not found.** presents the current FDR locations in North America. The network is continuously expanding as new hosts are being added. Figure 1-4 shows the FNET worldwide coverage of more than 20 countries.

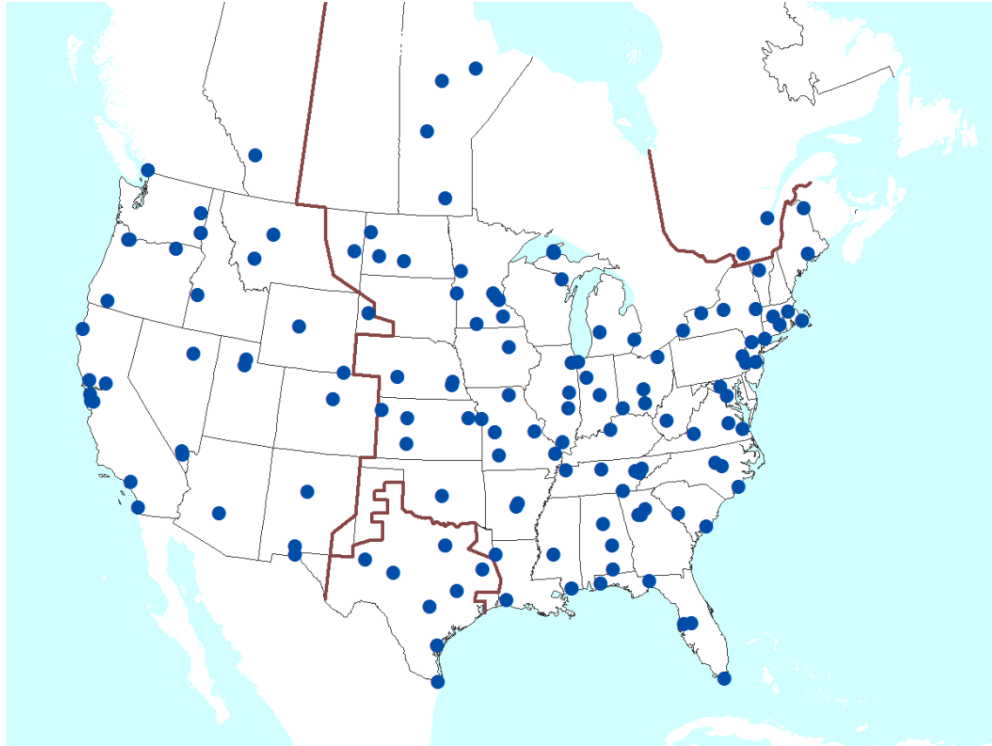


Figure 1-3 FDR Location Map (As of October 2014)



Figure 1-4 FNET World-wide Deployment Map

Chapter 2 EASTERN INTERCONNECTION MODEL REDUCTION BASED ON PHASOR MEASUREMENTS

2.1 Power System Dynamic Model Reduction

The research in dynamic reduction of power system can date back to the late 1960s when several methods such as modal equivalent, coherency-based equivalent and evaluation equivalent have been developed [2]. The modal equivalent method suggests eliminating those buses that are not easily affected by the disturbances in some areas. Since it is difficult to find these undisturbed buses and additional modification has to be made in the original dynamic simulation programs in order to make use of the state matrix of the equivalent equations, this method is not widely applied. In the 1970s, a novel coherency based method was presented, with the corresponding dynamic reduction programs, DYNRED [6], developed by the Electric Power Research Institute (EPRI). It identifies the coherent generators on the basis of the swing curves obtained by time domain simulations. The typical way of dynamic equivalence done by DYNRED is to model in sufficient detail of the system within the boundaries of a control center and approximate the external system. The external model needs to be commensurate with the dynamic problems at hand. For example, for transient stability problems it is necessary that the external model is accurate during the first swing as stability is determined during this period. Although this approach suffices for the operator of this control area, it does not provide sufficient modeling needs if one is interested in observing the propagation of a disturbance in a larger geographical region or control area. The NETOMAC program is based on the evaluation equivalent method [7], in which the complete structure and parameters of the external system are not required. Slow coherency technique [10] based on singular perturbation theory was developed in the early 1980s, which defines the coherent generators by means of modal analysis and coherency analysis.

2.2 Dynamic Equivalence of EI System

The procedure of building the dynamic equivalent of EI system based on FNET measurements is demonstrated in Figure 2-1. The first step is coherency determination

from FNET angle response, followed by the aggregation of generators and loads, and network reduction. The reduced EI system model is then built and simulated in PSS/E, and the simulation results are benchmarked with FNET measurement again.

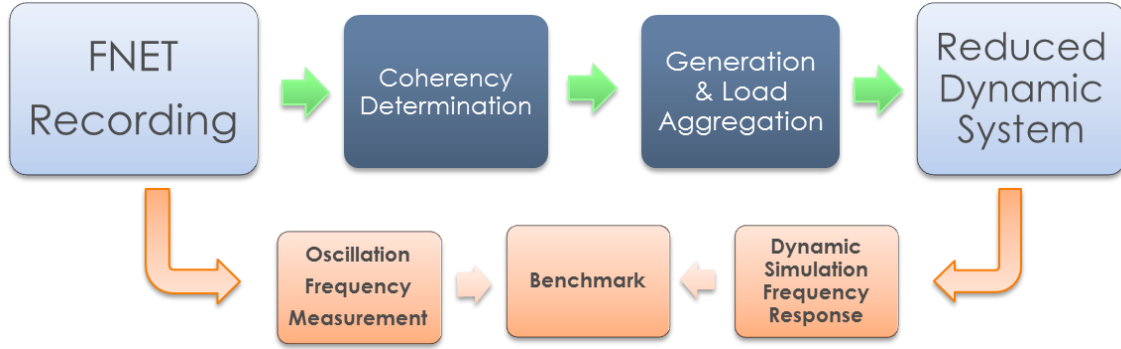


Figure 2-1 Voltage angle response from FNET

2.2.1 *Coherency Determination*

I. Methodology

To identify the coherent regions, clustering algorithm was applied on a data set consisting of the time-domain voltage angle responses of all FDRs in EI system during and following an oscillation. For a given oscillation event, the data set to be clustered can be presented by the following matrix.

$$\phi = \begin{bmatrix} \varphi_1(t_1) & \varphi_1(t_2) & \cdots & \varphi_1(t_n) \\ \varphi_2(t_1) & \varphi_2(t_2) & \cdots & \varphi_2(t_n) \\ \vdots & \vdots & \ddots & \vdots \\ \varphi_N(t_1) & \varphi_N(t_2) & \cdots & \varphi_N(t_n) \end{bmatrix} \quad 2-1$$

Where:

φ : is the voltage angle.

t_n : is the time of the oscillation event.

N : is the number of FDRs.

An example of the time domain plot of voltage angle is shown in Figure 2-2. Coherency between FDR units can be determined from such a data set.

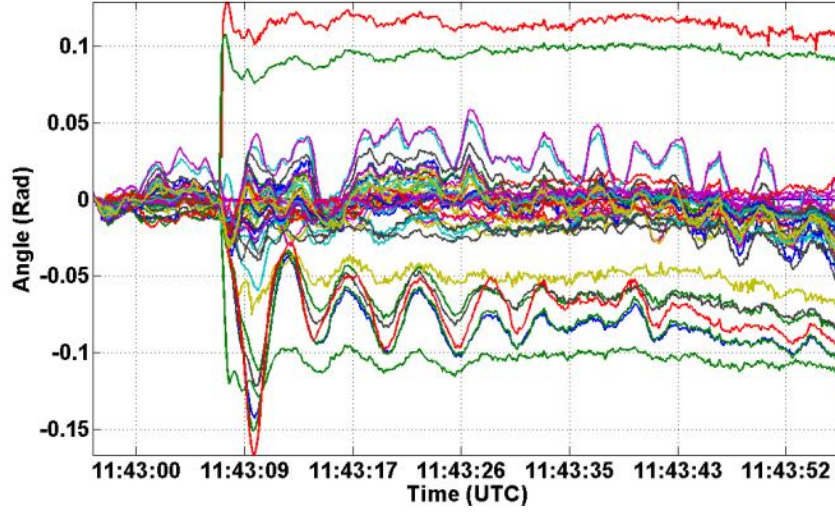


Figure 2-2 Voltage angle response from FNET

K-means is one of the most commonly used clustering algorithms. It is performed by minimizing the Euclidean distances between items and their corresponding centroids. However, K-means involves random generation of the initial centroids and the cluster number K must be given as a parameter, so the results often reach the local optima.

As in the coherency determination case, the total cluster number K in most cases are unknown, so this work introduces the K-means based divisive hierarchical clustering algorithm. It starts from applying K-means clustering algorithm, while K=2, to the original data set, which is identified as level 0. After the clustering, it calculates the Euclidean distance between the two centroids found by K-means from Equation 2-2.

$$d = \sqrt{\sum_{t=t_1}^{t=t_n} (c_i(t) - c_j(t))^2} \quad 2-2$$

Where d is the Euclidean distance between centroid i and centroid j.

The K-means based hierarchical clustering algorithm utilized to group the FDR units into coherent clusters is described by the flow chart in Figure 2-3. The Euclidean distance

reflects the dissimilarity between each FDR unit in their response to the encountered oscillation.

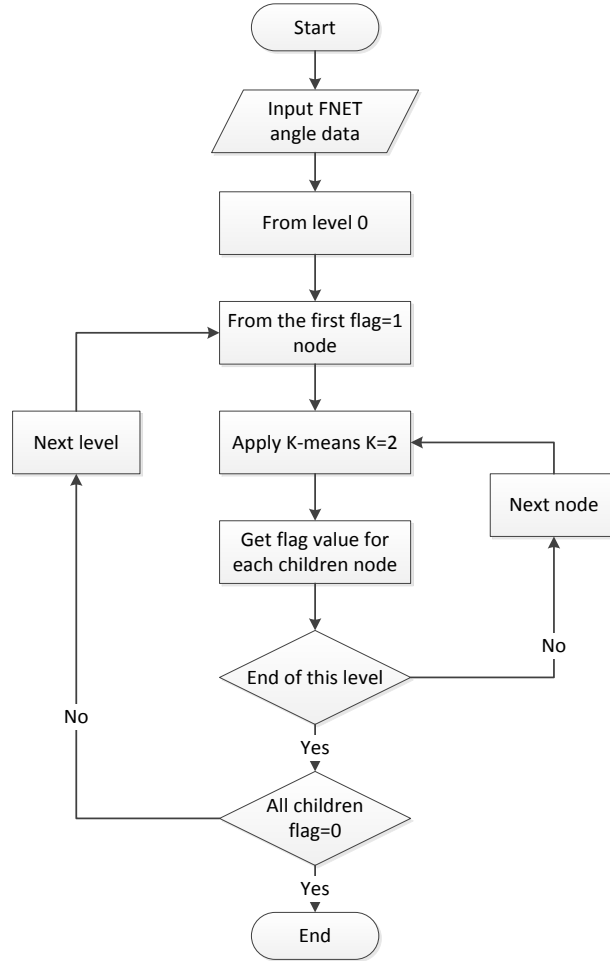


Figure 2-3 The flowchart for the clustering algorithm

Based on the distance obtained by Equation 2-2, a flag vector is then assigned to recognize the two clusters on the current level. When the distance is smaller than a threshold, the flag value is set to zero, which means it will stop splitting. Otherwise, the flag value is set to one and the K=2 K-means will continue to apply on this node. The flag vector for next level is updated by calculating the distance between new centroids. The algorithm will automatically stop when all the flag values in the vector of that level are set to zero.

II. Numerical results

A. Case selection

In order to test the proposed algorithm, certain cases need to be selected based on the following criteria: First, the selected disturbances result in large oscillations; and second is that the selections of event locations are evenly distributed in the geographical area of the EI system [4].

By following these two criteria, twenty typical oscillation cases detected by the FNET are selected from the EI in the past three months, from April 2012 to July 2012. The locations of the twenty cases are shown in Figure 2-4. And four typical cases located geographically far from each other are selected for results demonstration. Note that the location here only indicates the location of the first FDR unit that detected the oscillation.



Figure 2-4 Distribution of selected cases

B. Clustering Results

Based on the data from these cases, the coherency determination is processed by the proposed K-means based divisive hierarchical clustering method. By inputting the voltage angle data recorded by FNET, the coherency results for the selected four cases are outputted as in Table 2-1. The numbers in the table indicate FDR numbers.

For cases 1, 2 and 3, there are 19 coherent groups; as for case 4, 20 coherent groups found are instead. The number in each cell distinguishes the FDR units of each cluster. The clusters number and sequence may vary case by case; however, they don't have any influence on the final results.

Voting technique is then applied to all twenty results in order to get the final clustering results based on the following rules: First, units belonging to one cluster in most cases can automatically be seen as one cluster. Second, an exception of the previous rule is when the units are geographically too far from each other, they are treated as two clusters separately. Third, unit jumping from one cluster to another in different cases is separated as an independent cluster.

The final clustering results are listed in Table 2-2. By statistically analysis, final groups of coherent FDR regions are shown in Figure 2-5.

2.2.1 Generation and Load Aggregation

After obtaining the coherent regions from FNET angle measurements, we are assuming that angle shifts from generation level to distribution level does not change the inner coherency of generators. Therefore, all EI generators can be associated to the determined clusters by their geographical locations. According to the 2011 Energy Visuals Model, over 27,000 substations are spread around the whole EI system. The total generator and load capacities for each cluster are calculated based on the detailed model and the results are listed in Table 2-3.

Table 2-1 Clustering results of selected cases

	Case1	Case2	Case3	Case4
1	682,684	686	786	767
2	707,733	785	623	715,719
3	601,621	601	663	664,665
4	696,785	682,684	767	713
5	523,692, 770	696	523,692,770	720,739,760 777,781,832
6	623	715,719	669,673,753	667,682,684,733
7	710,713, 753,797	720,726,729,730,740	686,688,756	620,710,755,778
8	620,670,679, 686,688,755 778	620,688,710,713,755, 778, 797,830	620,621,670,713,781, 830	670,679,686 688,696,803
9	663	733	720,729,730,740	621
10	664,665	712,750,760,777,832	682,684	623
11	672,673	664	664,665	672,673,674
12	715,726	667,707	715,719	663,669
13	759,786	621,670,679,753	679,712,750,777	523,601,692,785
14	720,739,760 777,832	756,759,781	739,760,832	726
15	767	523,692,770,786	672	729,730,740
16	712,750,756	623,663	710,755,759,778,797	797
17	729,730,740	669,672,673	696,707	712,750,756,759
18	669	665	733	707
19	781	739	726	786
20				753

Table 2-2 FDR clustering results

Cluster	1	2	3	4	5	6	7
FDR NO.	682,684	712,715	664 665	715 719	729,730 740,726	720,739, 760,777, 832	620 755 778
Cluster	8	9	10	11	12	13	14
FDR NO.	667 707 733	523 692 770	601 785	623 663	672,673 669,674 753	710,713 797,830	670 679
Cluster	15	16	17	18	19	20	21
FDR NO.	686 688	786	759	767	756 781	621	696

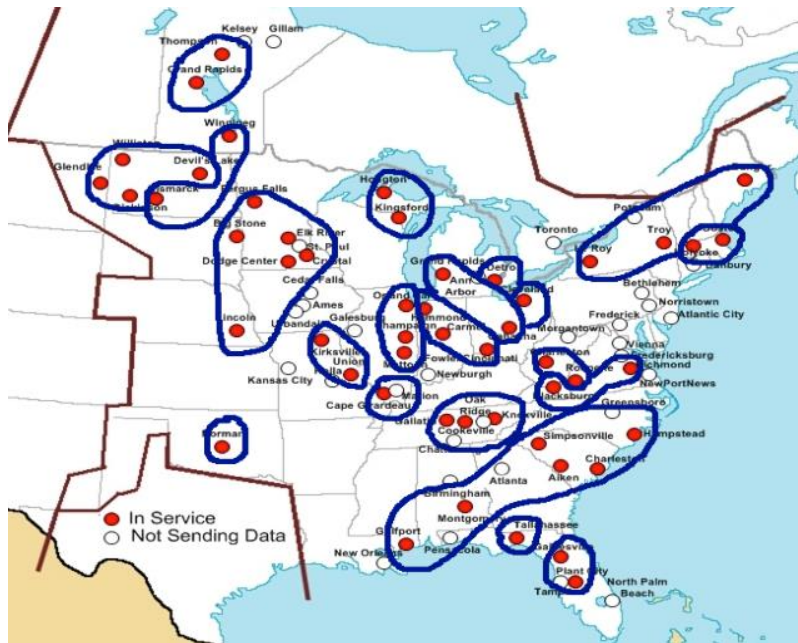


Figure 2-5 Coherent Regions Map

Table 2-3 Generator and load capacities for each cluster

Cluster Number	FDR Units Included	Generation Capacity (MW)	Load Capacity (MW)
1	682,684	64613.99	71346.41
2	712,715	12868.78	10350.22
3	664,665	1581.87	4758.34
4	715,719	5439.64	442.83
5	729,730,740,726	11964.96	7117.85
6	720,739,760,777,832	26013.61	28615.81
7	620,755,778	46947.41	46110.48
8	667,707,733	29907.66	18789.02
9	523,692,770	44738.59	37712.85
10	601,785	77598.79	82824.38
11	623,663	49752.82	52439.02
12	672,673,669,674,753	54369.59	50860.93
13	710,713,797,830	23986.32	24832.3
14	670,679	6195.26	18585.12
15	686,688	59370.23	59916.54
16	786	25581.73	26042.5
17	759	53727.9	51992.95
18	767	55694.3	42274.88
19	756,781	25884.57	30334.01
20	621	24618.18	19062.76
21	696	50905.66	48127.22

2.2.2 Network Reduction

Load flows transferred between generators in each cluster of the detailed model are then calculated to determine if there is a tie line flow between clusters. One branch is then used to identify the tie line between two clusters. The tie lines are then retained in the reduced system, and all the other branches are eliminated. Then the structure of the proposed reduced EI model can be represented by Figure 2-6.

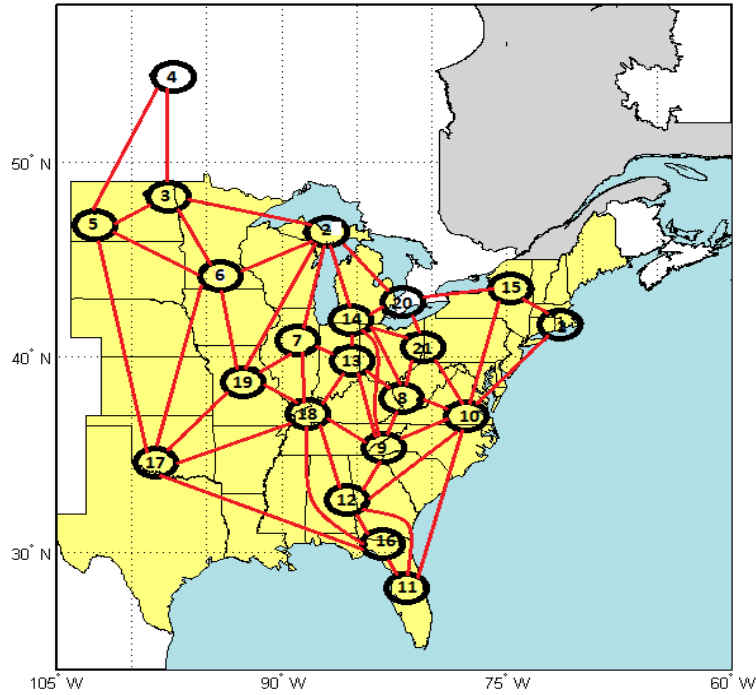


Figure 2-6 Reduced EI system Structure

2.3 PSS/E Model and Simulation Results

Since PSS/E can accomplish nonlinear time domain simulations for the large-scale power system efficiently, this work attempts to construct the equivalent model for the EI system under PSS/E with the procedure directly implemented in it. The equivalents are developed in both load flow model and dynamic model.

2.3.1 Load Flow Model

Based on the aggregation and network reduction results, the EI model is then built in PSS/E as shown in Figure 2-7.

Clusters are connected by phase shift transformers. The phase shifters are adjusted so that the power transfers between clusters preserve the network loadflow on the portions of the system retained in full detail [9].

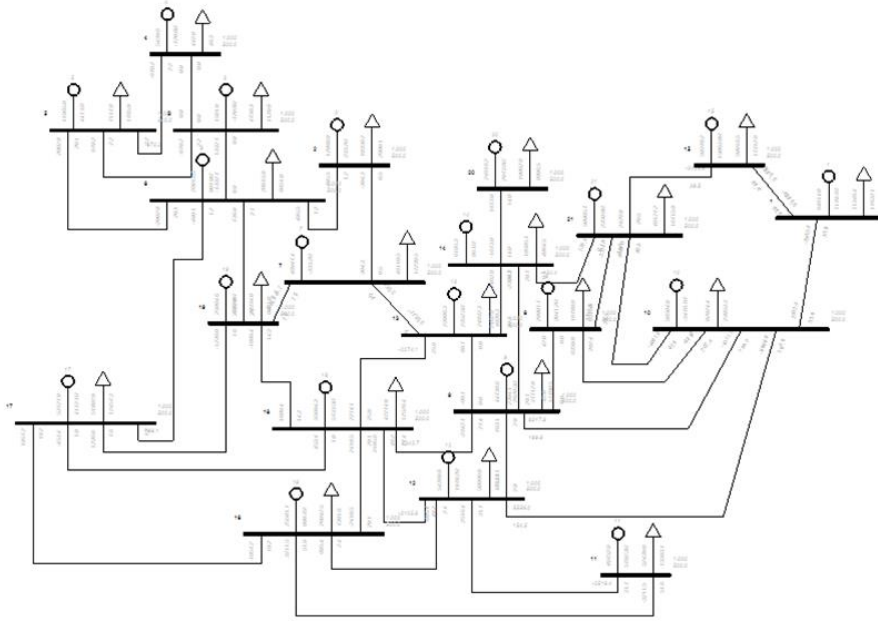


Figure 2-7 PSS/E load flow model

2.3.2 Dynamic Model

To study the dynamic characteristics of the reduced EI model, generator, exciter and governor models are adopted. All the generators are first modeled as round rotor generators. The inertia constant H for each generator is estimated based on the FNET measurements of oscillation frequency. Each generator is attached with a simplified exciter and steam turbine governor [11]. Future work is planned for more accurate generator

representation and includes other types of generators such as hydro, combustion turbine, etc. as needed.

2.3.3 Preliminary Simulation Results

To assess the validity of the reduced EI model, dynamic simulations are performed in PSS/E. As shown in Figure 2-8, an 1100MW generation trip at 0.5s was followed by an obvious frequency drop in the reduced EI system. Figure 2-9 shows the measurements of a real generation trip event in EI system detected by FNET. The estimated amount is also 1100MW. As we can see from both figures, the frequencies drop roughly the same amount of 0.06Hz during a period of 20s.

In Figure 2-10, a line fault on the transmission line from bus 2 to 7 was applied at 1.0 sec, and the fault was cleared after 10 cycles. The plot illustrates that the line fault causes dramatic oscillations in the EI system, and it is easy to visualize from the frequency deviation plot that there are at least two oscillation modes with one damped faster than the other. One of these modes is approximately 0.7Hz, which is close to an inter-area oscillation mode in the EI system [12].

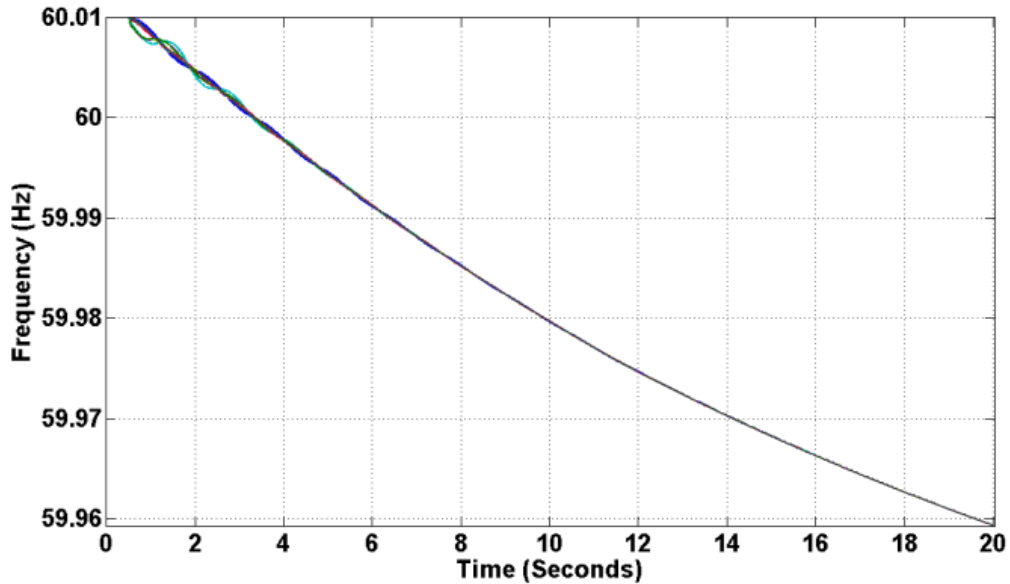


Figure 2-8 Simulation results of frequency deviations during a 1100 MW generation trip case

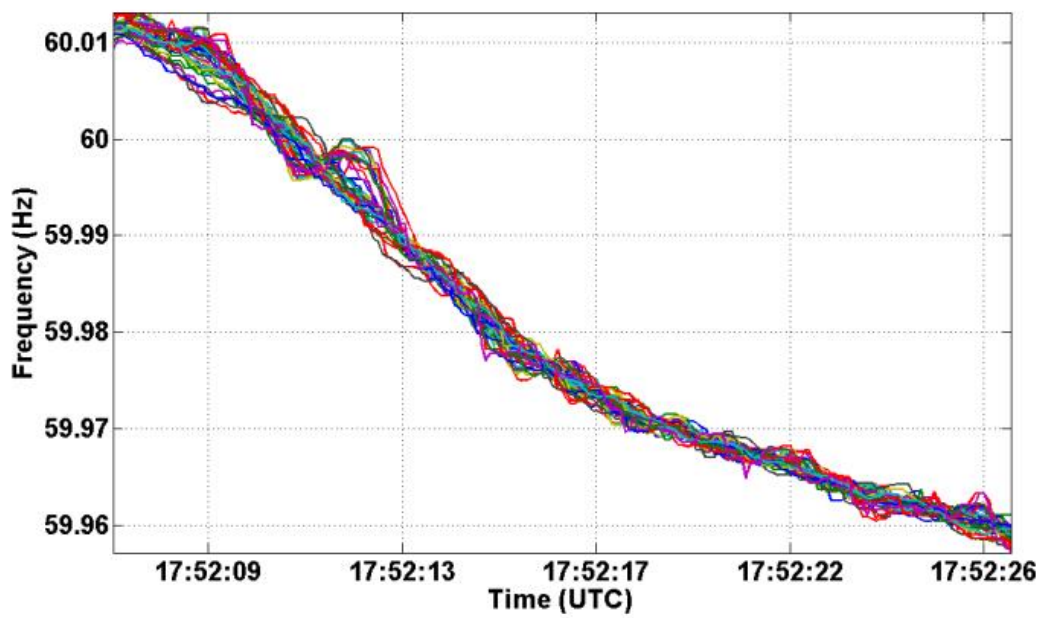


Figure 2-9 Frequency measurements of a 1100MW generation trip case

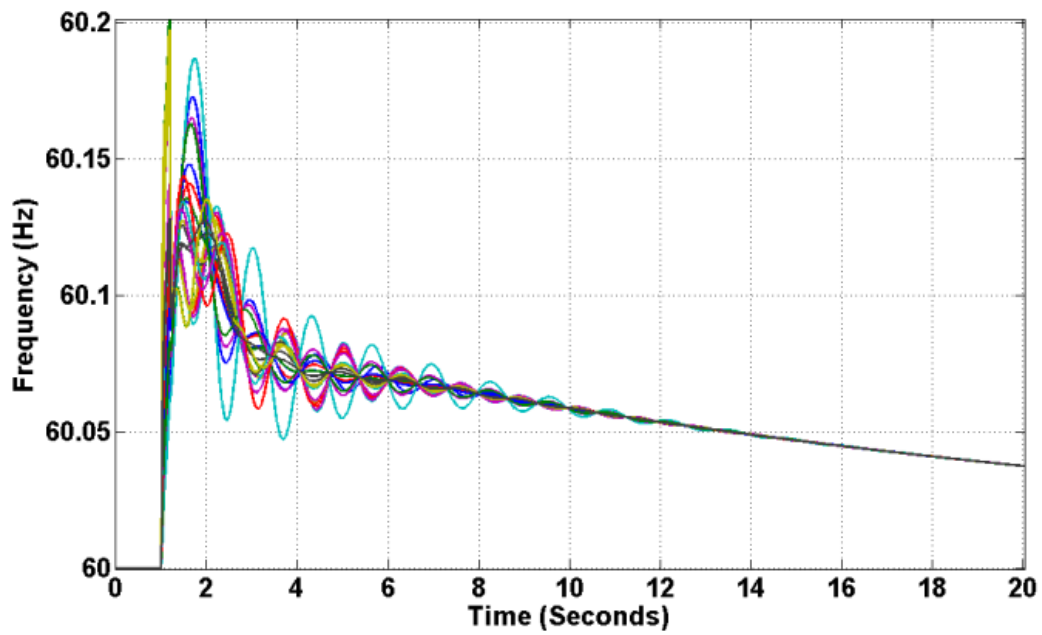


Figure 2-10 Simulated frequency deviations caused by a line fault

2.4 Conclusion

This chapter presents a procedure to construct the dynamic equivalent models of large-scale power systems using wide-area synchrophasor measurements. The procedure mainly consists of identification of coherent regions, aggregation of coherent generators and network reduction. The method is illustrated on the Eastern Interconnection and simulations in PSS/E are performed to assess the accuracy of the equivalent model. Results of the simulation show that the developed equivalent system has the capability in representing some of the dynamic characteristics of the original system. It is recognized that the accuracy of this model could not probably duplicate the more detailed model used in simulation. But for the target dynamical response, such high level models can be good decision aids for initiatives such as developing a national grid of a very large country like the United States. Another potential application could be simulating the faster than real time response of a large dynamic system as decision aids for power system operators.

Chapter 3 IMPACT OF SYNCHRONIZED HUMAN ACTIVITIES ON POWER SYSTEM FREQUENCY

3.1 Background

The impact of large-scale societal events on power system performance has drawn more attention in recent years. Reference [13] presents a thorough observation of power system frequency variation during Super Bowl XLII, and reference [14] illustrates the impact of the 2010 FIFA World Cup and Super Bowl XLIV on power grids. Reference [15] points out a possible reason for the unusual rapid frequency change may be the synchronized load changes of many television sets across the grid when the screens are changing from bright to dark back and forth simultaneously. All of the above papers demonstrate that a large group of people engaging in a synchronous, energy-intensive activity can affect the power system as a whole. This work summarizes and analyzes the impact of Super Bowl games on the system frequency from some other perspectives using FNET measurements.

3.2 Super Bowl Information

The Super Bowl is the annual championship game of the National Football League (NFL), the highest level of professional American football in the United States. The Super Bowl has frequently been the most watched American television broadcast of the year. Super Bowl XLIX, played in 2015, became the most-watched American television program in history, drawing an average audience of 114.5 million viewers and taking over the spot held by the previous year's Super Bowl. An estimated total audience of 168 million had watched that game, according to Nielsen, meaning that over half of the American population watched at least some of the initial broadcast. Table 3-1 lists the audience ratings of the last six Super Bowl games, which are studied in this work, as measured by Nielsen Company [16]. The Nielsen ratings represent an average percentage of all television-equipped households tuned in to Super Bowl games at any given moment.

Table 3-1 Super Bowl Audience Rating

Super Bowl #	Date	Stadium Location	Participating Teams	Nielsen Ratings
XLIV	Feb 7 th 2010	Miami Gardens, FL	New Orleans Saints, Indianapolis Colts	45.0 National 106.5 million
XLV	Feb 6 th 2011	Alington, TX	Pittsburgh Steelers, Green Bay Packers	47.3 National 111 million
XLVI	Feb 5 th 2012	Indianapolis, IN	New York Giants, New England Patriots	47.0 National 111.3 million
XLVII	Feb 3 rd 2013	New Orleans, LA	Baltimore Ravens, San Francisco 49ers	46.3 National 108.7 million
XLVIII	Feb 2 nd 2014	New York/ New Jersey	Seattle Seahawks, Denver Broncos	46.4 National 111.5 million
XLIX	Feb 1 st 2015	Glendale, AZ	Seattle Seahawks, New England Patriots	49.7 National 114.5 million

3.3 FNET Observations and Analysis of Power System Frequency

The analysis work in this study has paid particular attention to monitored power system frequency variations during the previous Super Bowl games. The FNET database has stored information of power grid performance since 2003. In the FNET system, the IMS is continuously analyzing the incoming frequency data. Once the rates of frequency change in several FDRs exceed an empirical threshold, a power system event is declared. Typical event types are frequency rise, frequency drop and oscillation. Then, the frequency deviation of the disturbance is converted into the equivalent active power amount by using the empirical coefficient β [17]. This estimation has proven accurate after verifying with many confirmed EI system events.

3.3.1 *Observation 1: high density of frequency events during broadcasting period*

Large numbers of frequency disturbances were detected during the game time. These events all involved hundreds of megawatts of power system variation. The FNET event

trigger is set at 400 MW. Figure 3-1 shows the histogram of daily triggered event numbers for the EI system. Typically, the EI has no more than 4 events per day. No four-hour period in the recorded events experiences as many events as there are during the Super Bowl. It is evidence that the high density of power system events during this time is tied to the behavior of the large number of people watching the game.

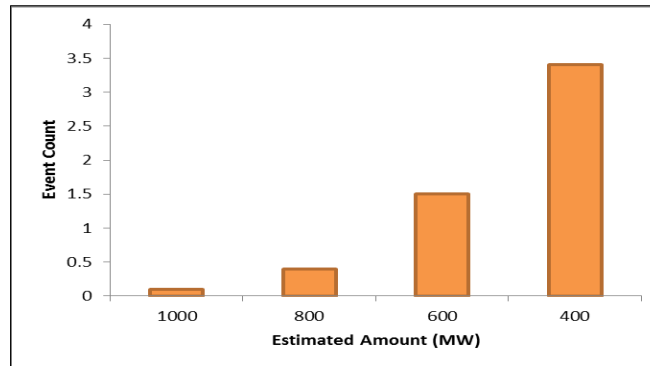


Figure 3-1 EI daily events histogram

The numbers of triggered events with magnitudes higher than 400 MW during previous four Super Bowl games are demonstrated in Figure 3-2 with their corresponding active power changes in MW. The events with magnitudes lower than 400 MW are considered as minor events, and are not included in the study.

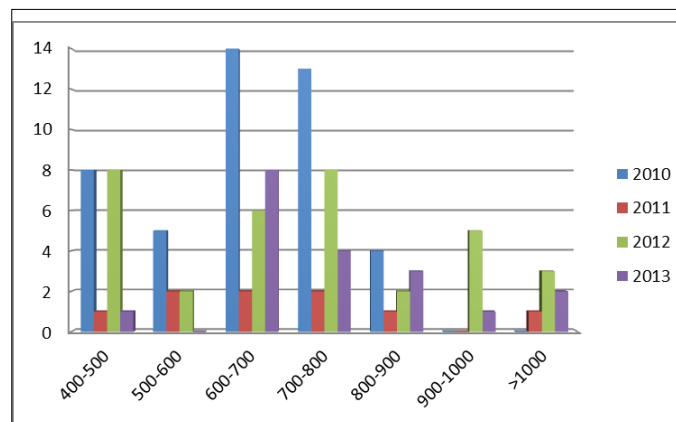


Figure 3-2 Super Bowl events histogram

3.3.2 *Observation 2: Frequency events tend to happen during commercial breaks*

It is elaborated in an online survey in reference [2] that during regular commercial breaks, the viewers are more likely to engage in other activities besides watching TV, such as using the restroom, getting food or beverages from the refrigerator, using a computer, stove, microwave, clothes dryer and washer, and other home appliances. Most of these activities involve the use of electricity. The increasing energy consumption explains why multiple grid frequency events occurred during the commercials. Figure 3-3 shows the distribution of FNET triggered frequency events for Super Bowl XLVI and XLVII.

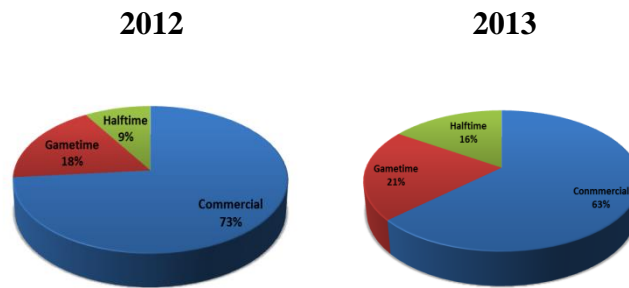


Figure 3-3 Frequency events occurrence distribution for Super Bowl XLVI, 2012 and XLVII, 2013

Consider that, on average, over 110 million people watch these games. Assume the power of the home electrical appliance is around 500 W. If only 1% of viewers use an appliance, the load level would increase by 550 MW. This has a measurable impact on the power system frequency.

3.3.3 *Observation 3: large frequency fluctuation during halftime show*

The general impact on the system is relatively larger during halftime show due to the longer period of break time and the increase of viewership, according to Nielson Company [5]. Figure 3-4 shows a 30 minutes frequency plot during the halftime show of Super Bowl XLVII, while Figure 3-5 plots the same 30 minutes time window frequency for an ordinary Sunday evening in late January.

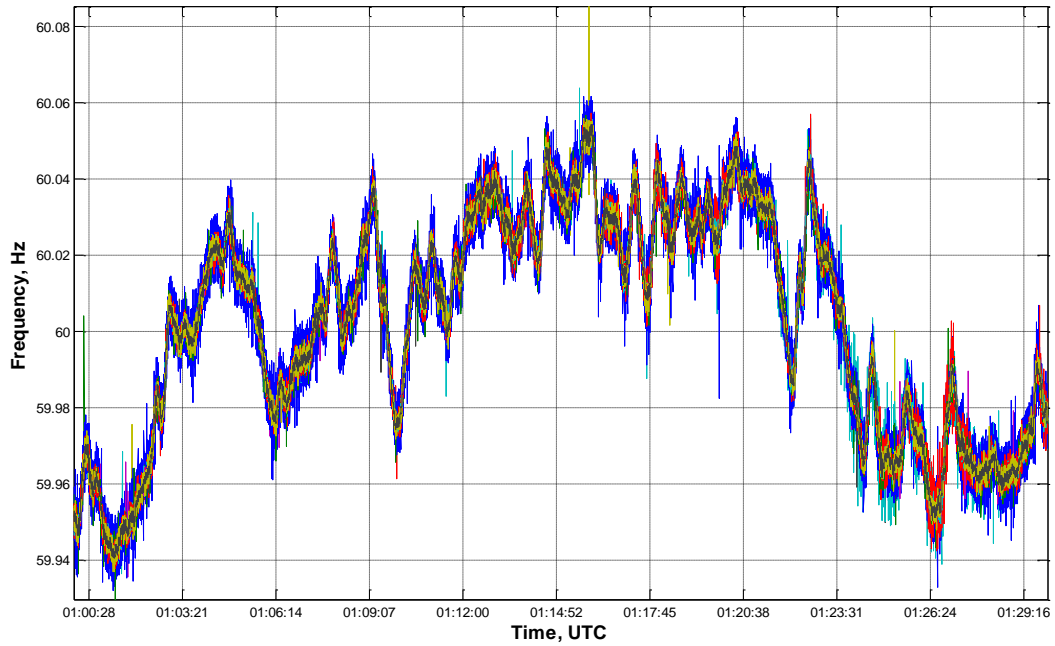


Figure 3-4 30 minutes frequency plot during halftime show on Super Bowl XLVII

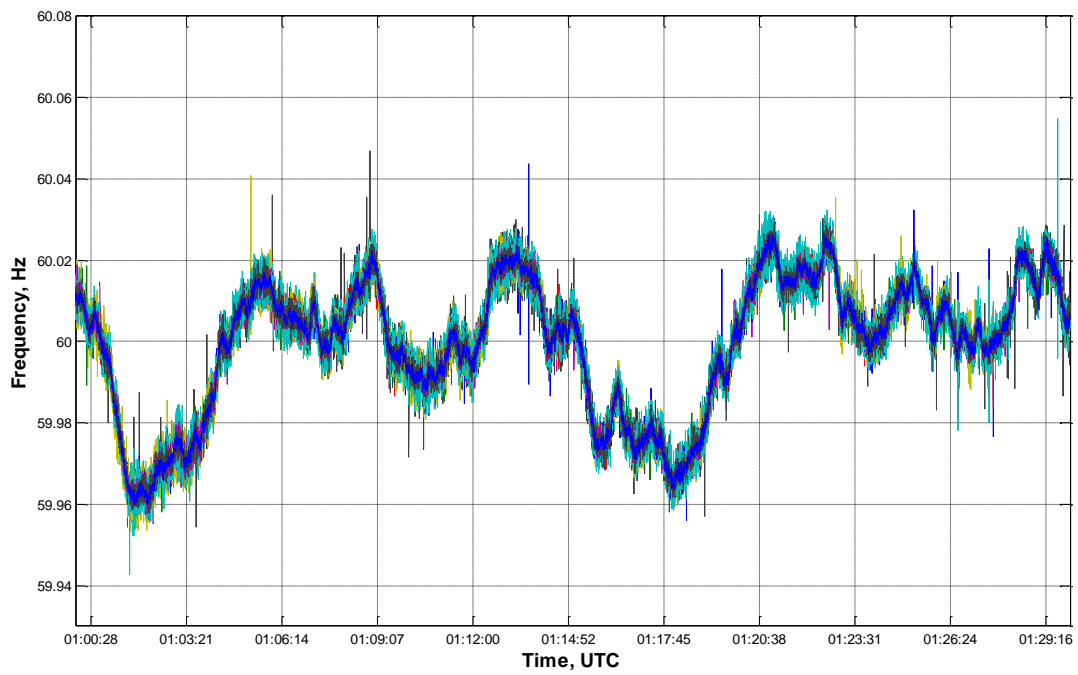


Figure 3-5 30 minutes frequency plot on an ordinary Sunday Evening

By comparison, we can clearly see that, the frequency experienced more fluctuation during Super Bowl halftime show time, a good quantity of sharp frequency rise and drop can be observed from the plot, which have strong relationship with human activities on that time period.

3.3.4 *Observation 4: Sharp drop of frequency at the beginning of halftime show*

The frequency response is tightly associated with the individual game progress and audience activities, so there is no uniform pattern that can be observed from year to year. However, there are some characteristics common to all Super Bowl games. For example, the power system frequency drops dramatically during the halftime break and increases once the third quarter begins. Figure 3-6 to Figure 3-9 shows the halftime break frequency data from the last four Super Bowl games. There were sharp frequency drops at the beginning of each halftime shows, the slope of the frequency drop is marked with a black line. It also seems reasonable that the audience would participate in other activities right after the halftime break, which would explain the drastic increases in electricity consumption and the resulting frequency drops.

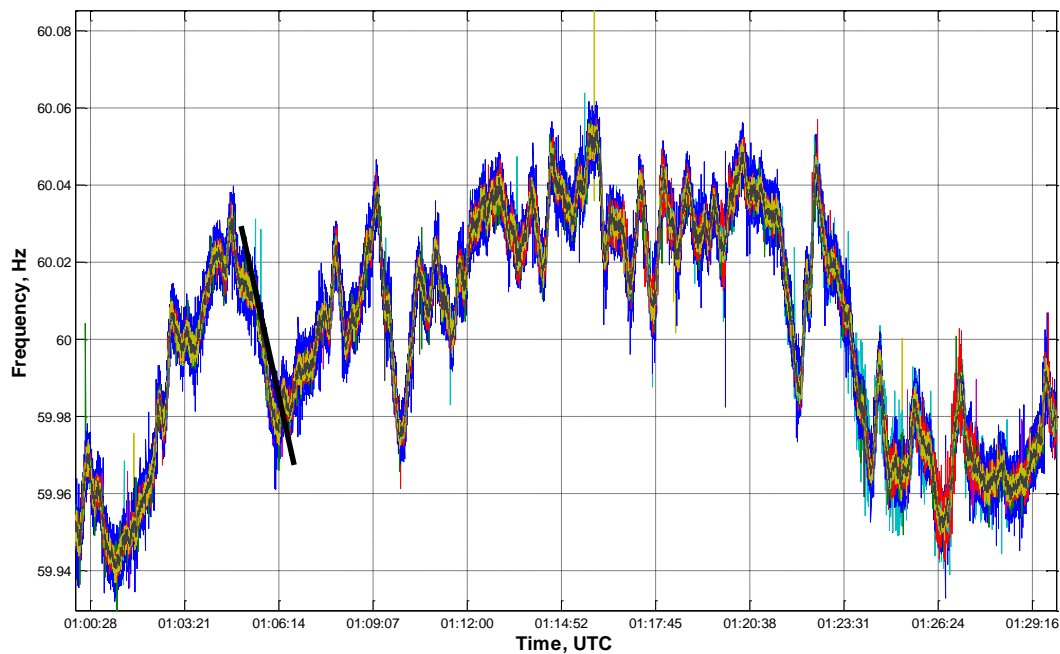


Figure 3-6 Halftime 30 minutes plot for Super Bowl XLVII, 2013

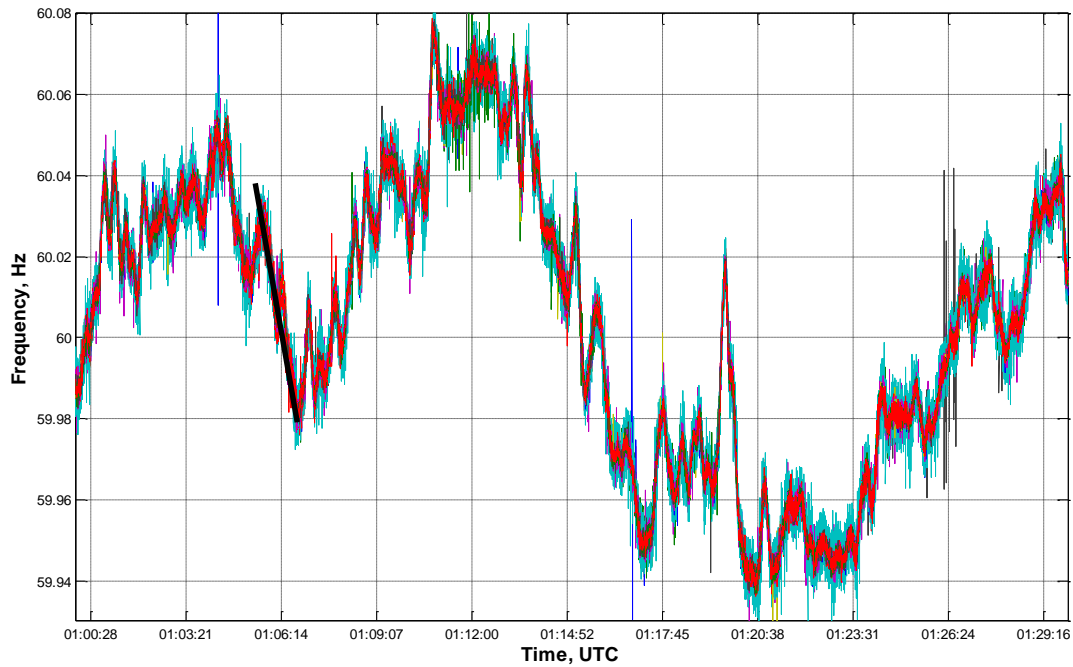


Figure 3-7 Halftime 30 minutes plot for Super Bowl XLVI, 2012

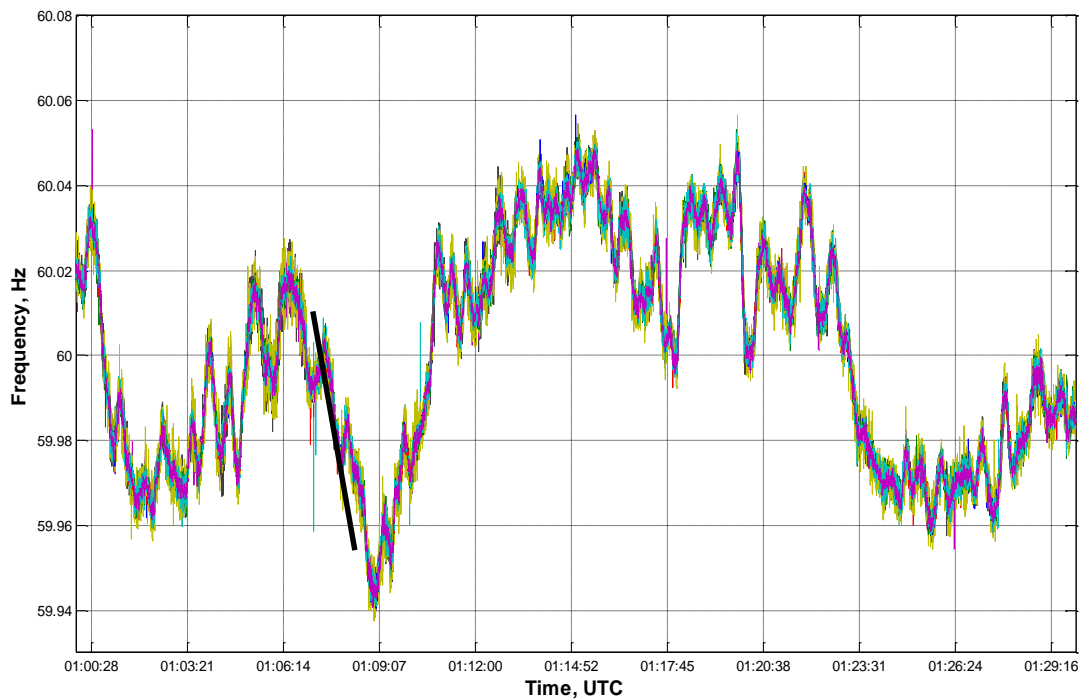


Figure 3-8 Halftime 30 minutes plot for Super Bowl XLV, 2011

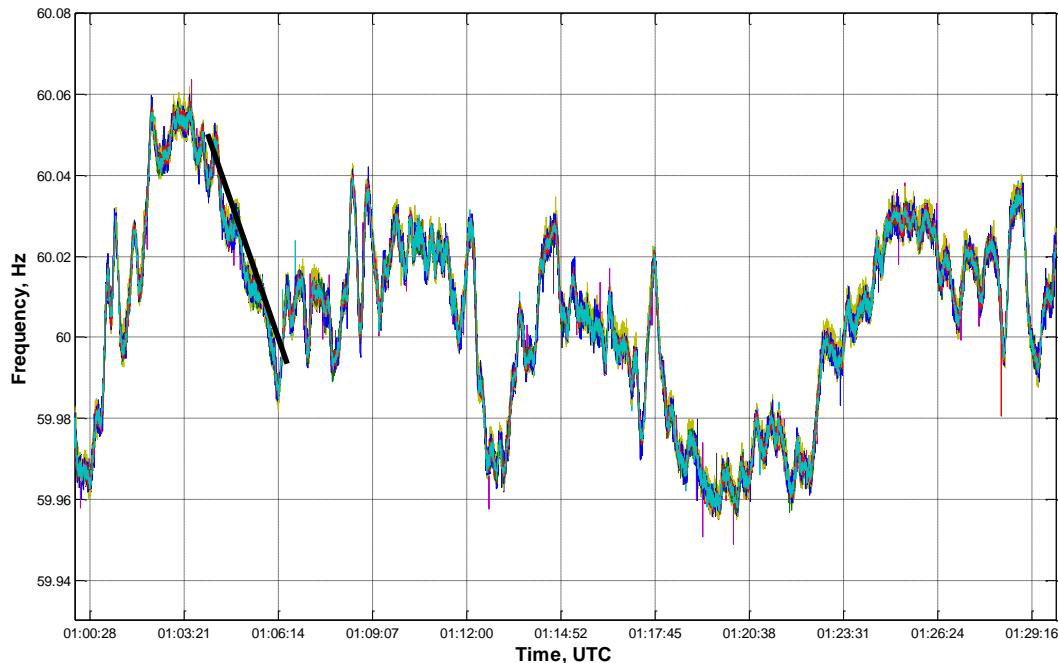


Figure 3-9 Halftime 30 minutes plot for Super Bowl XLV, 2011

3.3.5 *Observation 5: All US interconnections tend to oscillate together during large frequency disturbances*

The frequency event can also be observed in the West Electricity Coordinating Council (WECC) and Electric Reliability Council of Texas (ERCOT) Interconnection at the same time. Figure 3-10 shows the 30 minute frequency measurements of all three interconnections during halftime show on Super Bowl XLVII 2013, red frames show frequency swings observed at the same time. It can be seen that the impacts of nationwide events are also reflected in interconnections other than EI. Figure 3-11 shows the plots for an ordinary Sunday evening frequency in all three interconnections. We do not observe any consistency in these plots. These observations are also true for shorter time window events. As is shown in Figure.3-12, an EI triggered event can also be detected in WECC and ERCOT. Meanwhile, Figure 3-13 is a similar amount event trigger by FNET on non-Super Bowl time, we can see from this figure that the three interconnections do not always swing together during system events.

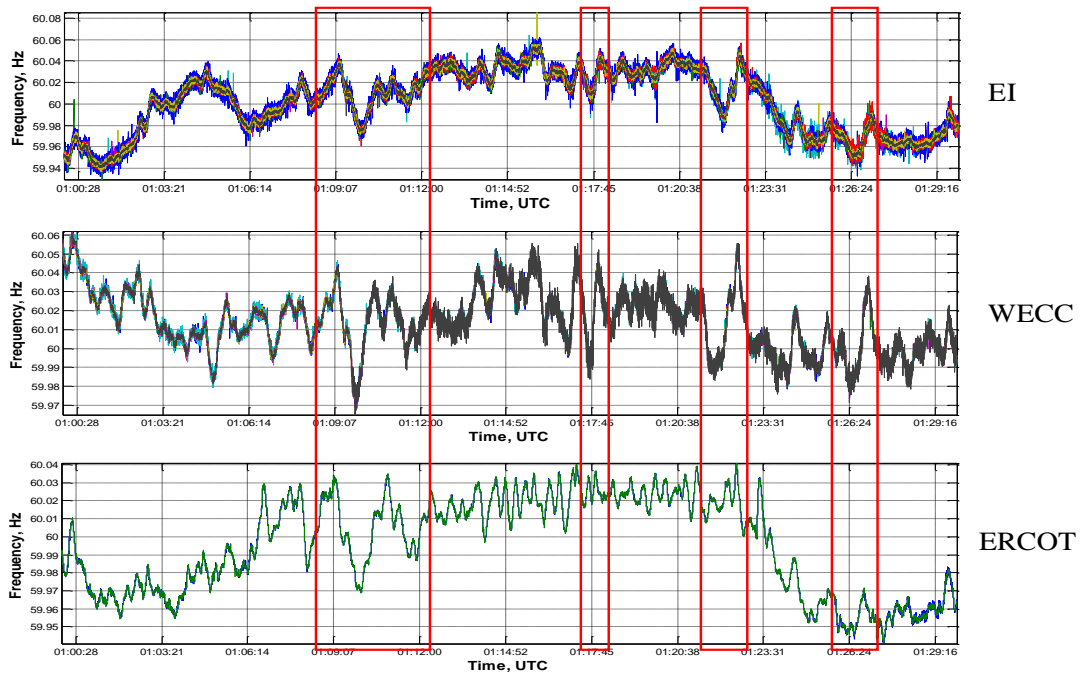


Figure 3-10 Different interconnections frequency swings during halftime 2013

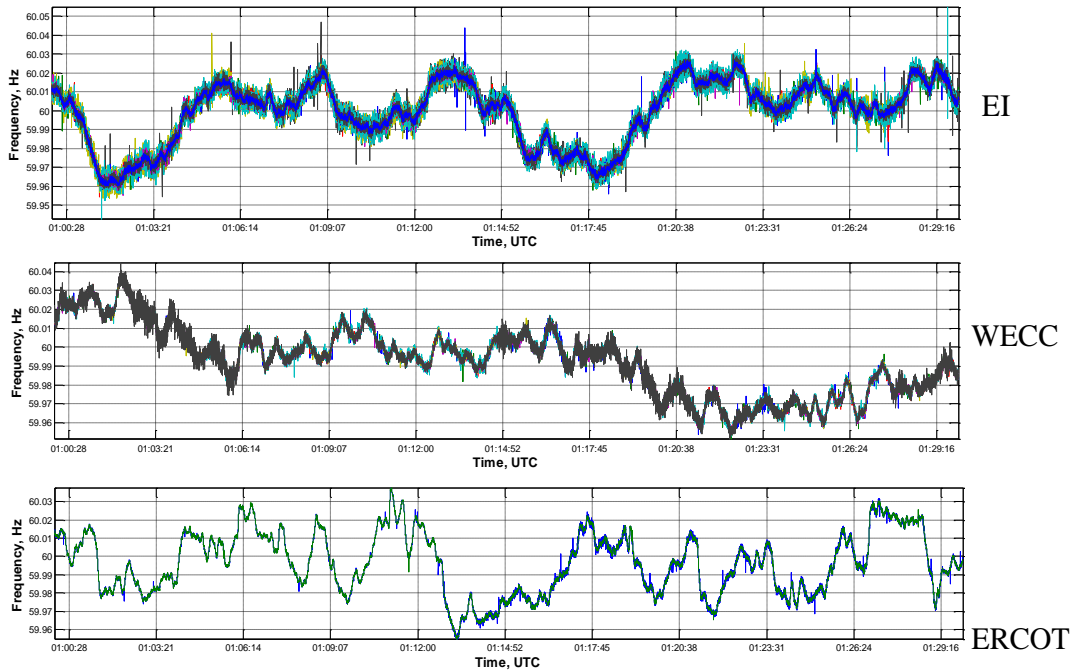


Figure 3-11 Different interconnections frequency swings on an ordinary Sunday evening

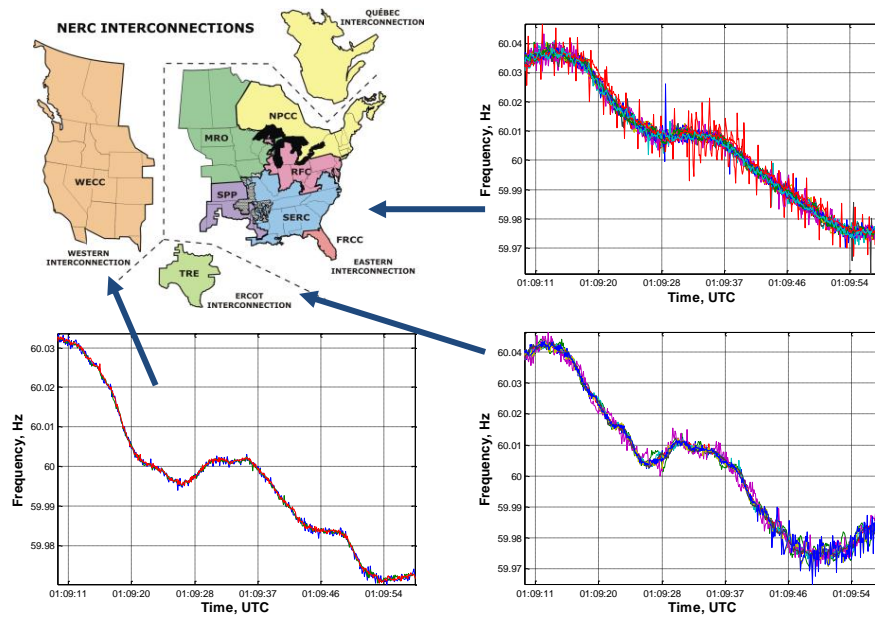


Figure 3-12 NERC interconnections frequency swings during Super Bowl XLVII
 [Image Courtesy of NERC] [18]

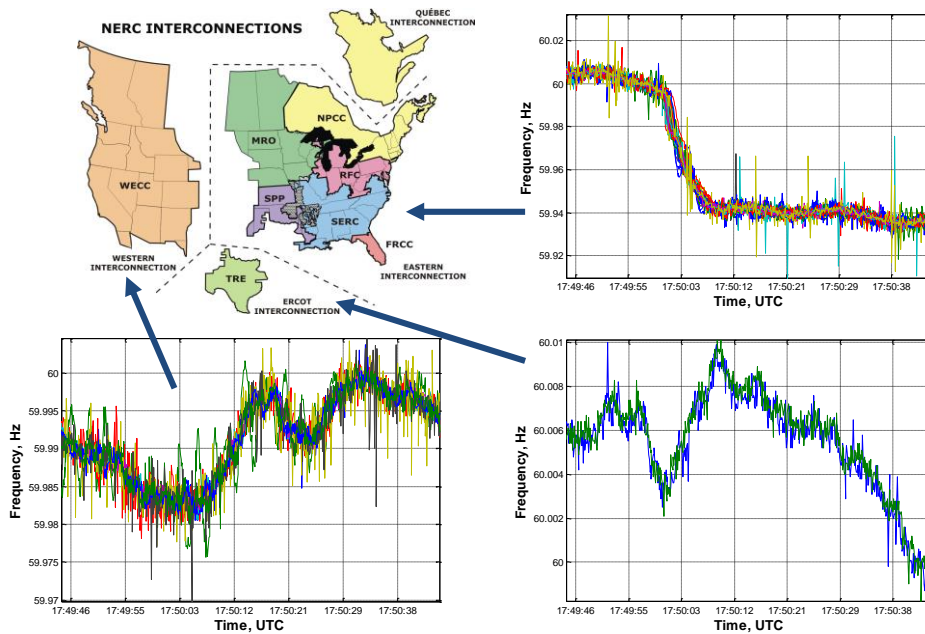


Figure 3-13 NERC interconnections frequency swings during random event
 [Image Courtesy of NERC] [18]

3.4 Conclusions

The statistical information of power system frequency behavior is investigated based on the real wide-area measurements taken in FNET from Super Bowl XLIV, 2010 to Super Bowl XLIX, 2015. It is apparent that large groups of people engaging in the same event at roughly the same time can have significant impacts on the power grid frequency. One common characteristic drawn from the system frequency recordings is the dramatic frequency drop during the halftime breaks. The relatively longer commercial and entertainment broadcasting time allows people to participate in other electric energy-related activities; hence, the introduction of greater frequency variability during this time.

Comparison of the Super Bowl data with non-game day data shows that there are far more power system events occurring in the former case. And most of the events occurred during the commercial breaks. Clearly, the impacts of the Super Bowl on power grid frequency in this work provide valuable information regarding the system dynamics of such popular events. The accumulation and statistical analysis of the FNET frequency data present an incisive point of view on the power grid frequency behavior during such events.

Understanding the relationship between large-scale societal events and power frequency has important implications for power system. With the development of smart grid technology, similar large-scale, synchronous activities would be observed. Individual consumers may decide to switch on their home electrical appliances when the electricity price is low. Such activities would have notable impact on the system frequency similar to the societal events discussed in this work. It is evident that the societal effects could play a very significant role in future smart grid implementation. The observations in this work will also provide valuable information in the study of responsive loads for power grid frequency regulation.

Chapter 4 WIND FREQUENCY CONTROL UNDER HIGH WIND PENETRATION ON AN NPCC SYSTEM MODEL

4.1 Background

Wind generation will play an important role in the total generation mix in future power systems in order to meet the needs of environmental regulations. Due to the different structure and control strategy of a wind turbine, its performance is different from conventional machines. It is crucial to maintain the power system frequency in specified range so that the power system is reliable and secure [19]. For conventional machines, in the first few seconds after a disturbance, the frequency dynamics are dominated by the inertial response of the on-line generation. Synchronous machines inherently contribute some of its stored inertial energy to the grid, reducing the frequency decline and allowing slower local governor actions to stabilize the system frequency [20]. However, most variable-speed wind generation does not exhibit this inertial response due to the lack of synchronization torque. Without special controls, the wind power plant does not participate in primary frequency response either [21].

These issues address a need to let the wind generation provide adequate frequency control. Many researchers have proposed different designs to allow wind power plants to provide capabilities similar to system inertial control and primary frequency response [22]. The work reported here adopts the modern technology of power electronics. Though the steady-state active power delivered to the grid solely depends on the mechanical energy transferred from a wind turbine, the electric power of variable-speed wind generators can be effectively controlled by modern power electronics devices in a fast manner. As a result, wind generation has significant capabilities to engage in frequency regulation when wind penetration is considerably high.

The Northeast Power Coordinating Council (NPCC) region system used in this study lies within the U.S. Eastern Interconnection (EI) and occupies the greater New England region of North America, covering the States of Maine, Vermont, New Hampshire, Massachusetts, New York, Connecticut, Rhode Island, and the Provinces of Ontario, Québec, New Brunswick, Nova Scotia and Prince Edward Island. NPCC also

has ties to non-NERC systems in Northern Canada. In terms of load served, NPCC covers 20% of the Eastern interconnection's total load demand, and 70% of Canada's entire demand [23].

4.2 Model Development

The purpose of this study is to evaluate the wind impact on system inertial response, as well as to study the potential contribution of variable-speed wind generation to frequency regulation using the PSS/E dynamic simulation software. A 700 MW generation trip is simulated in all cases to demonstrate the frequency responses under different conditions.

4.2.1 Base Case without Wind

The baseline model of NPCC system used in this study is a reduced model with 140 buses, and 48 machines. The total capacity of NPCC system is about 28 GW. Figure 4-1 shows the one-line diagram, and Figure 4-2 indicates the NPCC system topology geographically.

The PSS/E format of NPCC model is formulated based on the data in the MATLAB Power System Toolbox. Power flow data were formatted into PSS/E raw file directly. However, the dynamic data were formatted with some changes in order to meet the requirements of the reasonable relations among transient reactance and time constants of GENROU type generators. In addition, in order to make the system more realistic, a generic governor model was also added. The steps for adding the TGOV1 type of governor models into the NPCC system are described as follows:

1. Convert machine Mbase to 1.1 times its dispatch power, and change all generator reactance, machine inertia, machine damping constant correspondingly.
2. Add governor model, and decrease machine damping constant to match the response.
3. Tune governor droop (3%) to match EI Beta.
4. Change machine damping constant to 0, and tune excitation gain to match the original system response.

System response for each step is shown in Figure 4-3.

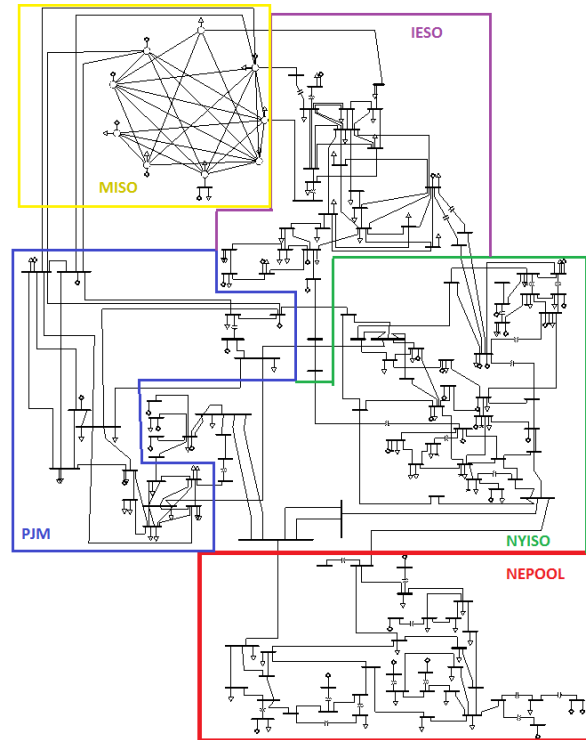


Figure 4-1 NPCC one-line diagram

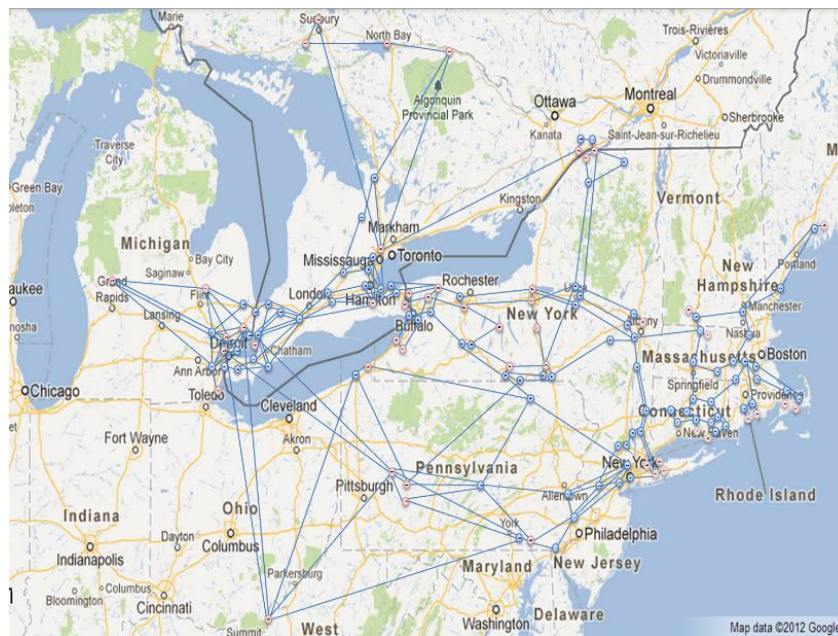


Figure 4-2 NPCC system topology

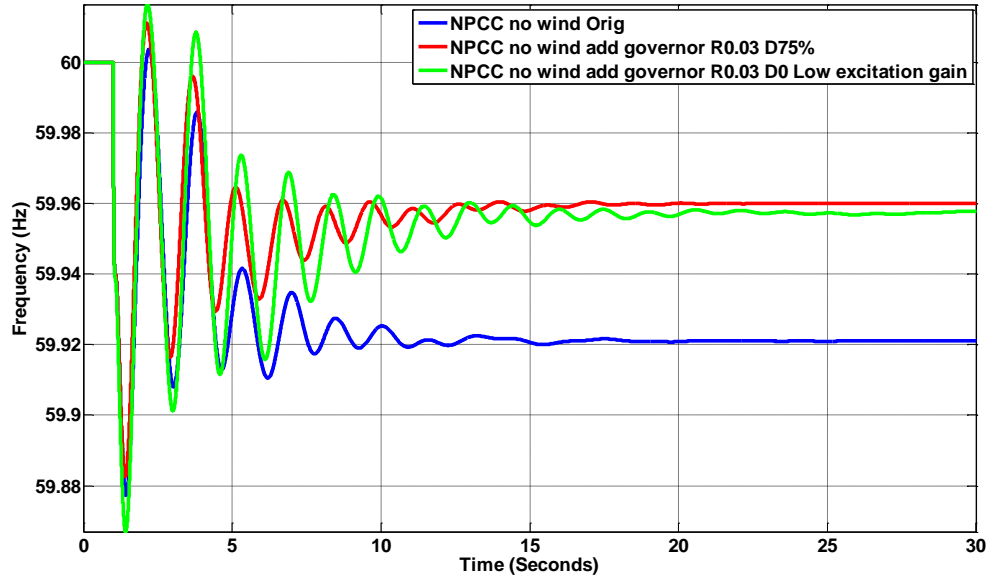


Figure 4-3 Base case tuning steps comparison

To verify the settle down frequency, the frequency deviation is calculated by Equation 4-1.

$$\Delta P = \sum \Delta f * S_{GENROU} / R + \sum \Delta f * D * S_{GENROU} + \sum \Delta f * D * S_{GENCLS} \quad 4-1$$

Where:

ΔP : generation active power deviation

Δf : frequency deviation

S_{GENROU} : complex power of each round rotor generator

S_{GENCLS} : complex power of each classic generator

R : governor droop

D : generator damping coefficient

Based on Equation 4-1, if a 700 MW generation is tripped, the frequency deviation should be around 0.04Hz, which matches the result shown in Figure 4-3. Figure 4-4 and 4-5 shows the system response to a 700MW generation trip in the base case.

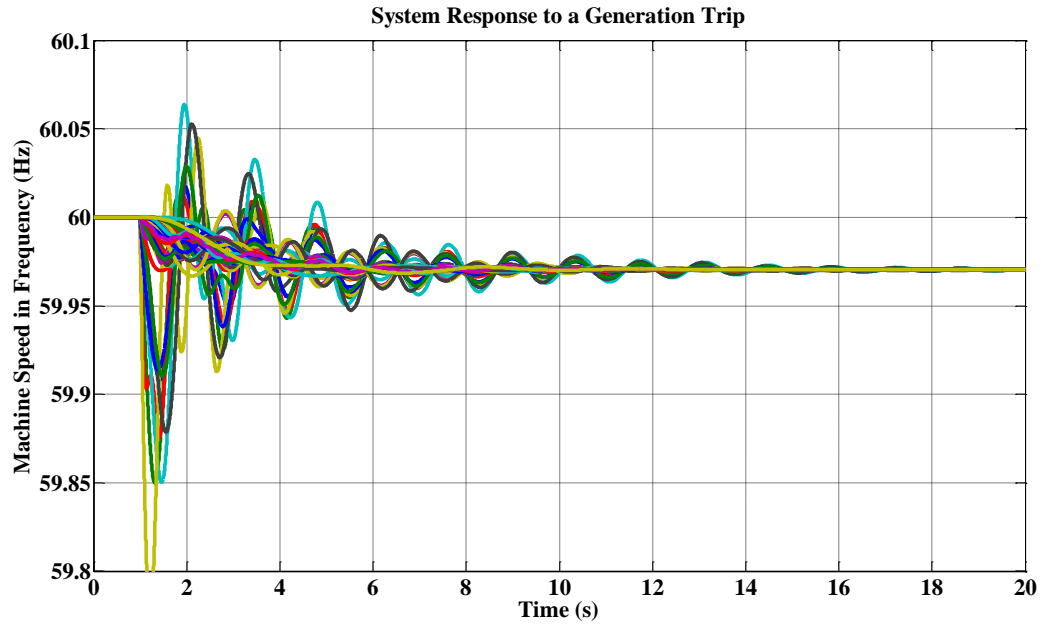


Figure 4-4 Machine speed deviation after a generation trip for base case

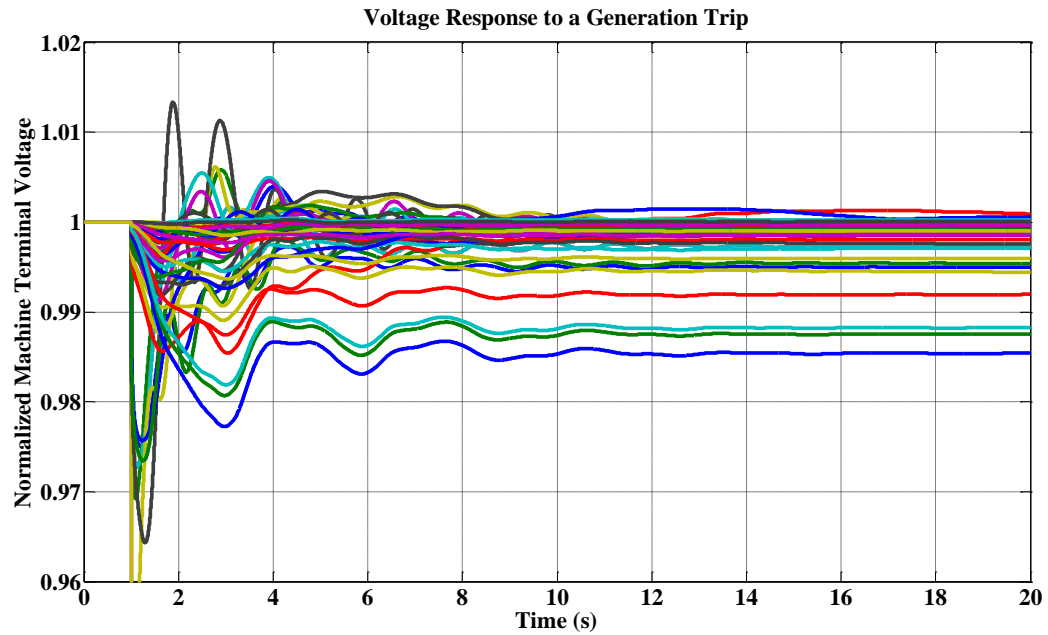


Figure 4-5 Machine terminal voltage after a generation trip for base case

4.2.2 Wind Case without Control

The typical WT3 wind turbine stability model in PSS/E is employed in this work to simulate the performance of a doubly fed induction generator (DFIG) with the active control by a power converter connected to the rotor terminals. There are four basic components for WT3 model (shown in Figure 4-6), namely:

- WT3G: generator/converter model
- WT3E: electrical control model
- WT3T: mechanical control (wind turbine) model
- WT3P: pitch control model.

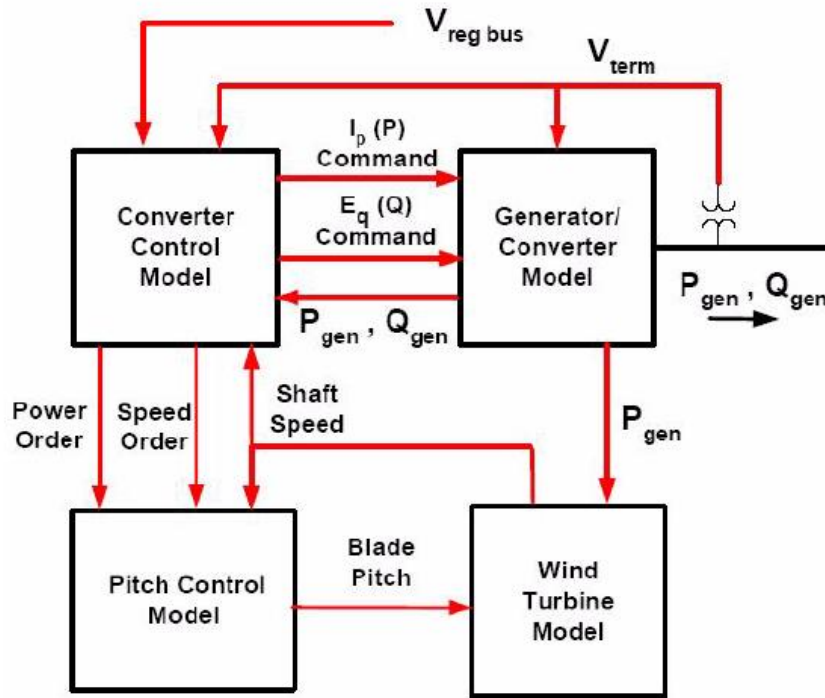


Figure 4-6 Structure of WT3 Wind Turbine Stability Model in PSS/E [24]

In the US, it is planned to increase wind penetration ratio to 20% by 2030 [31], so the 20% penetration level is chosen to be the first wind scenario. Please note that since pitch control and reactive power control are not considered in this study, WT3P part is ignored and

constant reactive power control mode is selected in all the simulations. Figure 4-7 indicates the wind farm locations for the 20% wind case. Locations are selected based on existing and planning wind farms.

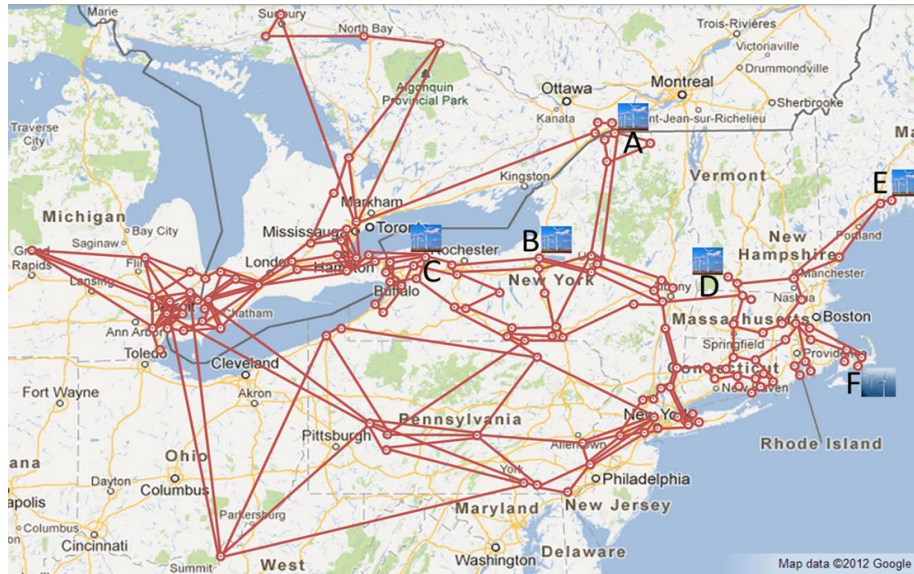


Figure 4-7 Wind farm locations for 20% wind case

An approach of replacing the existing conventional power plants with wind power plants is adopted, so that the modeling study does not address any issues to the transmission upgrades. The wind locations are chosen based on some current and potential wind farm locations in the detailed Eastern Interconnection 2030 model. Figure 4-8 and 4-9 shows the system response to a generation trip in the 20% wind case.

An extreme case of 100% renewable resources is then created to simulate the possible worst operation condition with the highest wind penetration level. Two hydro power plants involving five machines are retained in the system as there needs to be a synchronous reference in the system to ensure the simulation credibility in PSS/E, and all the rest generators are replaced by type 3 wind machines, which take about 90% of the total capacity. Figure 4-10 and 4-11 shows the system response to a generation trip in the 90% wind case.

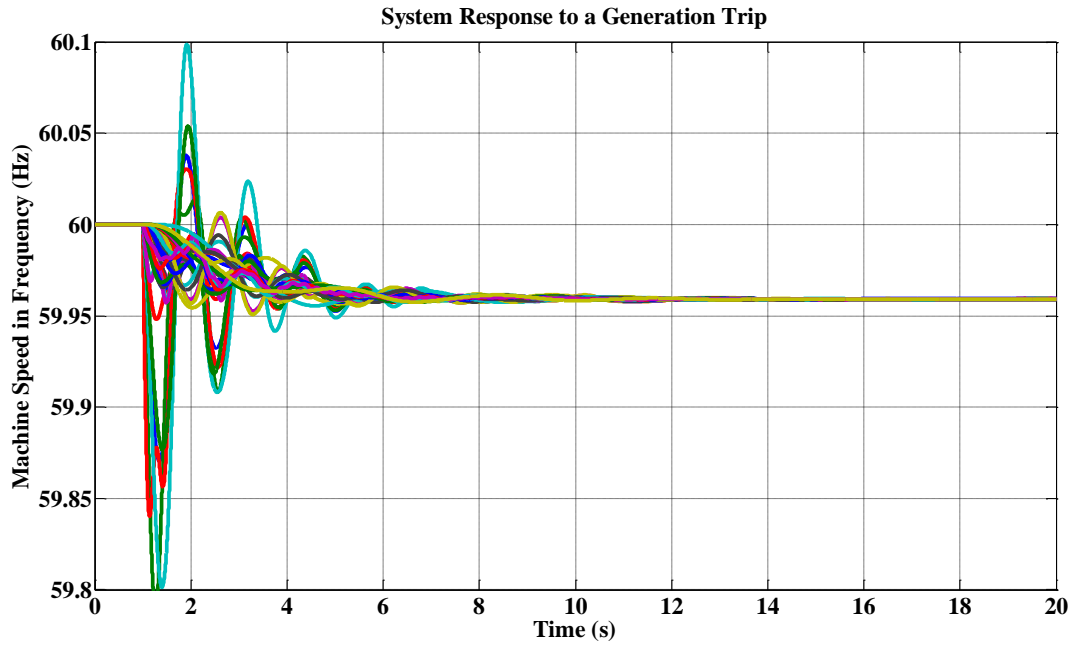


Figure 4-8 Machine speed deviation after a generation trip for 20% wind case without control

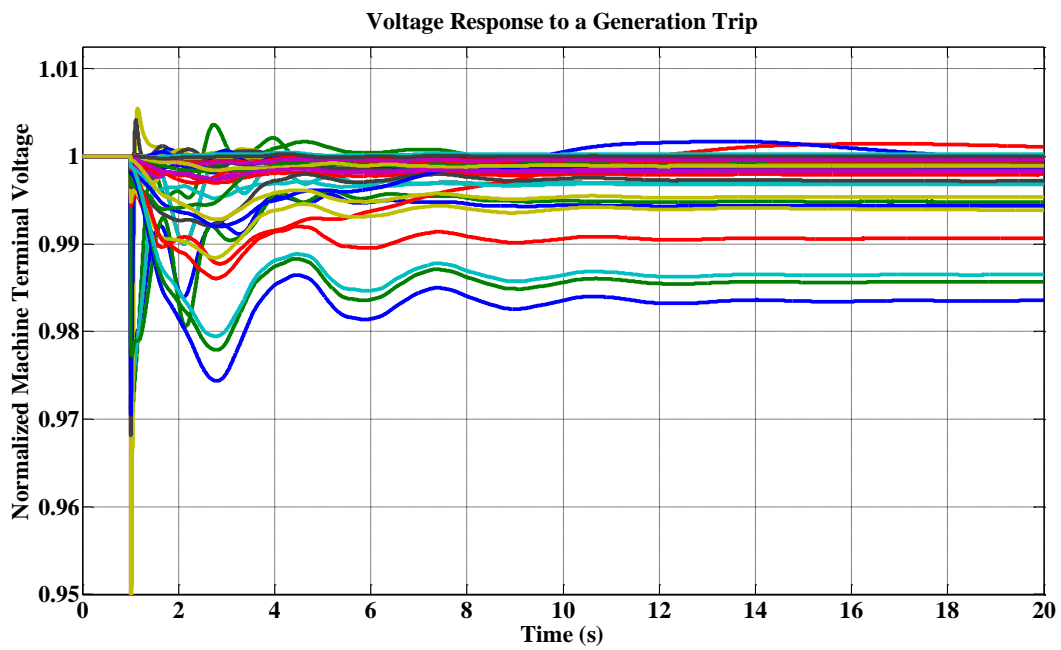


Figure 4-9 Machine terminal voltage after a generation trip for 20% wind case without control

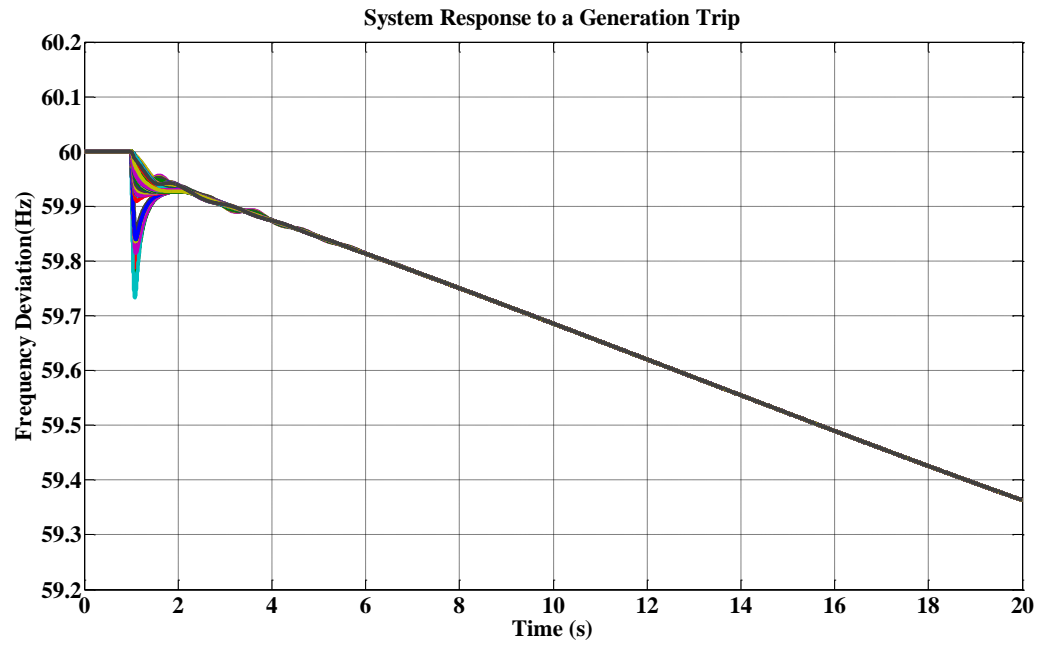


Figure 4-10 Frequency deviation after a generation trip for 90% wind case without control

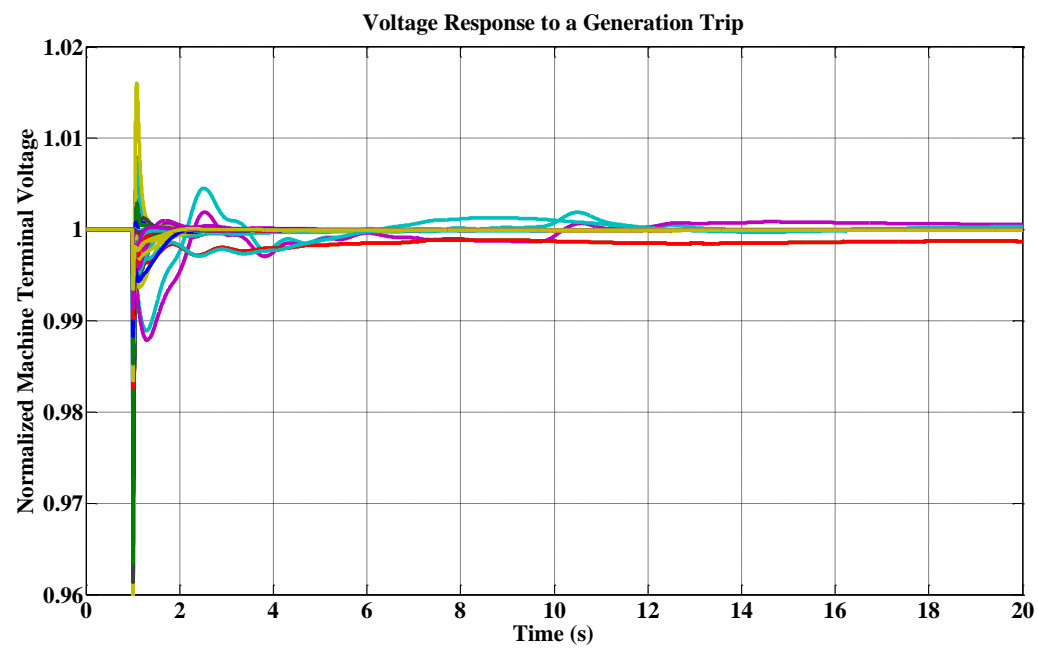


Figure 4-11 Machine terminal voltage after a generation trip for 90% wind case without control

As seen in Figure 4-10, the frequency decline is dramatic after the generation trip event, even lower than the under frequency load shedding (UFLS) trigger, as a result of losing a majority of system inertia and turbine governors.

4.2.3 Wind Case with Control

In order to allow variable-speed wind generation to engage in frequency regulation, several controllers are included in the user-written electrical control model, namely wind inertia control, and wind governor control.

A. Wind Inertia Control

Wind inertia control here is of the same philosophy as GE WindINERTIA™ technology, whose objective is to let wind generations provide inertia response. Droop control is employed to produce temporary active power output change which is proportional to the frequency deviation and given by

$$\Delta f = f_{msr} - f_{ref}$$

where f_{msr} is the measured system frequency and f_{ref} is the reference frequency. The structure of wind inertia control is shown in Figure 4-12.

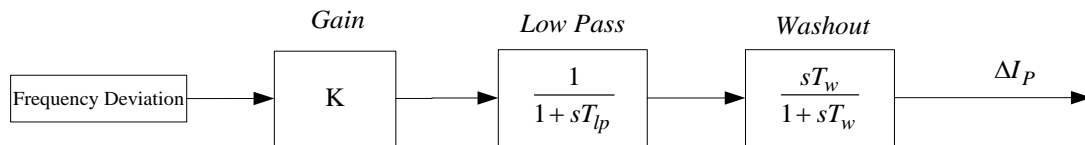


Figure 4-12 Wind Inertia Control Structure

B. Wind Governor Control

If working in over-speeding zone, wind turbines could decrease their rotational speed to release the reserve in seconds. Therefore, the “governor response” could be achieved on wind generation utilizing reserve. Again, droop control is used and the control structure is shown in Figure 4-13.

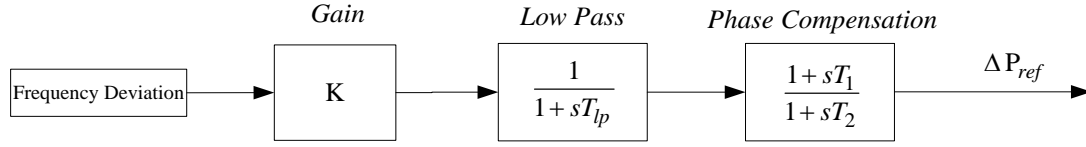


Figure 4-13 Wind Governor Control Structure

In the 20% wind case, two of the standard wind electric control models are replaced by a user-written model. Figure 4-14 and 4-15 shows the system response with wind controls in the 20% wind case, while Figure 4-16 and 4-17 shows the system response with wind controls in 90% wind case, in which 6 electric control models are implemented in each area respectively. The simulations results will be compared and discussed in the later section.

4.3 Simulation Results Comparison

4.3.1 Wind Impact of System Inertial Responses

Inertia frequency response is defined as “The power delivered by the Interconnection in response to any change in frequency due to the rotating mass of machines synchronously connected to the bulk power system, including both load and generation”[25]. As is shown in Figure 4-18, both the frequency nadir and the transition time between the beginning of the disturbance and the frequency nadir are decreased with higher penetration of wind generation. It is clear that wind penetration caused the system to lose inertial response.

4.3.1 Wind Frequency Control

As shown in Figure 4-19 to Figure 4-22, if only with inertia control, the wind generator increases its active power temporally in several seconds following the disturbance using the kinetic energy stored in the wind blades. Apparently, this control can help reduce the frequency drop nadir. If only with the wind governor control, the wind generation would ramp up and the active power output increases proportional to the frequency deviation, which is typical “governor response”. With both the wind inertia and governor control, the frequency nadir will be reduced further and the steady state frequency also decreases.

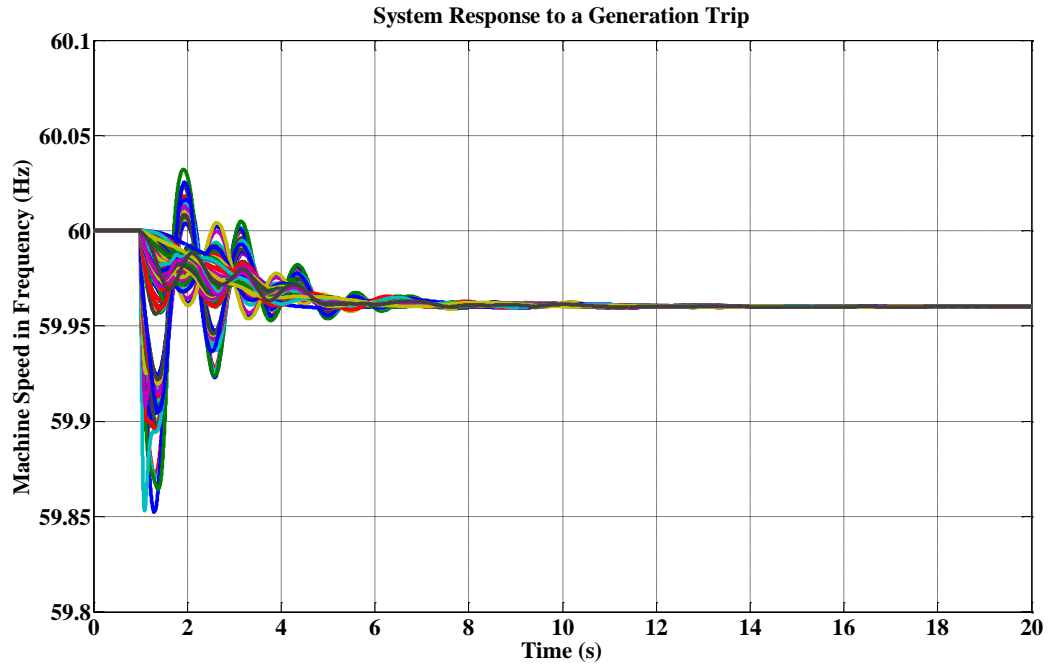


Figure 4-14 Machine speed deviation after a generation trip for 20% wind case with control

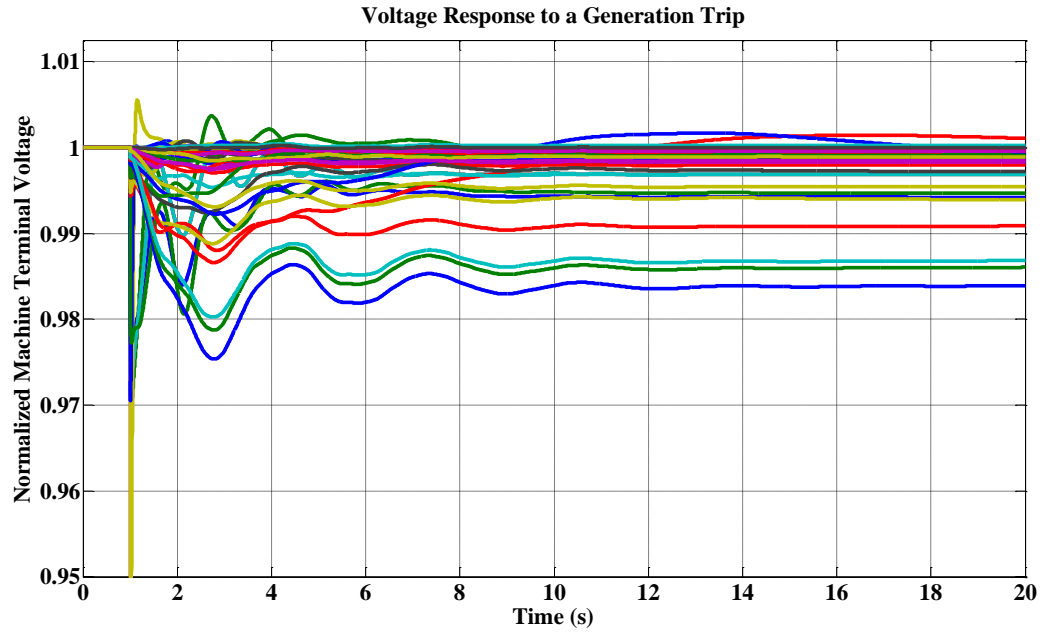


Figure 4-15 Machine terminal voltage after a generation trip for 20% wind case with control

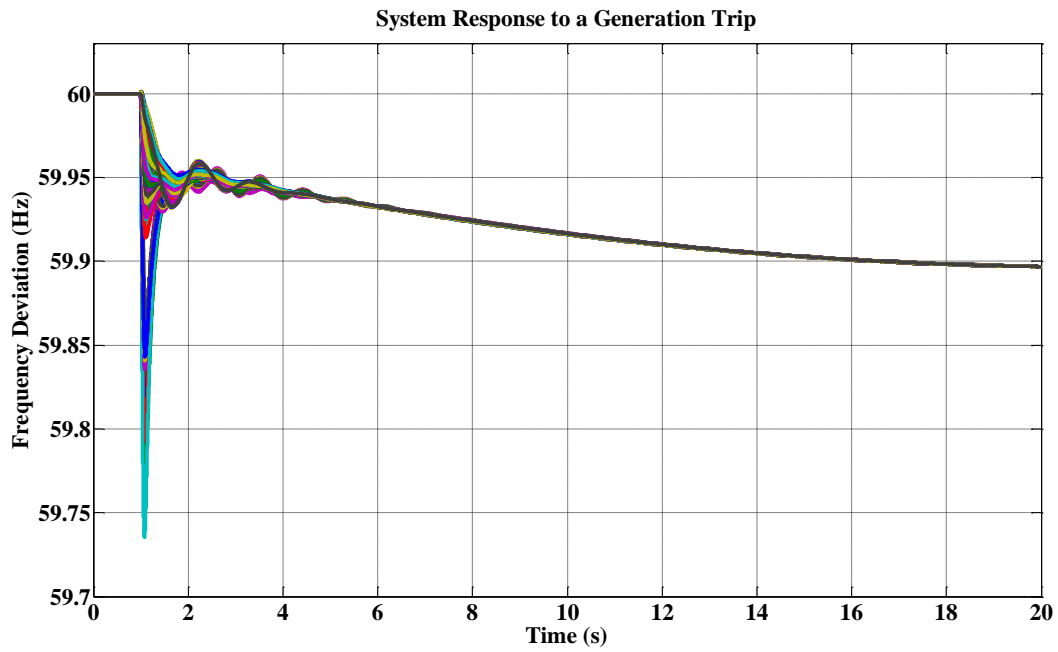


Figure 4-16 Machine speed deviation after a generation trip for 90% wind case with control

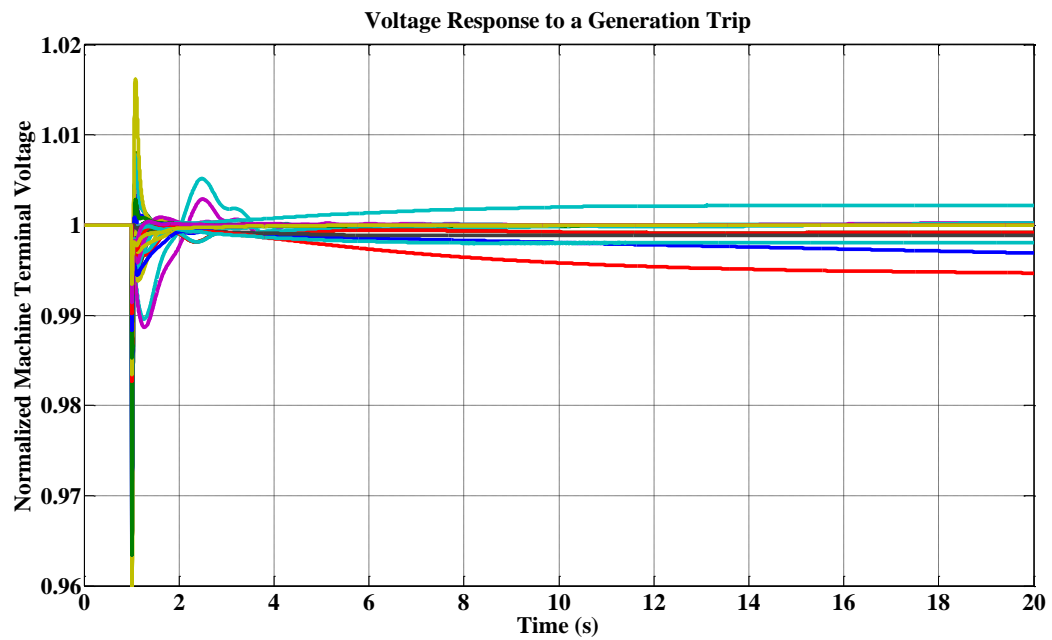


Figure 4-17 Machine terminal voltage after a generation trip for 90% wind case with control

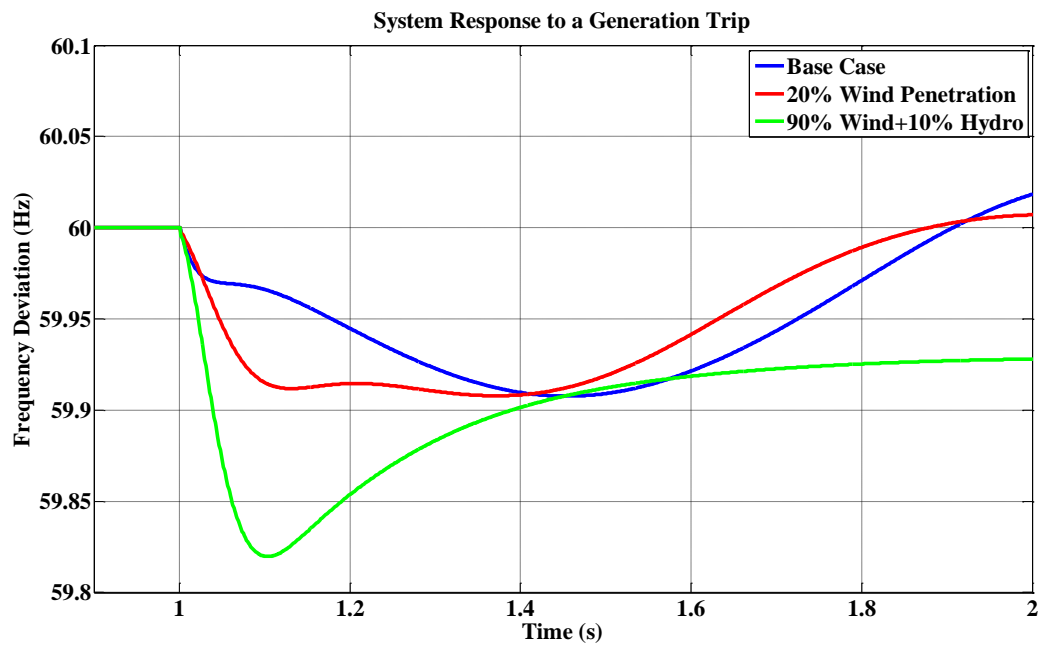


Figure 4-18 Frequency deviation after a generation trip under different wind penetration levels

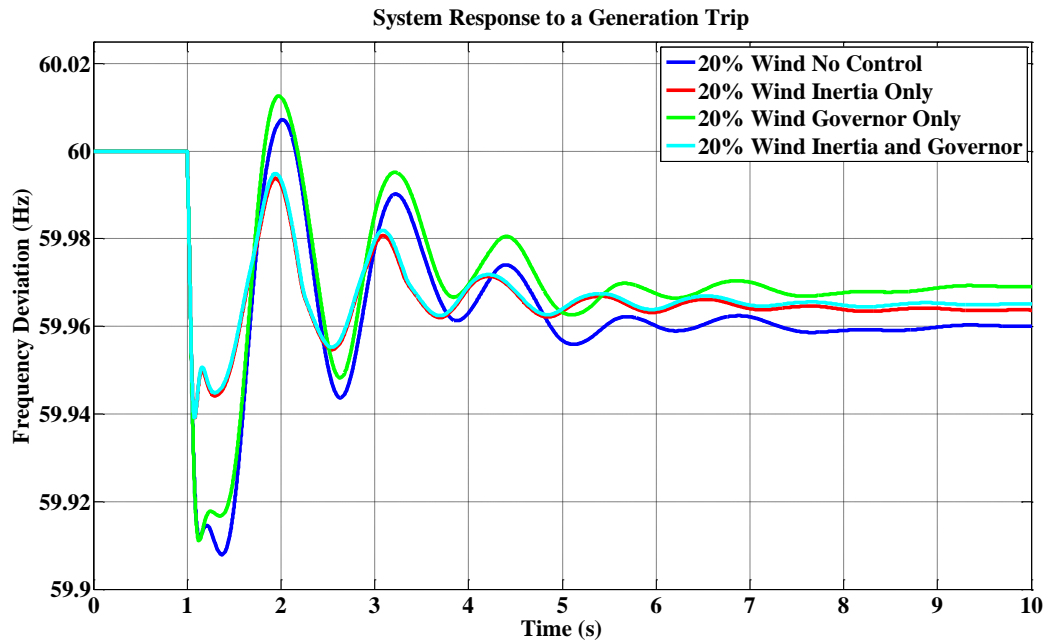


Figure 4-19 Frequency deviation after a generation trip for 20% wind case with different controls

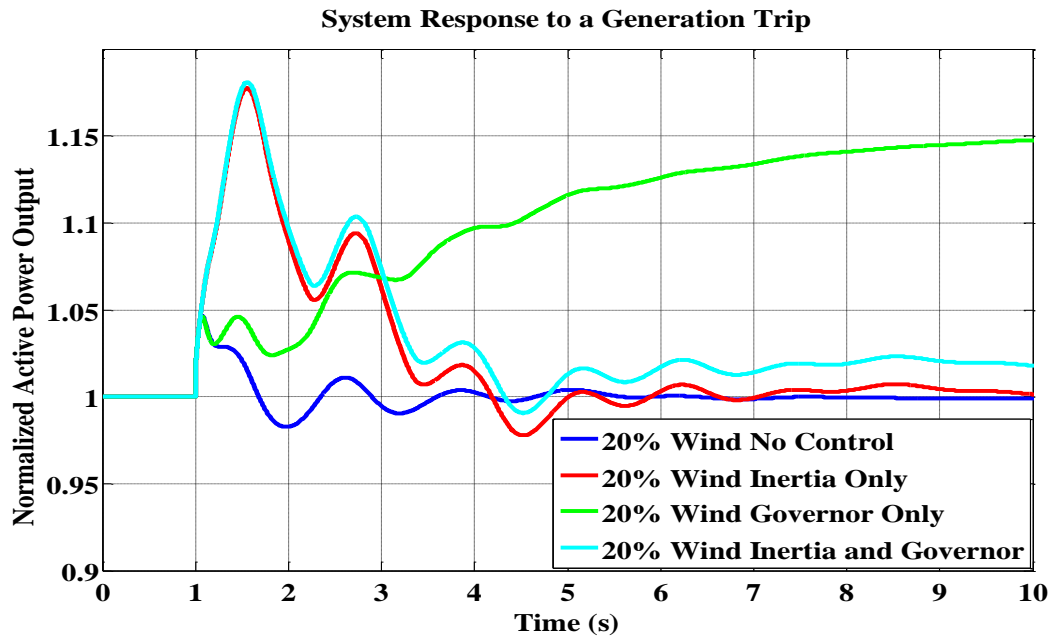


Figure 4-20 Active power output after a generation trip for 20% wind case with different controls

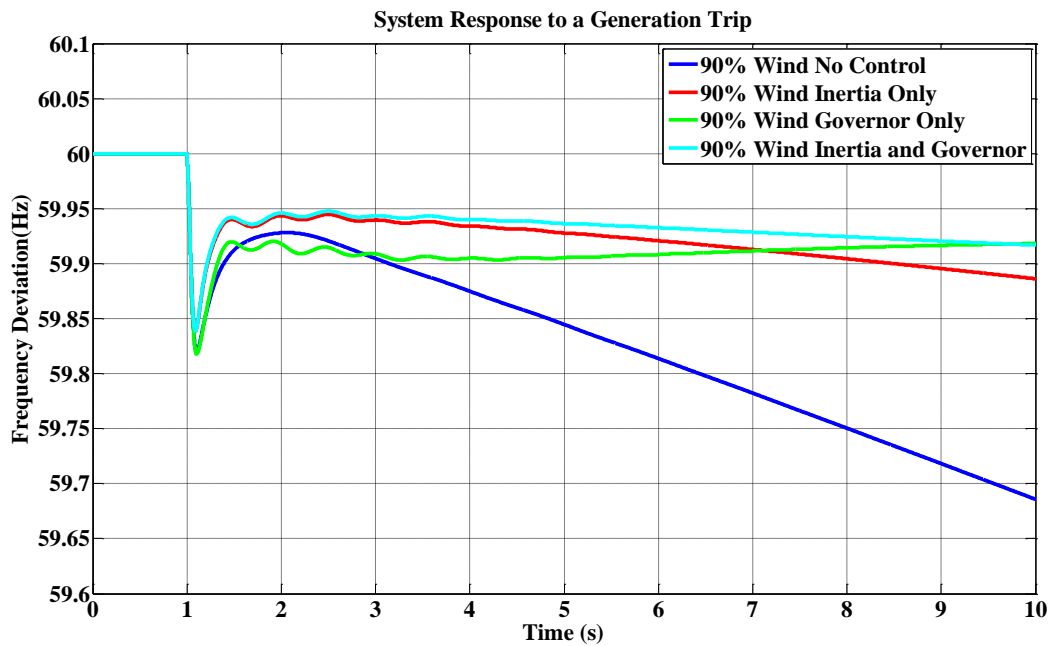


Figure 4-21 Frequency deviation after a generation trip for 90% wind case with different controls

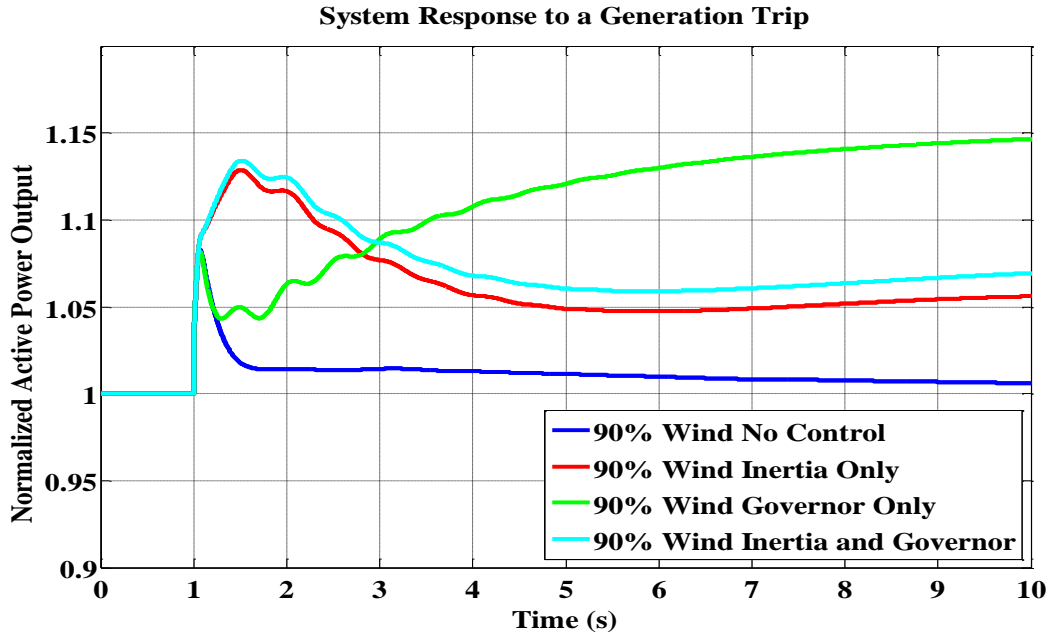


Figure 4-22 Active power output after a generation trip for 90% wind case with different controls

Fig. 4-19 and 4-20 shows the frequency deviation and active power output of the 20% wind penetration level. In this case, as the conventional generators and their governor response are still dominant in the system, the settling frequency after the disturbance is not changed significantly. However, in the 90% wind case, the wind control can bring the frequency back to steady state without triggering the UFLS.

4.4 Conclusion

In this chapter, several simulation cases of the NPCC system are developed to investigate the high wind penetration impact to NPCC system. A PSS/E user-defined electric control model was employed to implement fast active power controls, including wind inertia control and wind governor control. As demonstrated by the simulation results comparison, wind generation penetration decreases the system inertia significantly. And the wind generation effectively contributes to the frequency regulation. The simulation results provide insight in designing and operating wind generation active power control to an interconnected power system. Moreover, considering the fact that may bulk power system

around the world may have similar high wind penetration profiles, the control strategies discussed in this work holds great potential.

Chapter 5 VSC-HVDC MODEL DEVELOPMENT

5.1 Background

Since the first commercial High Voltage Direct Current (HVDC) link in the world was built in 1954, to transfer 20 MW electric power under 100 kV direct voltage from mainland Sweden to the Gotland [26], HVDC technology has been developed dramatically over the past several decades. The ratings of HVDC projects have been gradually increased to 7200 MW with direct voltage ± 800 kV in the Xiangjiaba-Shanghai HVDC project in China [27]. These projects were all using Current Source Converter based HVDC (CSC-HVDC) technology which adopt thyristor as switching devices in the converter. Since 1990s, a new type of HVDC technology, mainly using Insulated Gate Bipolar Transistor (IGBT), has been developed. It is called Voltage Source Converter based HVDC (VSC-HVDC). The first VSC-HVDC commercial project was put into operation also in Gotland, Sweden, in 1999 [28]. Many VSC-HVDC projects have been put into operation or are in planning for the near future. Generally, the CSC-HVDC has much larger power rating than VSC-HVDC, which makes it suitable for the high voltage bulk power transmission over long distance. Meanwhile, VSC-HVDC has advantages such as power flow control flexibility, fast response to disturbances and also capability of multi-terminal configuration, which makes VSC-HVDC a more attractive technology.

Most of the HVDC modeling are done in MATLAB Simulink, and switching models are constructed which make it computationally difficult for HVDC modeling in large power system. In order to study the impact of HVDC integration on large power system, it is necessary to have HVDC models representing all features in power system modeling tools. In this chapter, the available HVDC models in power system simulation tools are first investigated. Then a method of modeling multi-terminal VSC HVDC in Powertech Transient Stability Analysis Toolbox (TSAT) is discussed.

In PSS/E, there are CSC and VSC sourced model for two terminal and multi-terminals, as shown in Table 5-1. However, the multi-terminal VSC HVDC model, also called HVDC light model, is created by ABB and it's not public accessible.

Table 5-1 PSS/E convertor models

	Current Sourced Converter (LCC/CSC)	Voltage Sourced Converter (SCC/VSC)
Two-terminal	CDC4/CDC6/CDC7	VSCDCT
		HVDC PLUS
Multi-terminal	MTDC1T/MTDC3T	HVDC Light (ABB)

In PowerWorld, there is a MTDC model of pacific intertie, however, it's hard coded and all parameters are not subject to change. In TSAT, the VSC converter is modeled as shown in Figure 5-1. Therefore, it is possible to build a multi terminal VSC HVDC configuration under user defined model editor.

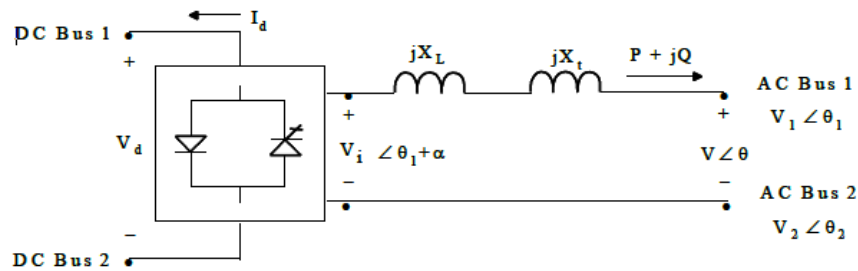


Figure 5-1 Voltage-Sourced Converter Model in TSAT[29]

5.2 Multi-terminal VSC HVDC Model Development

One common application of VSC HVDC transmission line is for wind energy integration, especially offshore wind. Based on the actual location of the first offshore wind farm Cape Wind in US, a traditional meshed topology for four-terminal HVDC is adopted to mimic the connection of offshore wind generation to main AC grid in NPCC system, as shown in Figure 5-2.

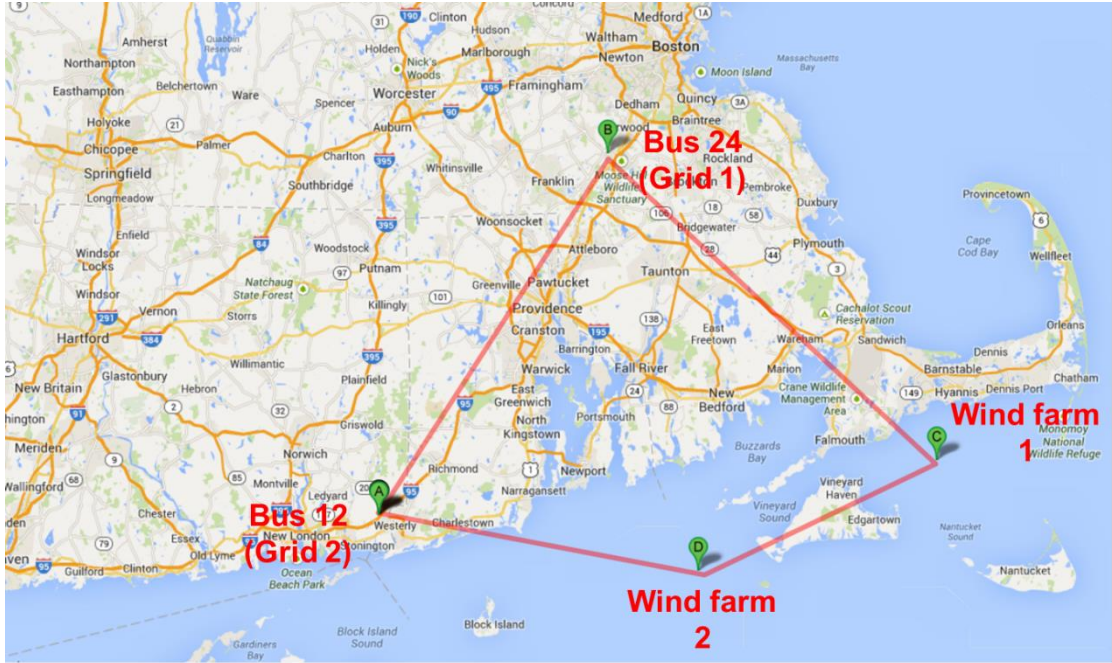


Figure 5-2 Four terminal VSC HVDC in NPCC system

5.2.1 Static Model

The static model of the proposed 4TDC system is built in PSAT (Powerflow and Short circuit Analysis Tool), as shown in Figure 5-3. Suitable parameters for VSCs are chosen in order to make both DC equations and AC power flows solved without any problem. The power flow benchmark with MATLAB 4TDC detail model is shown in Table 5-2.

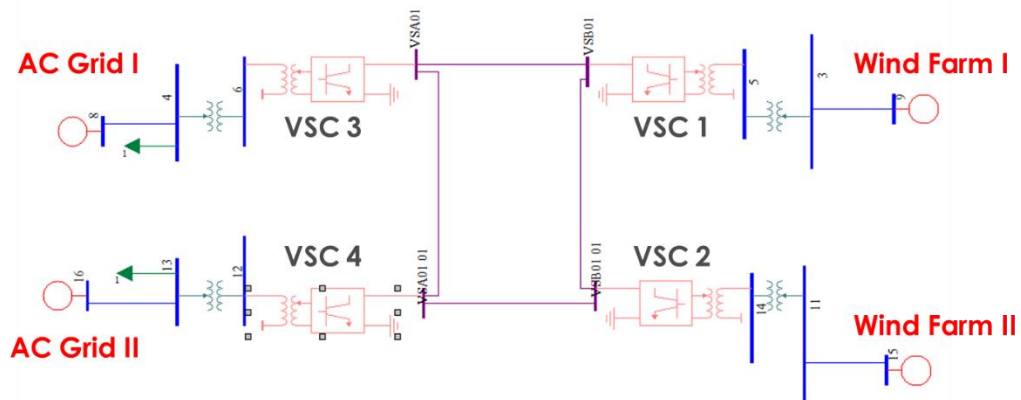


Figure 5-3 Static MTDC model in PSAT

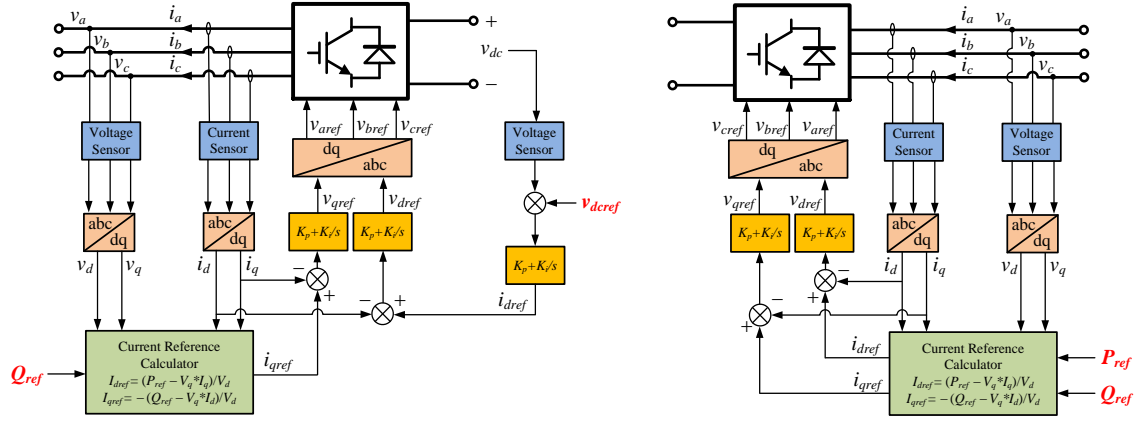
$$V_{dc3}=300\text{kV}, P_{dc1}=150\text{MW}, P_{dc2}=200\text{MW}, P_{dc4}=-150\text{MW}$$

Table 5-2 Power flow results comparison in TSAT and Matlab

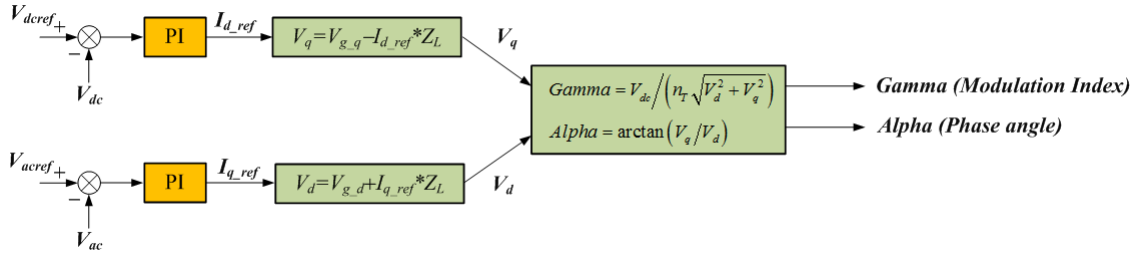
Parameters	TSAT	Matlab
V_{dc1}	1.0049	1.0049
V_{dc2}	1.0057	1.0058
V_{dc3}	1.0000	1.0000
V_{dc4}	1.0023	1.0022
I_{cable1}	-0.8289	-0.8289
I_{cable2}	0.8945	0.8943
I_{cable3}	-0.0907	-0.0910
I_{cable4}	0.1379	0.1378

5.2.2 *Dynamic Model*

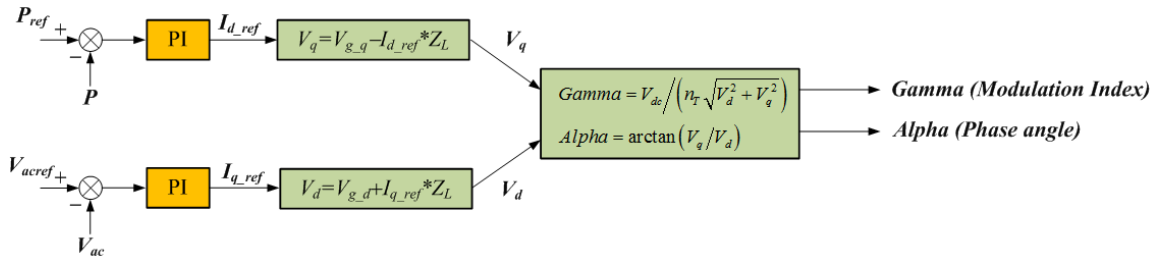
The dynamic model of the four-terminal DC system is written in TSAT (Transient Stability Assessment Tool) User Defined Mode editor, with both graphic interface and ASCII code. The dynamic model of each converter has three parts: converter parameters, control flags, and controller. The main functions in the controller are: DQ transfer, Phase Locked Loop (PLL), control functions such DC voltage control, active power control and reactive power control, also the modulation index and phase angle calculation. For the four-terminal topology system shown above, VSC3 controls the DC voltage and all the other converters control active power. Figure 5-4 (a) depicts different structures for the outer loop converter control of DC voltage and active power respectively, and Figure 5-4 (b) and (c) shows the inner current loop control for DC voltage and active power control.



(a) Outer voltage loop for DC voltage and active power control



(b) Inner current loop for DC voltage control



(c) Inner Current loop for Active power control

Figure 5-4 Control diagrams of MTDC converters

5.2.1 Simulation Results

The four-terminal VSC HVDC model is then tested with NPCC 140 bus system model. The system responses of a 350MW generation trip at bus 24 in the NPCC system is shown in Figure 5-5. It can be seen from the results that the converter DC voltage and active power is will control as a stable value, and the VSC converter is capable of generating reactive power during disturbance for voltage support.

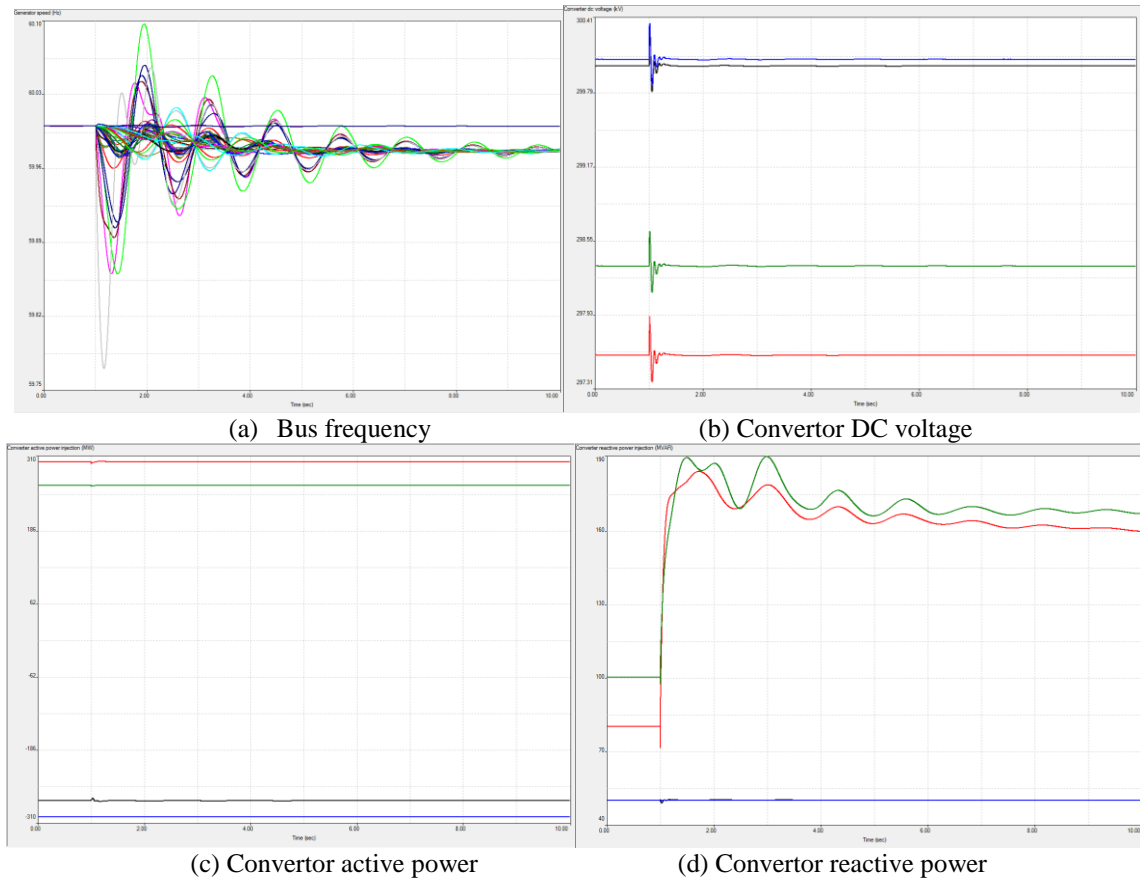


Figure 5-5 System response for a 350MW generation trip

5.3 VSC HVDC Supplementary Control

Although advanced HVDC technology has many advantages in transmitting large amount of power with lower losses, it is a fact that HVDC transmission network may reduce the system effective inertia due to the decoupling of mechanical and electrical systems, and

the generators connected by a HVDC transmission system will also be prevented from responding to system frequency changes. Moreover, there is no damping effect of the HVDC for network disturbances if only using the constant power output and constant AC voltage control. With the anticipated increase of HVDC links for renewable energy sources such as large offshore wind farms or onshore wind farm bases, there are ascending requirements for the HVDC connected generation system to participate in network support, such as frequency regulation and power oscillation damping. Therefore, a frequency droop control and inertia control is implemented in the VSC HVDC model, an oscillation damping function is also discussed and could be implemented in future work.

5.3.1 Frequency Droop Control

If the system has a high penetration of wind power, it will be necessary to have frequency droop in the HVDC loop. Otherwise, the frequency variation due to the load or generation change will be too large. The idea is the same as the frequency droop in the turbine governor in a synchronous generator. The control diagram for frequency droop control is shown in Figure 5-6.

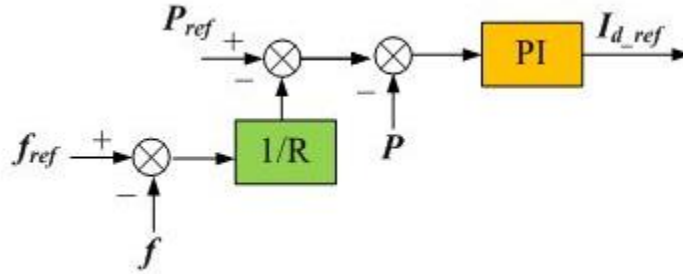


Figure 5-6 Control diagram for frequency droop control

5.3.2 Inertia Control

Due to the fact that system inertia will be decreasing as the integration of wind power and decoupling from AC network with DC transmission, it is necessary to include inertia support in VSC HVDC link for frequency regulation. The control diagram of HVDC inertia control is shown in Figure 5-7. The deviation of system frequency is obtained to modify

the power reference. A wash out function and a low pass filter are used to get rid of steady state DC component and noise measurements.

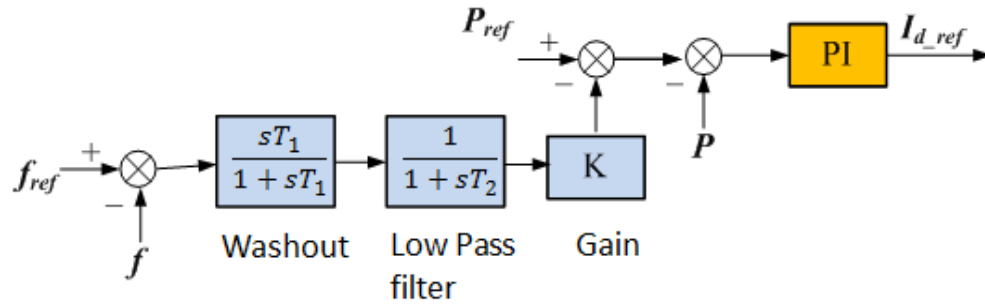


Figure 5-7 Control diagram for inertia control

5.3.3 Oscillation Damping Control

It is also necessary to exploit the oscillation damping function of the VSC-HVDC system to improve the system operation. By implementing a damping controller to active power modulation, the HVDC should mitigate the lower frequency oscillation, as shown in Figure 5-8. The frequency error is used as the input signal of the damping controller. The frequency error is processed through a wash out function to eliminate its steady-state DC component. A lead-lag damping regulator is applied to provide a phase shift on the interested frequency range. A limiter is applied to the output of the damping controller to ensure the reference current remains within the operating range.

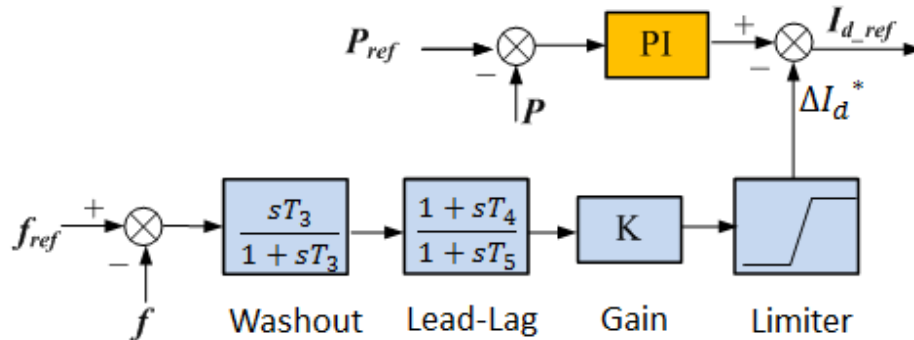


Figure 5-8 Control diagram for oscillation damping control

5.3.4 Test system and results

A simple test system as shown in Figure 5-9 is then constructed to test the functions of the supplementary control for VSC models in TSAT. This system can mimic a wind farm connected to AC grid through a VSC HVDC link. Figure 5-10 and Figure 5-11 shows the system response with or without frequency droop control and inertia control, respectively. It can be seen with the frequency droop control the settle down frequency deviation is smaller, and the convertor active power decreased during a load shedding disturbance. As for the inertia control, the system settle down frequency remain the same, however, the frequency nadir decreased apparently. In Figure 5-12, the effective control results are further illustrated. It is clearly that with both the inertia and frequency droop control, the frequency nadir will be reduced further and the steady state frequency also decreases.

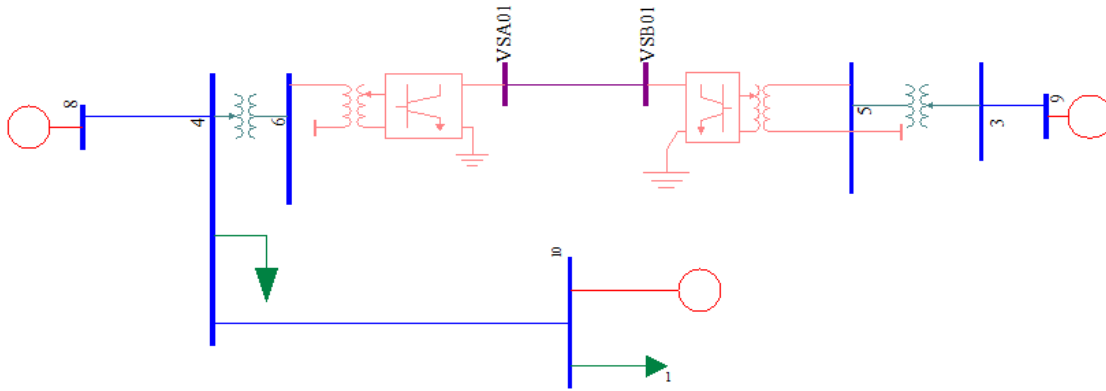
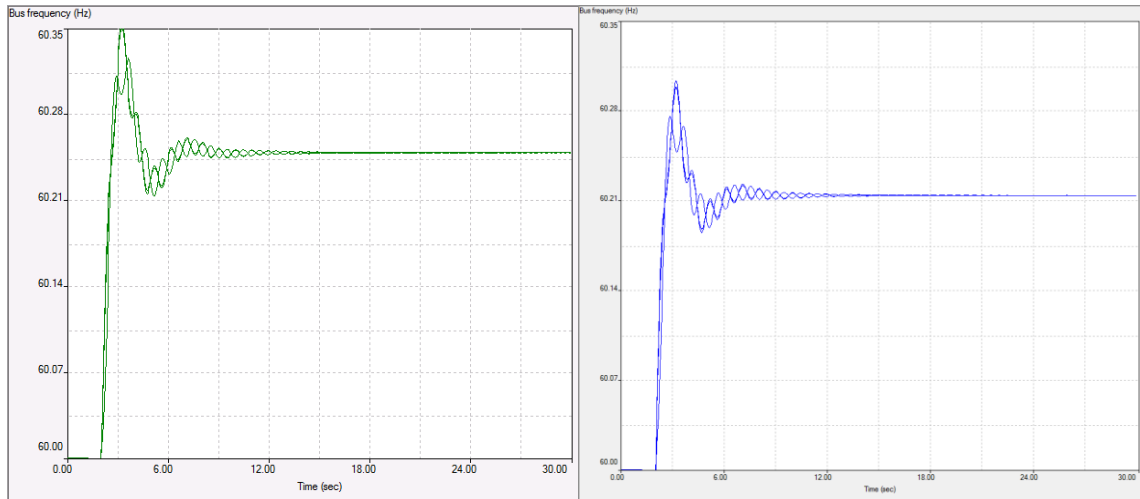
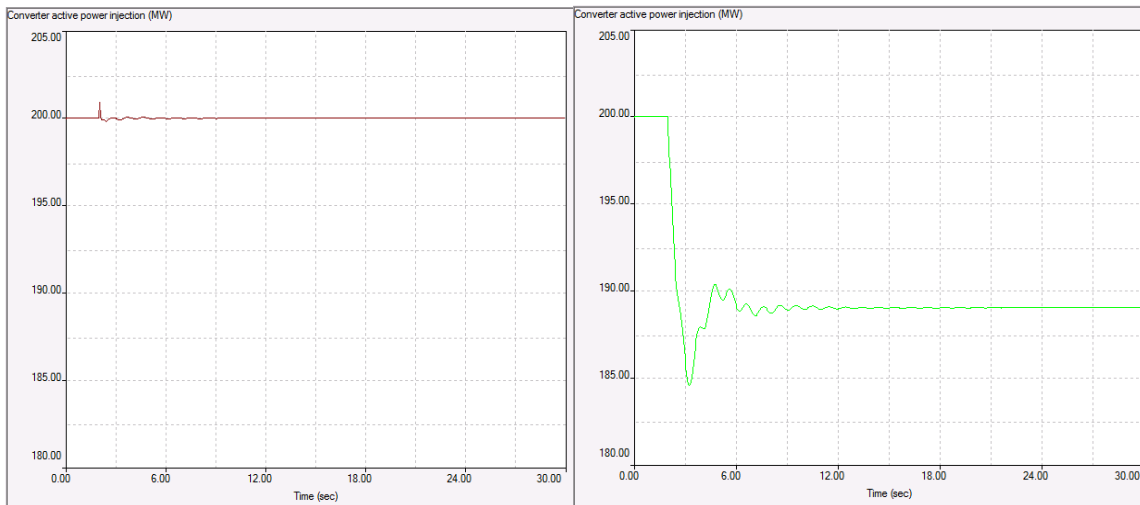


Figure 5-9 Test system topology for HVDC controls



(a) Bus frequency without droop control

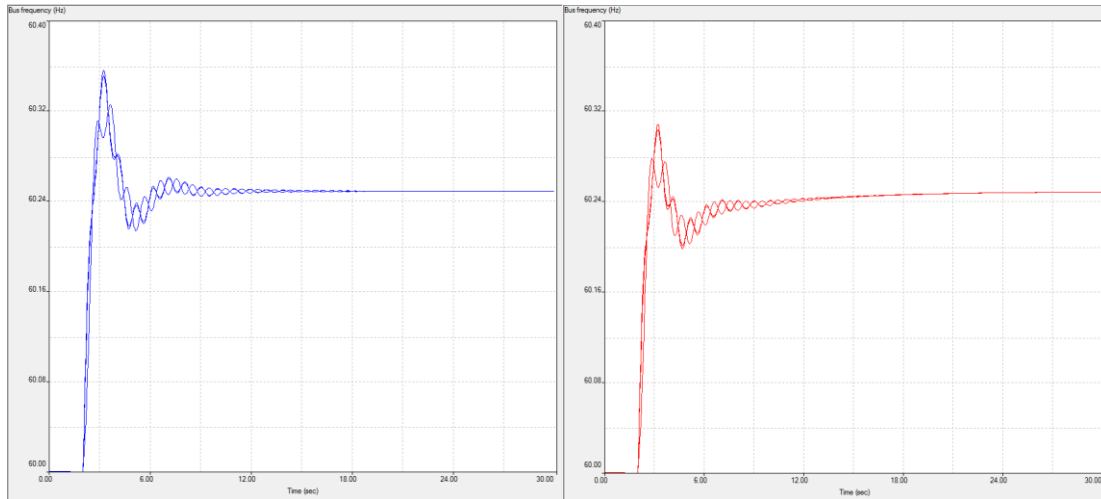
(b) Bus frequency with droop control



(c) Converter active power without droop control

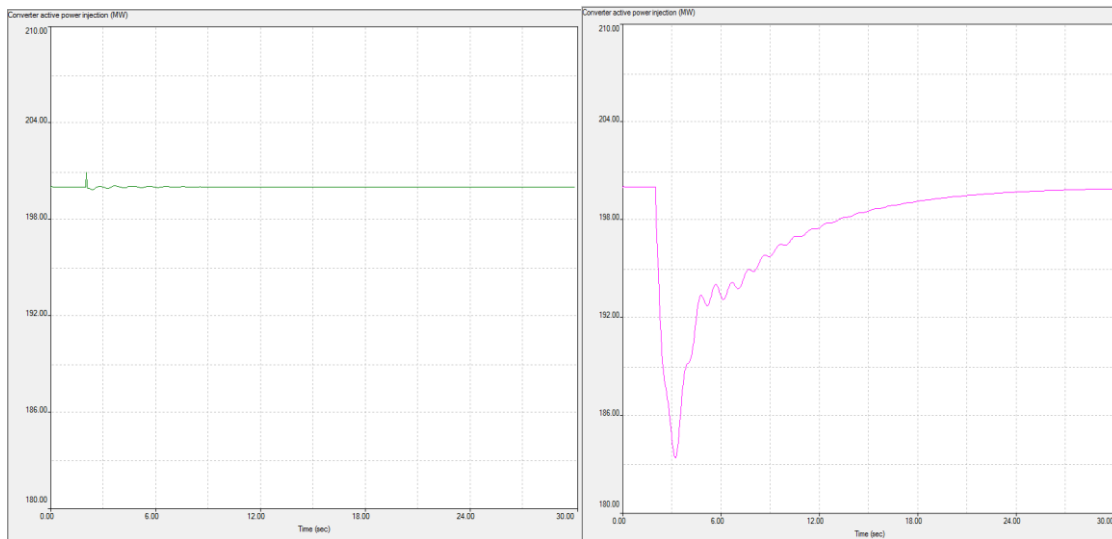
(b) Converter active power with droop control

Figure 5-10 System response with or without frequency droop control



(a) Bus frequency without inertia control

(b) Bus frequency with inertia control



(c) Convertor active power without inertia control

(b) Convertor active power with inertia control

Figure 5-11 System response with or without inertia control

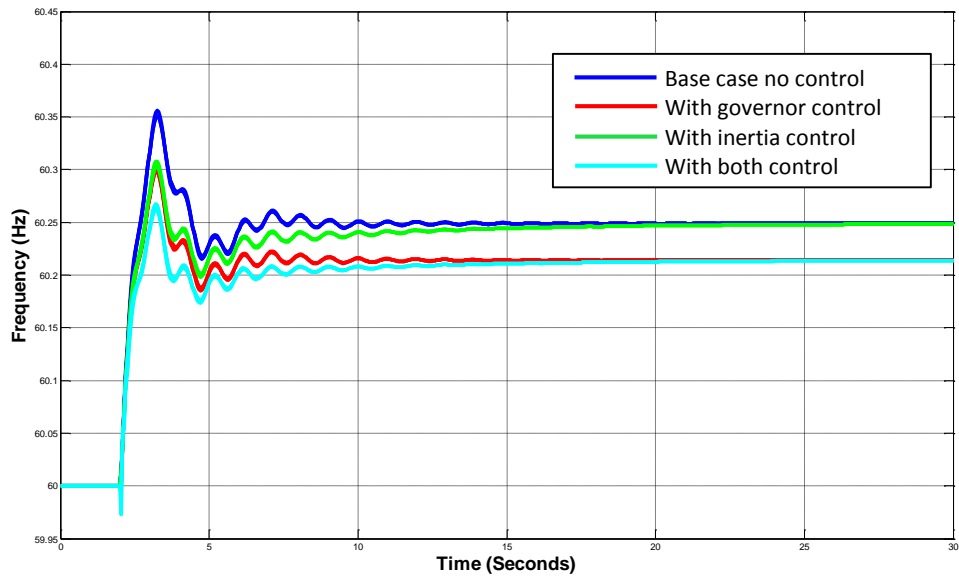


Figure 5-12 System response comparison

5.4 Conclusion

This chapter presents a method to model multi-terminal VSC HVDC in power system simulation toolbox and study the impact. The model is constructed in Powertech DSAtools, and then implemented with the NPCC 140 bus system to integrate an offshore wind farm in New England. Furthermore, to prevent the loss of system inertia due to HVDC connection and renewable integration, supplementary frequency control functions are also discussed. The supplementary control demonstrates effectiveness of inertia enhancement and primary frequency control during system load or generation change.

Chapter 6 BUILDING AN HVDC OVERLAY FOR US POWER GRID USING MULTI-TERMINAL VSC-HVDC TECHNOLOGY

6.1 Background

The notion of a Supergrid has been drawing increasing interests in many countries, especially in Europe, where a large amount of renewable energy is available on remote locations such as offshore or near the sea [30]. Meanwhile, in the US, with the 20% wind scenario planed by the Department of Energy (DOE), more and more wind power plants, which are far from load center, will be integrated to the existing power grid [31]. Furthermore, according to a report prepared by U.S. Energy Information Administration (EIA), the electricity demand in the US will increase by 29% from 2012 to 2040 [32]. These changes will result in a fundamental increase in the transmission of large amounts of power over longer distances.

There are many existing and ongoing national wide system projects that are or will be overlay grids all over the world. China has several long distance High Voltage Direct Current (HVDC) transmission lines in operation to transfer various energy sources from west to load centers in east coast [33]. One of the longest ± 800 kV HVDC transmission lines in China brings about 6400MW from southwest China to Shanghai [34]. The European Network of Transmission System Operators for Electricity (ENTSO-E) has proposed inter-regional high capacity transmission lines, which are termed as electricity highways [35], to interconnect their rich renewable resources geographically distributed across the continent. There are also many visions of European overlay grids proposing different grid and transmission technologies, most of which involves Voltage Source Converter (VSC) HVDC transmission technology as a preference for such transmission grids [36].

In US, there have been many conceptual national transmission overlay designs conceived by many organizations. However, most of them are planned as HVAC project. Regionally, Southwest Power Pool (SPP) has proposed an Extra High Voltage (EHV) Overlay, which is a collection of 500+ kV transmission projects to be added to the existing

transmission system to facilitate the economic transfer of power and reduce congestion across the grid [37]. Nationally, American Electric Power (AEP), in partnership with the American Wind Energy Association (AWEA), developed a conceptual 765 kV interstate transmission system with the ability to interconnect up to 400 GW of generation. It covered a majority portion of the United States (US) connecting areas of high wind resources with major load centers as shown in Figure 6-1[38].



Figure 6-1 AEP conceptual 765kV backbone system

With the improvement and deployment of HVDC technology, it is desired to build a DC overlay for US to transmit large amount of power with lower losses. However, design and construction of such an overlay grid is not only a major investment but also a completely new technological approach. It will fundamentally alter power grid in the way it is operated and planned. Therefore, the topology and technology of such a new overlay grid must be well conceived and analyzed in depth.

6.2 Required Characteristics of the Overlay Grid

To achieve the visions of future energy capacity expansion, the overlay grid must fulfill different technical requirements in order to determine the most suitable technology for the overlay grid [39][40].

First of all, since most onshore renewable resources are located in the West or Mid-west of US as shown in Figure 6-2, and most electric consumption is in the East, the overlay grid should be able to handle long distance transmission with low losses. As both the east and west coasts have large amounts of wind resource, the ability to connect the offshore wind, for example using undersea cables, is also a must in order to take good advantage of the offshore wind generation.

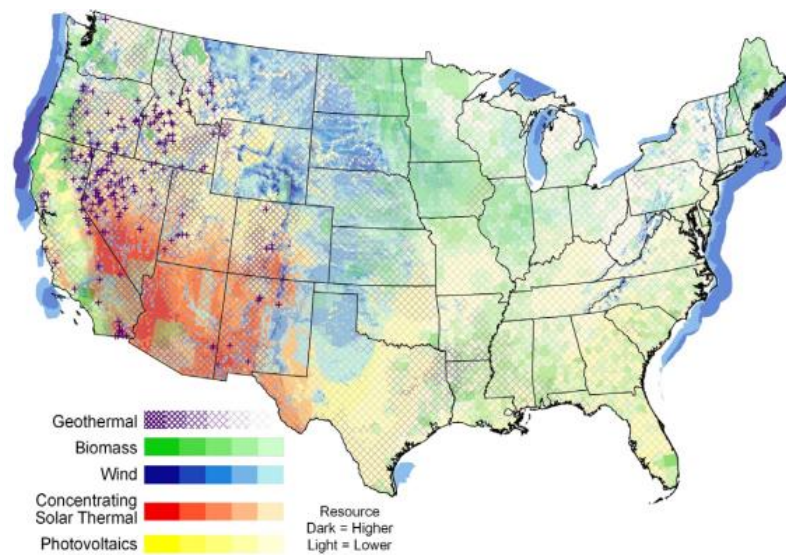


Figure 6-2 Renewable energy map, United States (Image courtesy of NREL)

Secondly, the new overlay grid should be an essential upgrade with respect to power transfer capacities, which requires a technology that is able to transmit electrical power at a significantly higher rating. This would require that the transmission happen at a higher voltage level than currently used in order to avoid excessive losses.

Thirdly, the new overlay grid should be compatible with the current transmission grid not only in a manner of the operational procedures, but also the resulting power flow of the overlay grid should not cause any problem of the existing one.

Lastly, there should not be any increasing risk of the overall system security. Concepts such as N-1 and coordinated frequency and voltage stability control must be applied to the overlay grid as well.

6.3 Transmission Technology

6.3.1 HVAC Technology

Currently the focus of transmission technological challenges is centered on the HVDC technology. However, HVAC technology should not be discarded, as it remains being very competitive. Extension and upgrade of the existing grid infrastructure can be an easy start of building an overlay system, as previously mentioned in SPP and AEP proposals. EHVAC solutions generally have lower investment cost than HVDC for distances of less than about 400 miles. There are commercialized Ultra High Voltage (1000kV and above) AC projects running in Russia, Japan and China [41][42].

However, if the overlay grid has also to rely on long and high capacity HVAC connections, then considerable parts of these connections will have to be built as underground cables or gas insulated lines, as the growing public resistance against overhead transmission lines. This brings new technical challenges and comes at a cost. In addition, the charging currents limit the distance of the connection when AC technology is used, although it is possible to provide reactive compensation.

6.3.2 HVDC Technology

HVDC is well-known to be an attractive option for bulk power transmission in three types of applications:

- Transmission of electricity at high voltages across large distances at a low cost and high efficiency.
- Connecting asynchronous electric grids and creating Security.

- Submarine cables, connecting ocean energy resources.

These attributes make HVDC an ideal technology for regional power grid development and the incorporation of clean energy sources.

Most of the existing HVDC projects in the world are well established by line commuted (LCC) HVDC. However, VSC HVDC shows its superiority in recent research. It can change the direction of power flow without reversing the polarity of the voltage of the DC cables. This feature makes it more suitable for multi-terminal HVDC than LCC HVDC, as LCC is more troublesome to control in a parallel multi-terminal configuration. Additionally, VSC HVDC is particularly suitable for offshore wind farm connection due to its capability of reactive power support and black start.

The major drawback of the VSC technology is that it requires further development in terms of transmission capacity. Also with respect to DC grid operation and control, a lot of questions remain unclear. Furthermore, a large number of protection issues regarding VSC HVDC have to be solved to ensure a safe operation of a meshed HVDC grid.

6.4 Regional HVDC Overlay Planning

6.4.1 *Overlay HVDC grid for NPCC system*

The overlay grid model was developed based on the VSC HVDC model discussed in the previous chapter. The overlay grid built for the NPCC system has five terminals, as shown in Figure 6-3. Each terminal is allocated in one area. A strong AC node that can provide or absorb large amount of power is selected in each area to connect with the VSC via a common connection AC bus. The underlying AC system is assumed to remain unchanged in this test case. The main purpose of this overlay grid is to transfer the cheap renewables in the Midwest like wind or hydro and potentially large amount of offshore wind in New England to load centers in the NYISO area. The operation mode of the five-terminal VSC HVDC system is shown in Table 6-1, with one node controlling the DC voltage and the rest control active power, while all nodes have the ability of reactive power support which means AC voltage at all nodes are controllable. The frequency responsive control can be implemented in a future work.

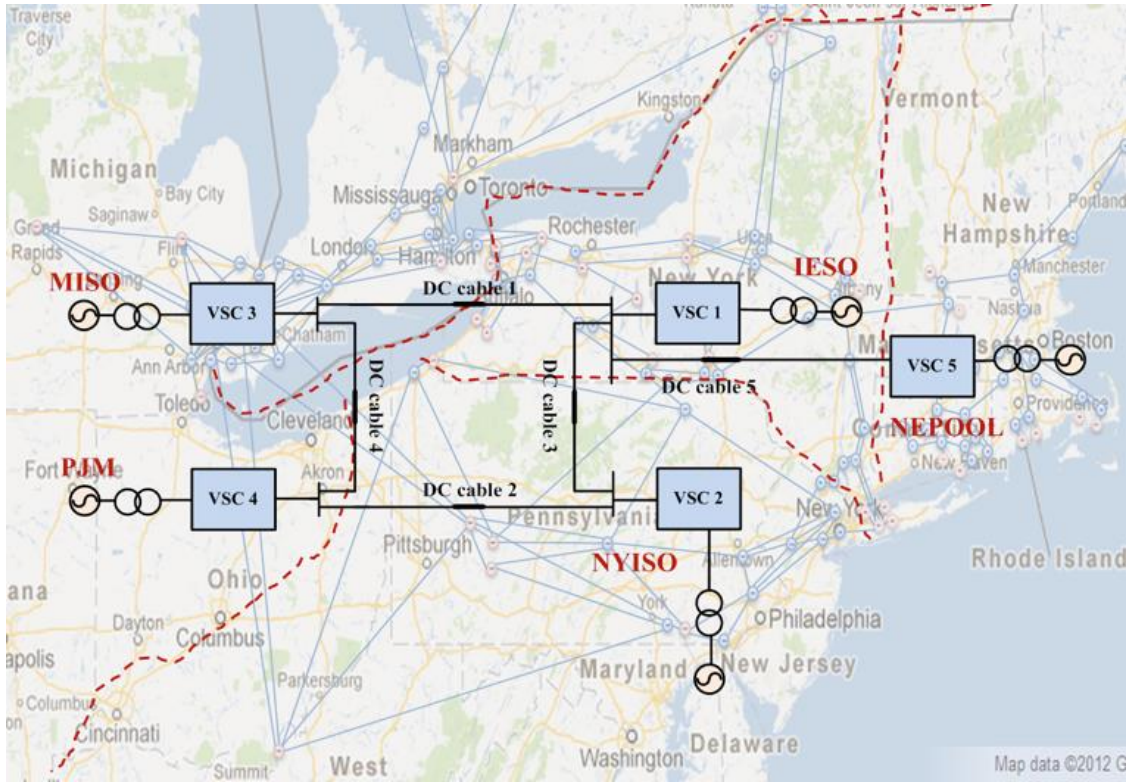


Figure 6-3 Five-terminal HVDC overlay of NPCC system

Table 6-1 Five-terminal VSC HVDC system operating mode

	VSC 1	VSC 2	VSC 3	VSC 4	VSC 5
System operating mode	VdcVac	PVac	PVac	PVac	PVac

6.4.2 Overlay HVDC grid for WECC and EI system

The overall HVDC overlay design is based on a topology proposed by Midwest Independent System Operator (MISO)[43], as shown in Figure 6-4. A WECC MTDC overlay system is then proposed on top of the 179-bus WECC system. It has 7 VSC converter stations, connecting wind in MT, solar in AZ with west coast load centers, and 3

potential terminals connecting with EI and ERCOT. The system topology is shown in Figure 6-5. As for the EI system, besides the MISO topology, the Eastern Wind Integration and Transmission Study conceptual transmission plan [44] is also considered to add two more terminals in New England and PJM area. The topology is shown in Figure 6-6.

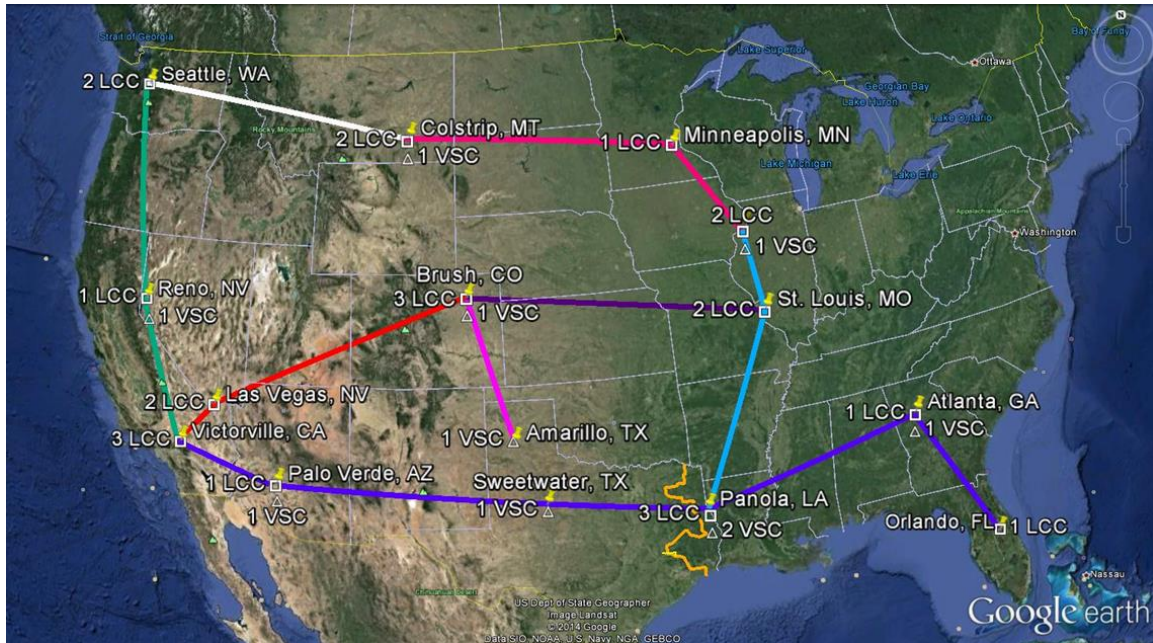


Figure 6-4 MISO proposed HVDC overlay topology

6.4.3 Simulation results with overlay grid

The general dynamic performance of the DC overlay grid is shown in Figure 6-7. An AC disturbance (generation trip) is added at 2 seconds. It can be seen that the DC voltage and active power are well controlled for each terminal during the disturbance. However, this is only a preliminary result with constant DC voltage and constant active power control, which is not practical in realistic. Advanced control functions should be added to this study later under different operation conditions for the HVDC overlay grid.

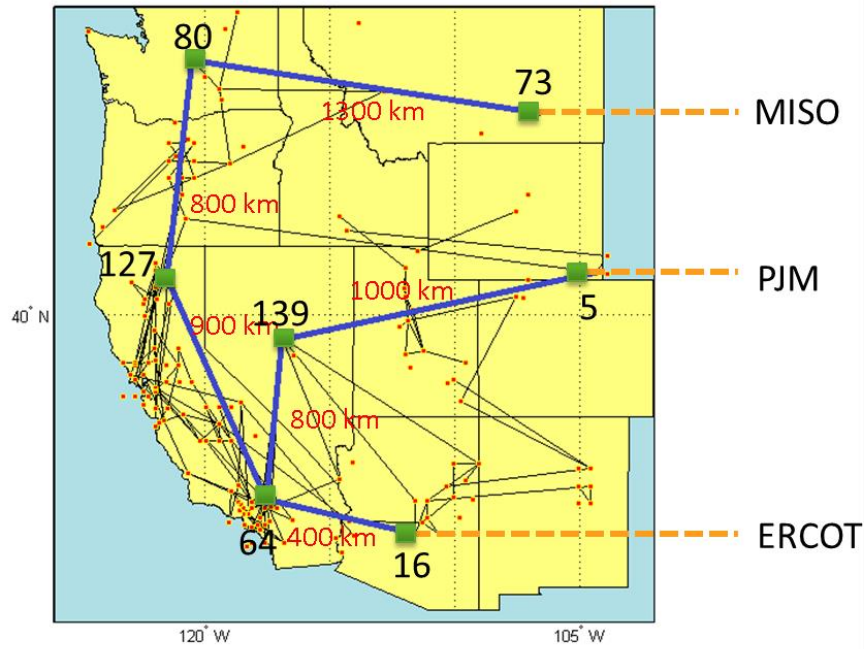


Figure 6-5 WECC system with HVDC overlay

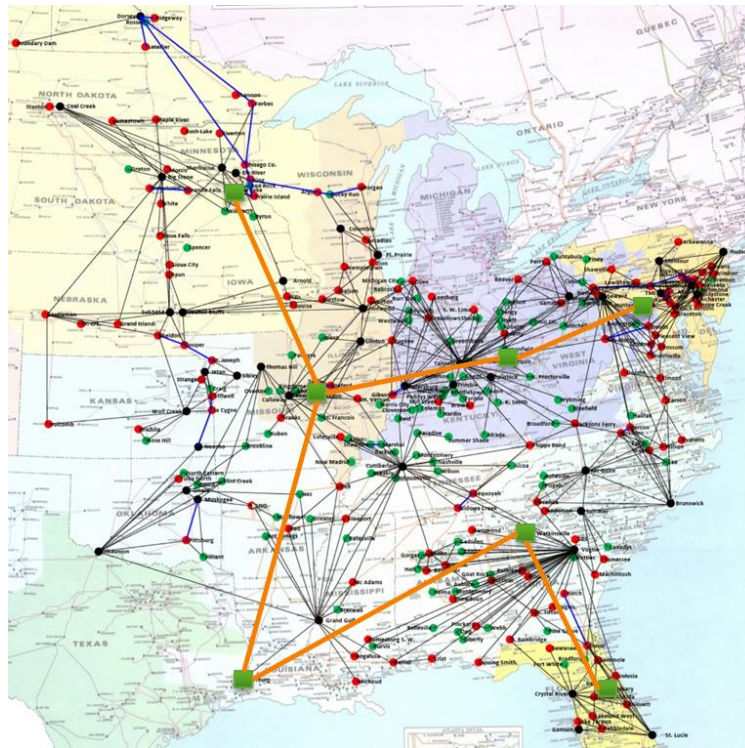
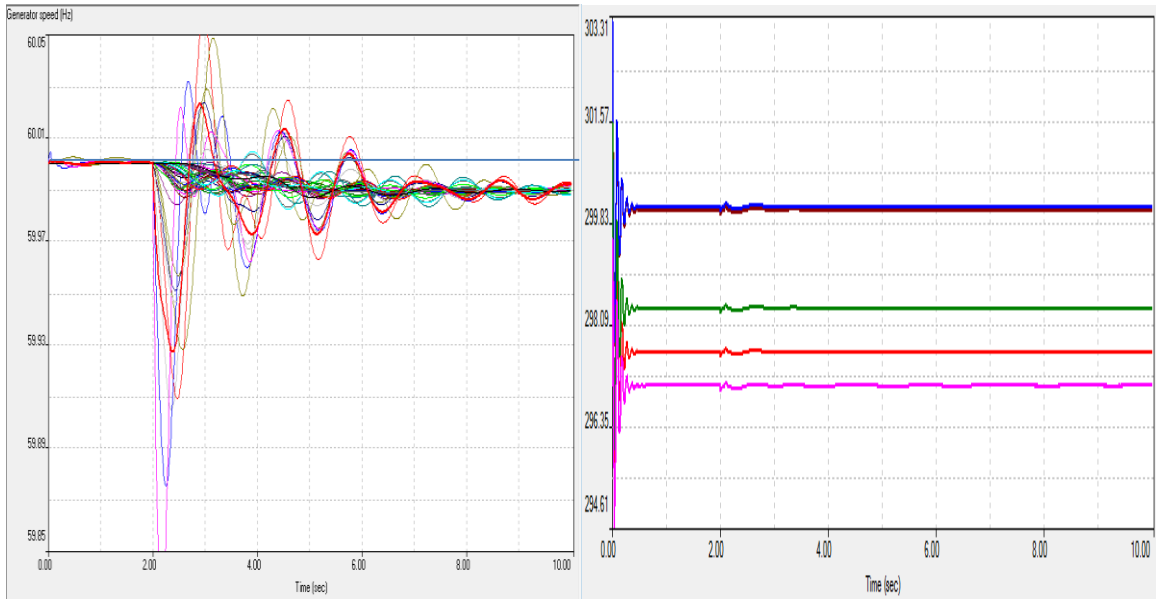
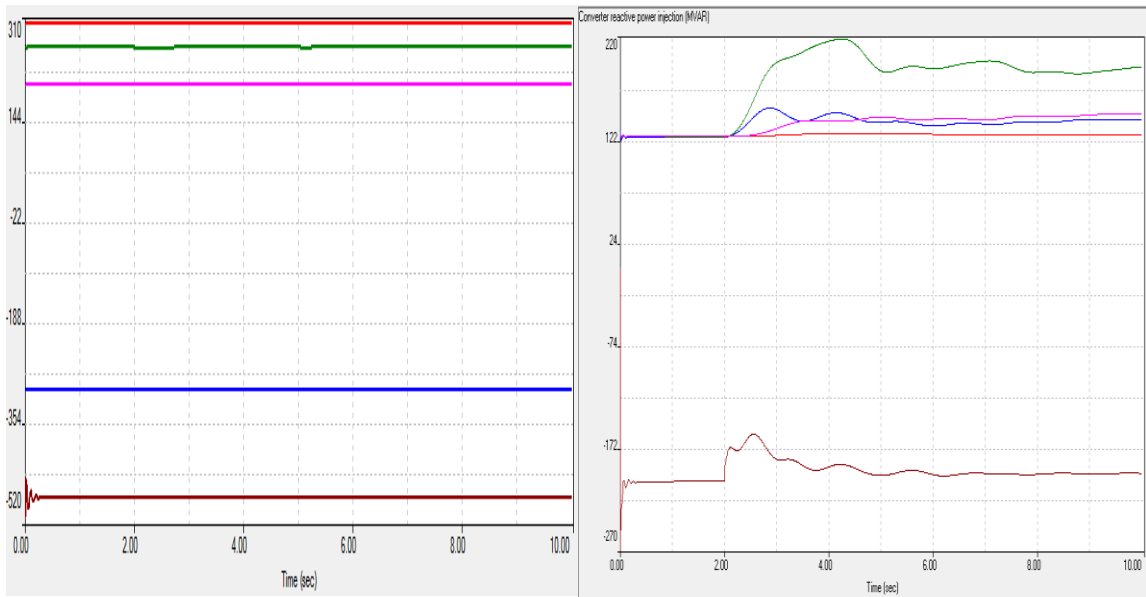


Figure 6-6 EI system with HVDC overlay



(a) Bus frequency

(b) Converter DC voltage



(c) Converter active power

(d) Converter reactive power

Figure 6-7 Overlay grid response

6.5 Conclusion

Under the scenarios of electricity demand growth and increasing renewable penetrations that are remote from load centers, the development of a nation-wide transmission overlay is becoming one of the primary goals for many countries. In US, this fundamental upgrade should also be conceived, and this will change the transmission grid significantly. This work analyzes the technical requirements of such an overlay grid and discusses some of the potential transmission technologies suitable for long distance bulk power transmission backbone. A multi-terminal VSC HVDC grid is considered to be the most optimal transmission technology for the essential transmission upgrade. And the primary implementation of the multi-terminal VSC HVDC overlay grid is on a regionally NPCC system, and eventually will cover the entire US grid. Advanced control methods should also be taking into consideration for practical operation conditions of the overlay grids.

Chapter 7 VIRTUAL GRID SIMULATOR

7.1 Background

In power industry, it is common to use Energy Management System (EMS) and SCADA (supervisory control and data acquisition) for electric utility grid monitor, control, and optimization. In order to study the system operation and control more realistic at the research level, it is desired to develop a real time grid operation platform which can continuously simulate the actual operation of a power grid under small or large disturbances, with communication and control action included under wide-area measurement. This ideal simulation platform is defined as Virtual Grid Simulator (VGS). The data structure of VGS is shown in Figure7-1.

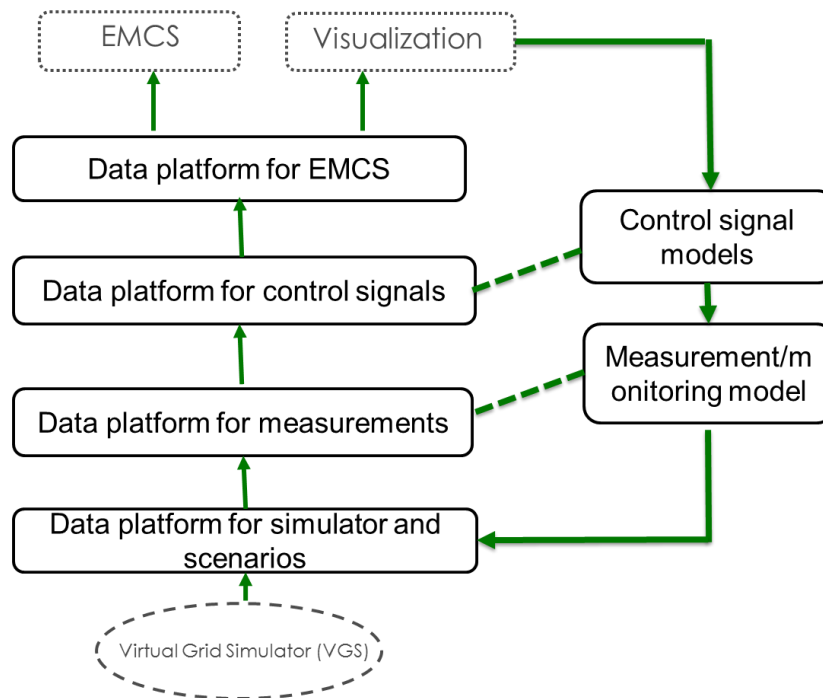


Figure 7-1 Data structure

Currently, the development of VGS is under two paths: one is research based tool which is Power System Analysis Toolbox, and the other path is commercial software like ePMU by

Powertech, PowerWorld Dynamic Simulator, and ePHASORsim by OPAL-RT. These tools will be demonstrated and evaluated in details respectively.

7.2 Different Toolboxes for Comparison

7.2.1 *Power System Analysis Toolbox (PSAT)*

PSAT is an open source MATLAB-based research aimed power system analysis tool, which can perform several power system analysis like continuation power flow, optimal power flow, small signal stability analysis, and time domain simulation and etc. PSAT support a variety of static and dynamic models, which include non-conventional loads, synchronous machines and controls, regulating transformers, FACTS, wind turbines, and fuel cells. Besides mathematical algorithms and models, PSAT also includes some additional tools like graphical user interface, Simulink library for one-line network diagram, data conversion to and from other formats, user defined model editor and installer, and command line usage. [45]

The test of PSAT has been carried on with IEEE 9 bus system. Hourly generation and load profiles are imported to mimic a 5 min dispatch in the simulation, as shown in Figure 7-2.

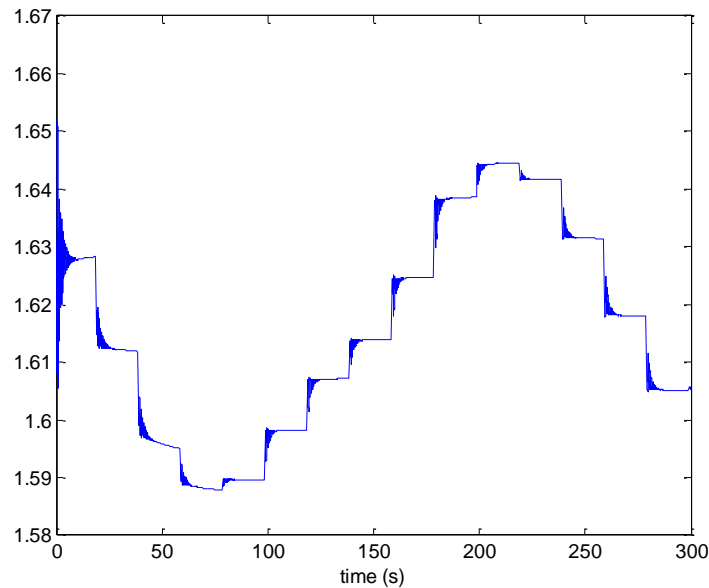


Figure 7-2 PSAT Results of adding load profile

7.2.2 *ePMU*

ePMU is an add-on module to TSAT and is built based on TSAT simulations. The main features and functions of ePMU are as follows: [46]

- Compatibility with all models supported by TSAT.
- Compatibility with all data formats supported by TSAT.
- Compatibility with TSAT user interface.
- Streaming generic IEEE C37.118 format data which can be captured by a Phasor Data Concentrator (PDC) such as openPDC.
- Capability of assigning PMUs at any bus, generator, and branch in the system using an approach similar to TSAT monitor data specification.
- Configurable PMU output reporting data rate.
- Configurable PMU data output TCP port.
- Support real-time external switching/control actions through IEEE C37.118 command frame.
- Replay and save simulation results of very large power system models.

The TSAT case contains all necessary data to perform simulations for a system model and parameters for running ePMU. ePMU operates along with the TSAT engine. As the TSAT simulation is calculated, ePMU ensures that the simulation is performed at real-time, and the simulation results are streamed out at specific reporting rate and TCP port in IEEE C37.118 format. All external PMU applications can receive the streamed PMU data and can also send switching/control commands to the ePMU module through designated TCP port. The structure of ePMU is shown in Figure 7-3.

The data are able to stream to openPDC, and commands from external applications can be sent via the PMU connection tester, the commands are programmed into the interface by C# code, as shown in Figure 7-4 and 7-5.

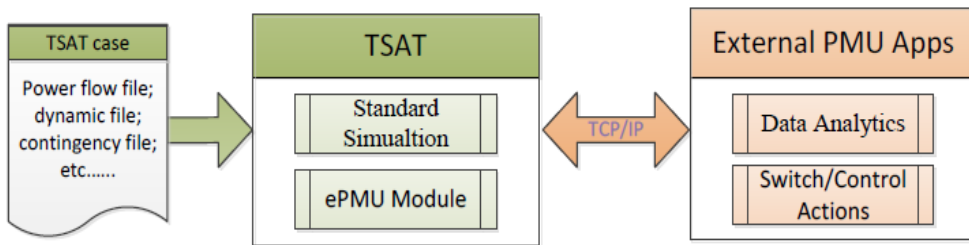


Figure 7-3 ePMU structure

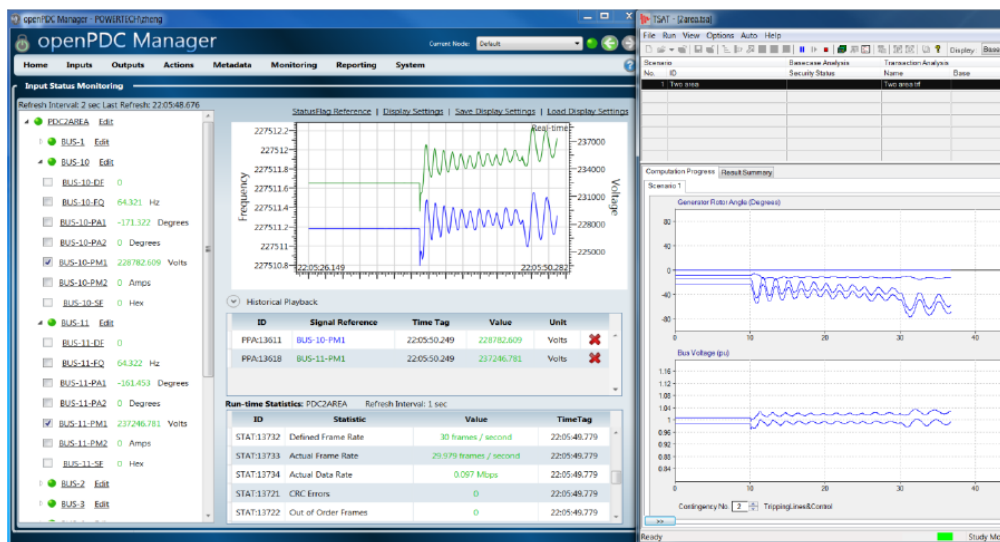


Figure 7-4 example of ePMU streaming data

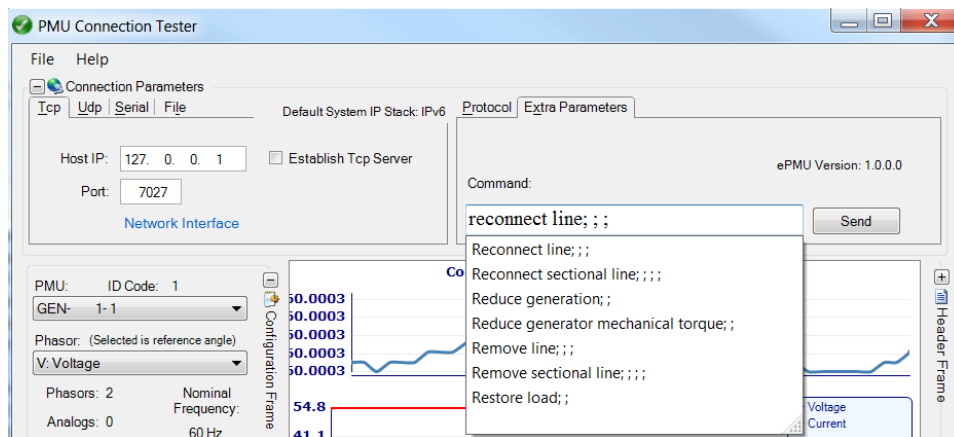


Figure 7-5 ePMU control command

7.2.3 PowerWorld Dynamic Simulator

The PowerWorld Dynamic Simulator (PWDS) is designed to provide an interactive power system simulation on the transient stability time scale (e.g., 1/4 cycle)[47]. It can be used either as a stand-alone single user simulation, or as the power system simulation server in a client-server environment. Clients communicate with the server using TCP/IP allowing clients to be anywhere. PWDS support a wide variety of transient stability models, including most of the model used by PSS/E and PSLF. There is no limit on the case size. And PowerWorld is adding models to support longer term dynamics, like AGC and load variation. Current PWDS code is still in beta, with new functionality being added, much of development work has focused on the stand-alone aspects. The user interface of PWDS is shown in Figure 7-6.

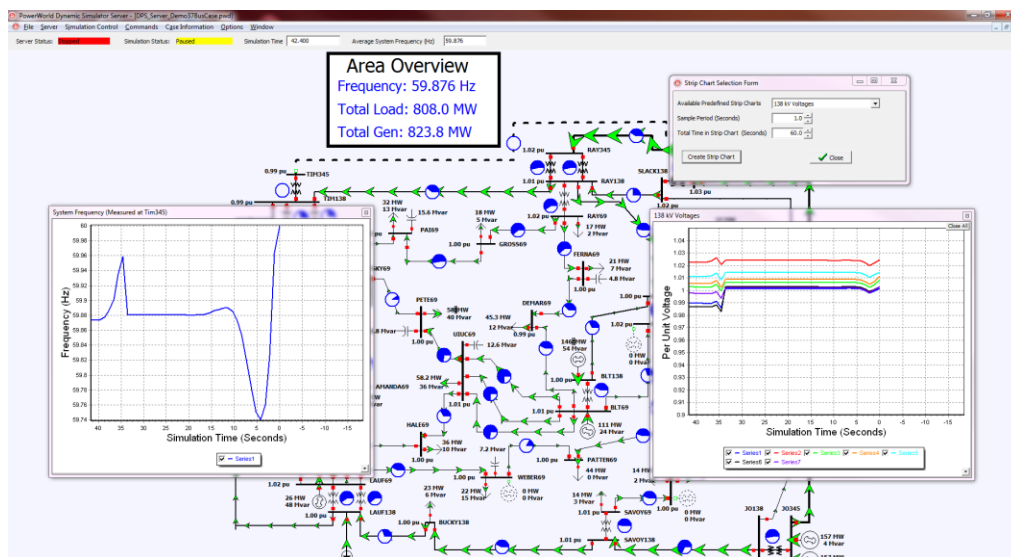


Figure 7-6 PWDS user interface

7.2.4 ePHASORsim

ePHASORsim simulates electro-mechanical transient stability phenomenon of very large power grids with thousands of buses, generators, transformers, transmission lines, loads and controllers.[48] It uses a fundamental frequency solver optimized to compute rms

values of voltages, currents, active and active power in real time, with a typical time step of 10 milliseconds.

The Solver block mask contains:

- Input File Format: Either an Excel file or a PSS/E Ver.32 file
- Excel File, which defines input/output pins.
- PSS/E RAW file and PSS/E DYR file.

ePHASORsim is ideal when implementing training simulators for system operators, testing SCADA systems, and developing and testing the performance of local protection and control systems, as well as complex global control systems and special protections. In such applications, the simulator receives commands and computes the new steady conditions and dynamic behavior of the simulated power grid in real time.[49] Voltages, currents, power, breaker status and critical control signals can be monitored in real-life applications. The control commands can be sent to the solver either directly or via Distributed Network Protocol (DNP3):

- Apply faults on buses.
- Apply faults on lines, with variable fault location
- In /Out-of-service commands for loads, capacitor banks, and transmission lines
- Generator outage
- Adjust tap position
- Adjust the reference for controllers
- Change load profile
- Open and reclose breakers

ePHASORsim is also capable of Hardware-In-the-Loop (HIL) simulation. Figure 7-7 shows an ePHASORsim HIL demo case. The left frame is OPAL 5600 simulator, with different subsystems running on different cores at multiple rates. The first block is

ePHASORsim solver, which runs at 10ms, and second block is analog I/O, which up-sample positive sequence phasor to time domain V and I waveforms, then send analogue signal to relay. The third block is communication block. C37.118 master and slave blocks are built inside. The right green frame is running on PC, which is the user interface, where user can monitor the system measures and send corresponding control commands. Figure 7-8 shows a benchmark simulation in ePHASORsim compared with PSS/E simulation results with user created governor and exciter models in OpenModelica.

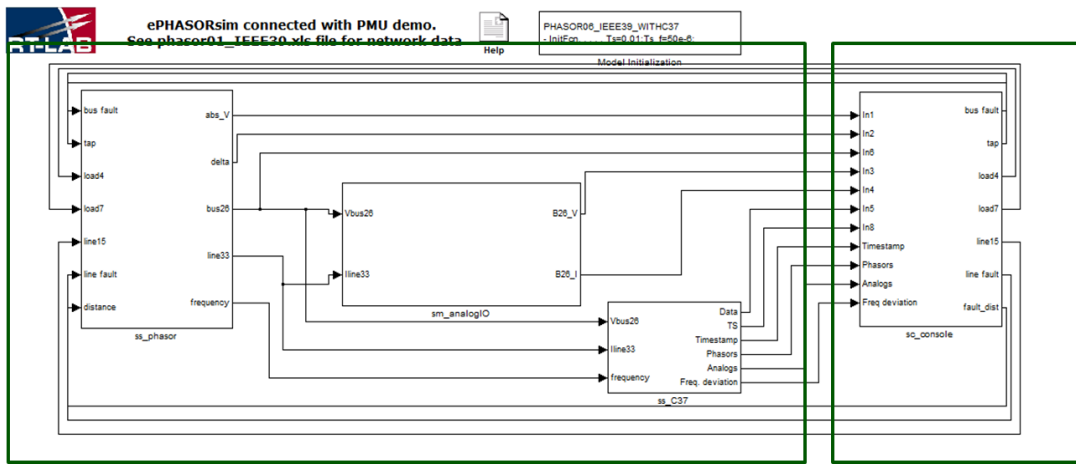


Figure 7-7 ePHASORsim HIL demo

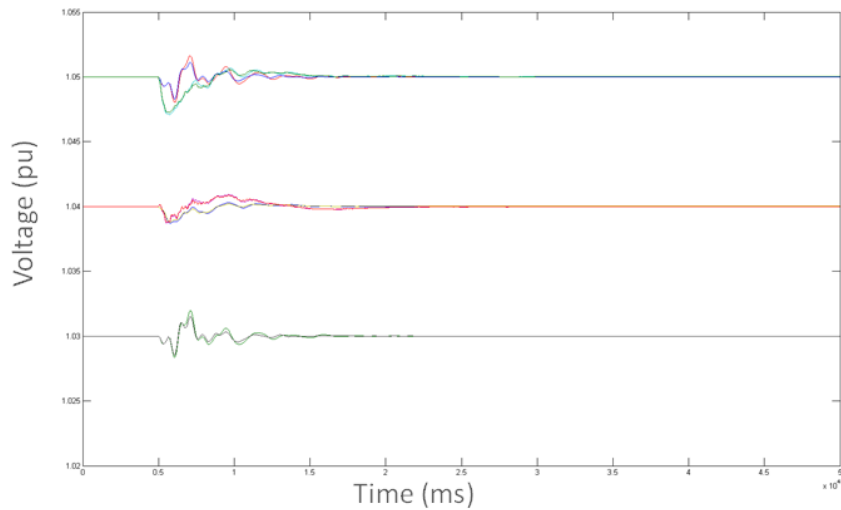


Figure 7-8 Simulation results validation with PSS/E

7.3 Conclusion

The purpose of VGS is to establish the platform which can run simulation continuously to mimic the real power grid with consideration of load change, economical dispatch as well as disturbances. Also the VGS should be able to communicate with Energy Management and Control System via standard data format under certain communication protocol.

Based on the needs of VGS, the tools discussed above are evaluated. Research tool wise, PSAT is fully functional to run continuously simulation with load variation, generation dispatch, and disturbances in between. However, some more work needs to be done to improve computation efficiency, also a standard output format will be developed for communication purpose.

Commercial tool wise, ePMU, PWDS, and ePHASORSim are all reliable tools to run continuous simulation with interactive control. Considering the fact of simulation accuracy and model library completeness, ePMU did slightly better than the other two. However, the user-defined model in TSAT has some limitations on block numbers, and the internal parameters of built-in models are difficult to access, so it causes problems for control implementation. And developing external control requires C# language. PWDS is still under beta version, and PowerWorld is working on adding new models as well as server/client side control commands. Therefore, ePHASORSim becomes a better choice. It supports a variety of PSS/E models, and users can create user defined models easily in OpenModelic, then import to ePHASORSim. With the freedom to define input/output pins, internal variables can be accessed. MATLAB/Simulink user friendly makes it a lot more flexible in terms of implementing control functions, dispatch programs, and etc. Validation with PSS/E simulation results shows credibility of ePHASORSim dynamic simulation results.

Chapter 8 CONCLUSIONS AND FUTURE WORK

8.1 Conclusions

The use of synchrophasor measurements system-wide has been providing significant assistance for grid dynamic monitoring, situation awareness and reliability improvement. Frequency Monitoring Network (FNET), as an academia-run GPS-synchronized phasor measurement system, utilizes a large number of Internet-connected low-cost Frequency Disturbance Recorders (FDRs) installed at the distribution level to measure power system dynamics and provide both online and off-line applications, such as event detection, event replay, oscillation modes online estimation, etc. This work aims to further explore applications of the FNET measurements and utilize measurement-based method in dynamic modeling.

Measurement-based dynamic reduction is an important application of synchrophasor measurement, especially considering the fact that when the system model is large, measurements provide a precise insight of system dynamics in order to determine equivalent regions. Chapter 1 presents a procedure to construct the dynamic equivalent models of large-scale power systems using wide-area synchrophasor measurements. The method is illustrated on the Eastern Interconnection and simulations in PSS/E are performed to assess the accuracy of the equivalent model. Results of the simulation show that the developed equivalent system has the capability in representing some of the dynamic characteristics of the original system. It is recognized that the accuracy of this model could not probably duplicate the more detailed model used in simulation. But for the target dynamical response, such high level models can be good decision aids for initiatives such as developing a national grid of a very large country like the United States. Another potential application could be simulating the faster than real time response of a large dynamic system as decision aids for power system operators.

Another important application is to investigate NFL Super Bowl games as an example to evaluate the influence of synchronized human activities on the power system using FNET measurement data. In chapter 2, the statistical information of power system frequency behavior is investigated based on the real wide-area measurements taken in FNET from

Super Bowl XLIV, 2010 to Super Bowl XLIX, 2015. It is apparent that large groups of people engaging in the same event at roughly the same time can have significant impacts on the power grid frequency. Comparison of the Super Bowl data with non-game day data shows that there are far more power system events occurring in the former case. Clearly, the impacts of the Super Bowl on power grid frequency in this work provide valuable information regarding the system dynamics of such popular events. Understanding the relationship between large-scale societal events and power frequency has important implications for power system. With the development of smart grid technology, similar large-scale, synchronous activities would be observed. It is evident that the societal effects could play a very significant role in future smart grid implementation. The observations in this work will also provide valuable information in the study of responsive loads for power grid frequency regulation.

Chapter 3 evaluates the impact of wind power on the system inertial response, simulation scenarios with different wind penetration levels are developed in PSS®E based on the U.S. Northeast Power Coordinating Council (NPCC) system. A user-defined electrical control model is also introduced to provide inertia and governor control to the doubly-fed induction generator (DFIG) – based wind generations. An extreme case of 100% renewable resources including 90% wind and 10% hydro generations is considered in this work and simulation results demonstrate that wind power has significant impact on system inertial response and is also promising in providing primary frequency supports.

Except for wind generation, the wide-area frequency regulation and oscillation damping can also be achieved by supplementary of HVDC transmission line. Chapter 5 presents a method to model multi-terminal VSC HVDC in power system simulation toolbox and study the impact. The model is constructed in Powertech DSAtools, and then implemented with the NPCC 140 bus system to integrate an offshore wind farm in New England. Furthermore, to prevent the loss of system inertia due to HVDC connection and renewable integration, supplementary frequency control functions are also discussed. The supplementary control demonstrates effectiveness of inertia enhancement and primary frequency control during system load or generation change.

As the expected increase in renewable generation and electricity demand, questions about how to transmit large amount of intermittent and remote renewable energy over long distance to load centers arises. Under the scenarios, the development of a nation-wide transmission overlay is becoming one of the primary goals for many counties. Chapter 6 analyzes the technical requirements of such an overlay grid and discusses some of the potential transmission technologies suitable for long distance bulk power transmission backbone. A multi-terminal VSC HVDC grid is considered to be the most optimal transmission technology for the essential transmission upgrade. And the primary implementation of the multi-terminal VSC HVDC overly grid is on a regionally NPCC system, and eventually will cover the entire US grid. Advanced control methods should also be taking into consideration for practical operation conditions of the overlay grids.

Finally, a Virtual Grid Simulator (VGS) is discussed, which is a platform that can run dynamic simulation continuously to mimic the real power grid with consideration of load variation, economical dispatch as well as disturbances. Several tools, including Power System Analysis Toolbox (PSAT), PowerWorld Dynamic Simulator, ePMU, ePHASORsim, are evaluated and compared based on the needs of VGS. ePHASORsim was eventually chosen as the commercial platform as it supports a variety of PSS/E models, and users can create user defined models easily in OpenModelic, then import to ePHASORsim. With the freedom to define input/output pins, internal variables can be accessed. MATLAB/Simulink user friendly makes it a lot more flexible in terms of implementing control functions, dispatch programs, and etc. Validation with PSS/E simulation results shows credibility of ePHASORsim dynamic simulation results.

8.2 Possible Future Work

- Implement the oscillation damping function into the VSC-HVDC model. The control function was discussed in this work, however, due to some software issue, the damping control function was not fully implemented.

- Enhance dynamic models of VSC HVDC, enable coordination control between different terminals. Implement the frequency regulation and damping control on the overlay system. This is important for overlay system control especially when operating with AC system together. Advanced communication and control schemes should be developed to enhance the system operation condition.
- Connect the overlay system for three major interconnections. This step should be done after test running for each individual interconnection overlay grid.
- The data analysis for Super Bowl events should also be continued. It is a critical evidence showing how human behavior can influence the power grid.
- Advanced control functions can be implemented with VGS under ePHASORSim platform.

LIST OF REFERENCES

- [1] B. Qiu, L. Chen, V. Centeno, X. Dong, and Y. Liu, "Internet-based Frequency Monitoring Network (FNET) ", in *IEEE Power Engineering Society Winter Meeting*, pp. 1166-1171, 2001.
- [2] Z. Zhong, C. Xu, Billian, B.J, Li Zhang, Tsai, S.-J.S., Connors, R.W.; Centeno, V.A., Phadke, A.G., Y. Liu, "Power system frequency monitoring network (FNET) implementation," *IEEE Trans. Power Systems*, vol. 20, pp. 1914-1921, Nov. 2005.
- [3] YC. Zhang, Markhan, P., T. Xia, L. Chen, Y. Ye, Z. Wu, Z.Yuan, L. Wang, Bank, J., Burgett, J., Connors, R.W., Yilu Liu, "Wide-Area Frequency Monitoring Network (FNET) Architecture and Applications," *IEEE Trans. Smart Grid*, vol. 1, pp. 159-167, Sept. 2010. I. S. Jacobs and C. P. Bean, "Fine particles, thin films and exchange anisotropy," in *Magnetism*, vol. III, G. T. Rado and H. Suhl, Eds. New York: Academic, 1963, pp. 271–350.
- [4] Z. Yuan, T. Xia, Y. Zhang, L. Chen, Markhan Peen, Gardner R.M, Y. Liu, "Inter-area oscillation analysis using wide area voltage angle measurements from FNET," *IEEE Power and Energy Society General Meeting* 2010.
- [5] H.A. Alsafih, R. Dunn, "Determination of coherent clusters in a multi-machine power system based on wide-area signal measurements," *IEEE Power and Energy Society General Meeting* 2010.
- [6] L. Wang, M. Klein, S. Yirga, P. Kundur, "Dynamic Reduction of Large Power Systems for Stability Studies" *IEEE Trans. Power Systems*, vol. 12, pp. 889-895, May 1997.
- [7] Y. Kang, X. Zhou, G. Xie, "Study of Power System Dynamic Equivalents in NETOMA", *Power Technology*, Vol. 22, No. 5, pp 21-24, May 1998.
- [8] J. H. Chow, R. Galarza, Raccari, W. W. Price, "Inertial and slow coherency aggregation algorithms for Power System Dynamic model reduction", *IEEE Trans. Power Systems*, vol. 10, pp. 680-685, May 1995.
- [9] J.T. Tou and R.C. Gonzalez, *Pattern Recognition Principles*, Massachusetts: Addison-Wesley, 1974.
- [10] J. H. Chow, *Power System Coherency and Model Reduction*, Springer, 2012
- [11] PSS/E 32.0.5 Program Application Guide: Volume II. Siemens Energy, Inc., Power Technologies International.
- [12] L. Vanfretti, J. H. Chow, "Identification of Dominant Inter-Area Modes in the Eastern Interconnection from PMU data of the FRCC 2008 Disturbance: an Eigensystem Realization Algorithm Illustration", White paper prepared for a Special Publication of the Task Force on Modal Identification of Electromechanical Modes, *IEEE Power and Energy Society*. July 2010.
- [13] X. Tao, et al., "FNET observations on the impact of super bowl xlii on the power grid frequency," in *Power & Energy Society General Meeting*, 2009. PES '09. IEEE, 2009, pp. 1-5.
- [14] L. Chen, P. Markham, C. Chen, and Y. Liu, " Analysis of Societal Event Impacts on the Power System Frequency using FNET Measurements," in *Proc. 2011 IEEE Power Engineering Society General Meeting*., pp. 1-8.

- [15] B. Starling, K. Thomas, R. Orndorff, J. Ingleson, E. Allen, "Effects of the Super Bowl on the Eastern Interconnection," in Georgia Tech Fault AND Disturbance Analysis Conference, 2013
- [16] "Super Bowl Ratings Record: Giants-Patriots Game Is Highest-Rated TV Show In US History". Huffington Post. Retrieved February 7, 2012. [Online]. Available: http://www.huffingtonpost.com/2012/02/06/super-bowl-ratings-record-tv-giants-patriots_n_1258107.html
- [17] R. Gardner, "A Wide-Area Perspective on Power System Operation and Dynamics," Ph.D. dissertation, Dept. Electrical Eng., Virginia Tech Univ. Blacksburg, 2008.
- [18] http://www.nerc.com/AboutNERC/keyplayers/Documents/NERC_Interconnections_Color_072512.jpg
- [19] Y. Zhang *et al.*, "Role of wind power in the primary frequency response of an interconnection," National Renewable Energy Laboratory (NREL), Golden, CO, USA, Oct. 2013.
- [20] N.W. Miller, K. Clark, and M. Shao, "Impact of frequency responsive wind plant controls on grid performance," In Proc. 9th International Workshop on Large-Scale Integration of Wind Power, Quebec, Canada, Oct. 2010.
- [21] R. G. de Almeida and J. A. P. Lopes, "Participation of doubly fed induction wind generators in system frequency regulation," IEEE Transactions on Power Systems, vol. 22, no. 3, pp. 944 - 950, Aug. 2007.
- [22] Joseph H Eto *et al.*, "Use of frequency response metrics to assess the planning and operating requirements for reliable integration of variable renewable generation," Ernest Orlando Lawrence Berkeley National Laboratory, Berkeley, CA, LBNL-4142E, December 2010.
- [23] http://en.wikipedia.org/wiki/Northeast_Power_Coordinating_Council
- [24] PSS/E 33.5 User Manual, October, 2013
- [25] NERC Frequency Response Initiative, April, 2010
- [26] "The Gotland HVDC link", ABB, [Online]. Available: <http://new.abb.com/systems/hvdc/references/the-gotland-hvdc-link>
- [27] "Xiangjiaba-Shanghai HVDC link," ABB, [Online]. Available: <http://new.abb.com/systems/hvdc/references/xiangjiaba---shanghai>
- [28] M. Byggeth, K. Johannesson, C. Liljegren, and U. Axelsson, "Gotland HVDC ight - The World's First Commercial Extruded HVDC Cable System," in CIGRÉ 2000, Paris, France, August, 2000.
- [29] TSAT User Manual, Powertech Lab
- [30] D. Van Hertem and M. Ghandhari, "Multi-terminal VSC HVDC for the European supergrid: Obstacles," *Renewable and Sustainable Energy Reviews*, vol. 14, no. 9, pp. 3156 - 3163, 2010.
- [31] 20% Wind energy by 2030 – increasing wind energy's contribution to US Electricity Supply. DOE/GO-102008-2567, July 2008. Available: <http://www.nrel.gov/docs/fy08osti/41869.pdf>

- [32] The U.S. Energy Information Administration (2014, Apr.). Annual Energy Outlook 2014 with Projections to 2040. [Online]. Available: <http://www.eia.gov/forecasts/aeo>
- [33] Pudney D. A review of HVDC in China. Transmission and distribution. Energize, April 2012. p. 31–4
- [34] Xiangjiaba-Shanghai, The first Ultrahigh Voltage Direct Current project in the world to go into commercial operation, in July 2010. [Online]. Available: <http://new.abb.com/systems/hvdc/references/xiangjiaba---shanghai>
- [35] European Network of Transmission System Operators for Electricity (ENTSO-E). “Study roadmap towards modular development plan on pan-European electricity highways system-way to 2050 pan-European power system”, Tech. rep., 2011.
- [36] A. Roehder, H. Natemeyer, S. Winter, A. Schnettler, “Coordinated Control of Active Devices in an Overlay Grid to Facilitate the Integration of Renewable Energy Sources in Europe”, *Powertech* 2013
- [37] Southwest Power Pool, 2008 EHV Overlay Report. [Online]. Available: <http://www.spp.org/publications>
- [38] H. Ergun, J. Beerten, and D. Van Hertem, “Building a new overlay grid for Europe,” in *2012 IEEE Power and Energy Society General Meeting*. July. 2012, pp. 1–8.
- [39] American Electric Power (AEP), Interstate transmission vision for wind integration, March 2007.
- [40] J. D. McCalley, V. Krishnan, “A survey of transmission technologies for planning long distance bulk transmission overlay in US,” *Int. J. Electrical Power and Energy Systems*, 2013, [Online]. Available: <http://www.sciencedirect.com/science/article/pii/S0142061513003396>
- [41] H. Huang, D. Kumar, V. Ramaswami, D. Retzmann, “UHV 1200kV AC Transmission”, Gridtech 2007, SIEMENS, [Online]. Available: http://www.ptd.siemens.de/070201_AC1000kV_GRIDTECH.pdf
- [42] Badenhorst Barrie, van der Merwe Chris, de Vos Jacques. China unveils 1000 kV AC transmission grid. Energize, July 2009. p. 41–2.
- [43] Dale Osborn, David Orser, Maire Waight, “Conceptual Interregional HVDC Network” [Online] Available: <https://www.misoenergy.org/Library/Repository>
- [44] Eastern Wind Integration and Transmission Study, January 2010.
- [45] Federico Milano, “A Brief Introduction to the Power System Analysis Toolbox (PSAT) for Power System Analysis Undergraduate Courses”, [Online] Available: <http://faraday1.ucd.ie/archive/psat/brieftutorial.pdf>
- [46] ePMU User Manual, Powertech Lab Inc.
- [47] Tom Overbye, “PowerWorld Dynamic Simulator”
- [48] ePHASORSim User Manual, 2014

- [49] V. Jalili-Marandi, F. J. Ayres, E. Ghahremani, J. Beilanger, V. Lapointe, "A real-time dynamic simulation tool for transmission and distribution power systems," Proc.IEEE/PES General Meeting, pp. 1-5, July. 2013

VITA

Yin Lei received the B.S. degree in electrical engineering from Xi'an University of Technology in 2009 and obtained the M.S. degrees in electrical engineering from University of Southern California in 2011, respectively. Her research interests include power system dynamics, wide-area power system modeling and control, renewable energy and HVDC integration.